PSU-IRL-SCI-456

Classification Numbers: 1.5, 1.5.1

THE PENNSYLVANIA STATE UNIVERSITY

IONOSPHERIC RESEARCH

Scientific Report 456

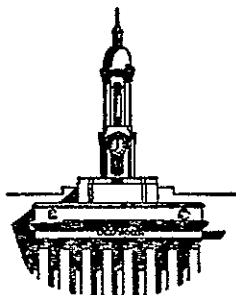# LABORATORY SIMULATION OF ROCKET-BORNE D-REGION BLUNT PROBE FLOWS

by

Lee Bernard Kaplan

May 18, 1977

IONOSPHERE RESEARCH LABORATORY

University Park, Pennsylvania

REPORT DOCUMENTATION PAGE		READ INSTRUCTIONS BEFORE COMPLETING FORM

1 REPORT NUMBER 456	2. GOVT ACCESSION NO.	3 RECIPIENT'S CATALOG NUMBER
4 TITLE *(and Subtitle)* Laboratory Simulation of Rocket-Borne D-Region Blunt Probe Flows		5. TYPE OF REPORT & PERIOD COVERED Scientific Report
		6. PERFORMING ORG. REPORT NUMBER PSU-IRL-SCI-456
7. AUTHOR(s) Lee Bernard Kaplan		8. CONTRACT OR GRANT NUMBER(s) NASA NGL 39-009-003 NASA MAP NSG-6004
9 PERFORMING ORGANIZATION NAME AND ADDRESS The Ionosphere Research Laboratory 318 Electrical Engineering East Building University Park, Pennsylvania 16802		10. PROGRAM ELEMENT. PROJECT, TASK AREA & WORK UNIT NUMBERS
11. CONTROLLING OFFICE NAME AND ADDRESS National Aeronautics and Space Administration Washington, D. C. 20546		12. REPORT DATE May, 1977
		13. NUMBER OF PAGES 161
14 MONITORING AGENCY NAME & ADDRESS(If different from Controlling Office)		15. SECURITY CLASS. (of this report) NONE
		15a. DECLASSIFICATION/DOWNGRADING SCHEDULE

16. DISTRIBUTION STATEMENT *(of this Report)*

17. DISTRIBUTION STATEMENT *(of the abstract entered in Block 20, If different from Report)*

18. SUPPLEMENTARY NOTES

19. KEY WORDS *(Continue on reverse side If necessary and Identify by block number)*

Ionosphere
D-Region

20. ABSTRACT *(Continue on reverse side If necessary and Identify by block number)*

The flow of weakly ionized plasmas that is similar to the flow that occurs over rocket-borne blunt probes as they pass through the lower ionosphere has been simulated in a scaled laboratory environment, and electron collection D-region blunt probe theories have been evaluated.

A scaled steady state plasma flow simulated the electron temperatures ($T_e \sim 10^2$ °K) and number densities ($n_e \sim 10^2$ cm^{-3}) characteristic of the lower ionosphere (D-region). A glow discharge was used to produce the source plasma; source electron temperatures and densities were controlled by varying the

electrode configuration. The test section conditions were also controlled by relaxation of the plasma from the cross flow in the discharge chamber and through a baffle system. Subsonic ($M_n = 0.3$) and supersonic ($M_n = 2.0$) flows were produced. Equivalence of the flow parameters ($M_n \sim 0.3$, $R_n \sim 10^2$, and $K_n \sim 10^{-2}$) was reproduced by appropriately scaling both the neutral gas density and probe diameter by two orders of magnitude.

The state of the plasma in the glow source and test section jet was indicated from a Langmuir (collisionless) double probe response. A scaled version of a rocket-borne blunt probe was also evaluated in this controlled flow experiment. The various blunt probe theories for particle collection were analyzed, and electron densities evaluated from double Langmuir and scaled blunt probe data using these theories were compared with mixed results. The theory by Mitchell, Hale, Hoult is felt to correctly describe the processes in the relatively thin perturbed layer adjacent to the probe surface that is dominant in ion collection. However, for electron collection, the theory proposed by Lai appears to more correctly describe the particle motion and processes occurring in the several perturbed layers adjacent to the blunt probe surface, and indicated number densities show better agreement with those indicated by the double probe.

PSU-IRL-SCI-456
Classification Numbers: 1.5, 1.5.1

Scientific Report 456

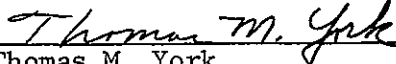Laboratory Simulation of Rocket-Borne
D-Region Blunt Probe Flows

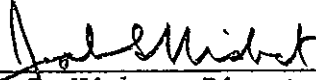by

Lee Bernard Kaplan

May 18, 1977

Submitted by:

.Thomas M. York
Associate Professor of
Aerospace Engineering

Approved by:

J. :S. Nisbet, Director
Ionosphere Research Laboratory

Ionosphere Research Laboratory

The Pennsylvania State University

University Park, Pennsylvania 16802

ACKNOWLEDGEMENTS

The author wishes to express gratitude and appreciation to Dr. Thomas M. York for his advice and continued guidance throughout the course of this work. Thanks are also expressed to Mr. R. Husted and Mr. T. Young for their help in the design and construction of the components for the test facility.

TABLE OF CONTENTS

LIST OF TABLES

LIST OF FIGURES

NOMENCLATURE

English Letter Symbols

A Cross sectional area

A_{COL} Area of blunt probe collector

A_E Exit plane area of nozzle

A_o Area of entrance of choked orifice

A_0 Area of collection surface

A_s Area of sheath

A_S Surface area of probe

C Pressure coefficient

$\bar{c}$ Random velocity of attracted particles

D_p Probe diameter

e Electron charge

E Total energy of particles

$\hat{E}$ Electric field

E_p Potential energy of attracted particles

g Stagnation point inviscid flow velocity gradient

i Conducted probe current

i_e Conducted electron current

I_e Dimensionless electron current

J Defined by Eq. (5.4.3)

j_e Electron current density

$j_{i,\infty*}$ Defined by Eq. (5) in Ref. (22)

J_e Electron current at plasma potential

J_i Ion current at plasma potential

J_s Defined by Eq. (5.4.7)

k	Boltzman constant
K_n	Knudsen number
l	Length of probe filament
m	Mass
$\dot{m}$	Mass flow rate
m_e	Mass of electron
m_i	Mass of ion
M	Molecular weight
M_n	Mach number
n	Neutral concentration
n_e	Electron number density
n_{eo}	Electron number density in undisturbed plasma
n_i	Ion number density
n_o	Particle number density in ambient plasma
$(n_e)_{col}$	Electron number density in collisionless regime
$(n_e)_{trans}$	Electron number density in transitional regime
P	Static gas pressure
P_E	Static pressure at exit plane of nozzle
P_i	Impact pressure
P_{ideal}	Impact pressure in free molecular flow
P_o	Static gas pressure at entrance of choked orifice
r	Radial displacement of attracted particles
r_{COL}	Radius of collector disc
r_n	Radial distance across exit plane of nozzle
r_o	Radius of collection surface
r_p	Radius of probe

R   Gas constant

R_e Electric Reynolds number

R_n Flow Reynolds number

Sci   Ion Schmidt number

t   Time for flow to proceed from center of plasma source to exit plane of nozzle

T   Heavy particle gas temperature

T_e Electron temperature

T_E Gas temperature at exit plane of nozzle

T_i Ion temperature

U   Flow velocity

$\bar{U}$ Defined by Eq. (5.4.4)

U_E' Flow velocity at entrance of test chamber (exit of nozzle)

U_o Flow velocity at entrance of choked orifice

v_r Radial velocity

$\dot{V}$ Volume flow rate

V_d Applied probe potential

V_D Electron drift potential

V_p Plasma potential

V_T Electron thermal velocity

y   Axial distance from center of source plasma

Z   Charge of attracted particles

Greek Letter Symbols

α Recombination coefficient

$(\alpha)_{CAL}$ Calculated recombination coefficient

$(\alpha)_{EXP}$ Experimentally determined recombination coefficient

α_p Defined by Eq. (5.4.6)

β $= \dot{m}_e \, m_i^{-1}$

Δ Shock position

δ Boundary layer thickness

δ_S Thickness of shock transition

γ Ratio of specific heats

γ^{-1} Defined by Eq. (2) in Ref.(22)

γ_A Radius of convection and mobility region

γ_B Radius of mobility layer

γ_0 Static perturbed thickness

Γ Nondimensional current conducted by Langmuir double probe

θ Degree of ionization

λ_{e-n} Electron-neutral mean free path

λ_D Debye length, defined by Eq. (5.2.2)

λ_{i-n} Ion-neutral mean free path

λ_{n-n} Neutral-neutral mean free path

λ_{s-n} Mean free path between neutral particles and attracted species

μ Viscosity

μ_e Electron mobility

μ_i Ion mobility

ν Kinematic viscosity

ρ Neutral gas density

ρ_E Neutral gas density at entrance of test chamber

ρ_0 Neutral gas density at entrance of choked orifice

σ Collision cross section

σ_+ Positive conductivity

σ_- Negative conductivity

σ_{e-n} Electron-neutral collision cross section

σ_i Ion collision cross section

σ_{s-n} Collision cross section between the attracted species and neutral particles

φ_d $= e\, V_d\, (kT_e)^{-1}$, nondimensional probe potential

φ_p $= e\, V_p\, (kT_e)^{-1}$, nondimensional plasma potential

$\varphi_{(r)}$ Local particle potential

Φ Potential distribution for a circular disc

Φ_p Potential distribution on surface of circular disc

Ω Angular momentum

T End-effect parameter

ABSTRACT

The flow of weakly ionized plasmas that is similar to the flow that occurs over rocket-borne blunt probes as they pass through the lower ionosphere has been simulated in a scaled laboratory environment, and electron collection D-region blunt probe theories have been evaluated.

A scaled steady state plasma flow simulated the electron temperatures ($T_e \sim 10^2$ °K) and number densities ($n_e \sim 10^2$ cm^{-3}) characteristic of the lower ionosphere (D-region). A glow discharge was used to produce the source plasma; source electron temperatures and densities were controlled by varying the electrode configuration. The test section conditions were also controlled by relaxation of the plasma from the cross flow in the discharge chamber and through a baffle system. Subsonic ($M_n = 0.3$) and supersonic ($M_n = 2.0$) flows were produced. Equivalence of the flow parameters ($M_n \sim 0.3$, $R_n \sim 10^2$, and $K_n \sim 10^{-2}$) was reproduced by appropriately scaling both the neutral gas density and probe diameter by two orders of magnitude.

The state of the plasma in the glow source and test section jet was indicated from a Langmuir (collisionless) double probe response. A scaled version of a rocket-borne blunt probe was also evaluated in this controlled flow experiment. The various blunt probe theories for particle collection were analyzed, and electron densities evaluated from double Langmuir and scaled blunt probe data using these theories were compared with mixed results. The theory by Mitchell, Hale, Hoult is felt to correctly describe the processes in the relatively thin perturbed layer adjacent to the probe surface that is dominant in ion

collection. However, for electron collection, the theory proposed by Lai appears to more correctly describe the particle motion and processes occurring in the several perturbed layers adjacent to the blunt probe surface, and indicated number densities show better agreement with those indicated by the double probe.

CHAPTER I

INTRODUCTION

1.1 Discussion of Problem and Earlier Work

The D-region is the lower part of the ionosphere, located between

the lower thermosphere and upper stratosphere; it extends from about

40 km to 90 km above a standard sea-level reference. The chemical com-

position of the D-region is poorly understood because of its complex

structure and general inaccessibility for probing. This region of space

is too high for balloon studies and too low for orbital satellite

research. The use of rocket-borne probes has overcome the inaccessibility

problem, but it has introduced a new degree of difficulty because of the

need to interpret the response of the probes. Accordingly, the correct

interpretation of the response from rocket-borne probes is of fundamental

interest in trying to understand the chemical composition of the

D-region.

The properties of the D-region (1), presented in Table 1 include

values for the pressure, P, density, ρ, neutral concentration, n,

temperature, T, electron-neutral mean free path, λ_{e-n}, ion-neutral, λ_{i-n},

and neutral-neutral, λ_{n-n}, mean free paths. The state of the medium

in the D-region is specified by the electron Knudsen number, defined as

the ratio of the electron-neutral mean free path to the characteristic

probe size (Eq. 1.3.2); it is about 9 to 90 km and 8×10^{-3} at 40 km. A

rocket-borne probe is typically on the order of 10 cm in diameter $(D_p = 2r_p)$

and descends through the D-region while passing from a collisionless

$(\lambda_{s-n} \gg r_p)$ medium at 90 km to a collisional $(\lambda_{s-n} \ll r_p)$ medium at

40 km. The D-region is weakly ionized with the degree of ionization,

Table 1: The Properties of the D-Region

ALT (km)	P (Torr)	ρ (g cm^{-3})	n (cm^{-3})	T ($^{\circ}$K)	λ_{e-n} (cm)	λ_{i-n} (cm)	λ_{n-n} (cm)
40	2.17	3.43×10^{-6}	7.2×10^{16}	284	8.0×10^{-2}	2.6×10^{-3}	3.2×10^{-3}
50	6.0×10^{-1}	9.93×10^{-7}	2.0×10^{16}	271	3.2×10^{-1}	6.7×10^{-3}	8.2×10^{-3}
60	1.5×10^{-1}	2.66×10^{-7}	5.7×10^{15}	253	1.2	2.0×10^{-2}	2.4×10^{-2}
70	3.5×10^{-2}	7.45×10^{-8}	1.61×10^{15}	210	4.2	6.7×10^{-2}	8.2×10^{-2}
80	6.77×10^{-3}	1.54×10^{-9}	3.24×10^{14}	197	2.0×10^{1}	4.5×10^{-1}	5.6×10^{-1}
90	1.25×10^{-3}	2.96×10^{-9}	6.4×10^{13}	185	9.0×10^{1}	1.6	2.0

defined approximately as the ratio of electron to neutral particle concentration ($\theta = n_e/n$), varying from 10^{-9} to 10^{-14} between 90 and 40 km, respectively. The Debye length, the characteristic electrostatic shielding length scale (defined in Chapter V), is approximately 10 cm at 40 km and 3 cm at 90 km.

Sounding rockets are used to carry diagnostic probes into the ionosphere where they are released; probes are flown in subsonic and supersonic flight conditions. With the parachute system, the probes will descend subsonically with velocities of about 300 m sec^{-1} at 90 km to about 40 m sec^{-1} at 40 km (2); the average descending velocity is 100 m sec^{-1}. Without a parachute drag system the probe's descending flight is supersonic with a terminal Mach number of about 4 (3); the probe's average flight Mach number is about 2.

The electrostatic blunt probe diagnostic was first used by Hale and Hoult (4) to study the chemical composition of the D-region. These probes were launched into the ionosphere and collected data in descent from 90 km to 40 km. The probes moved subsonically with the aid of a parachute drag system, having an average velocity of 100 m sec^{-1}. Other similar types of particle collecting probes have been flown supersonically. Gerdien condenser probes (5) recorded data that requires a knowledge of the flow field and shock wave characteristics for proper interpretation. In supersonic flow, as a shock wave forms in front of the probe, chemical effects on the electrically charged particles occur in the flow region surrounding the probe. If further ionization is caused by the shock, difficulties arise in trying to relate the recorded data to the basic atmospheric data. There are no foolproof means of

controlling the orientation of the supersonic probes, and this can result in an alteration of the composition of the plasma in contact with the probe. Bordeau, et al. (6) suggested that for a more satisfactory understanding of the data obtained from the supersonically flown probes, an improved analysis would be required. Chung, et al. (7) have presented a review of available electric probe theories in flowing plasmas. They also point out that ion and electron particle collection in the ionosphere is an important use of such probes, and that there have been many theories developed for the interpretation of data received from rocket-borne probes. In the present work, comparison and analysis of the various relevant probe theories, particularly for electron particle collection by subsonic, blunt probes, will be presented.

The Ionosphere Research Laboratory of The Pennsylvania State University has recently (October 1971 to February 1972) launched 11 electrostatic blunt probes into the D-region of the ionosphere. Hale (8) has pointed out that the interpretation of the electron data obtained from these subsonically flown probes needs further in-depth study. This thesis will explore laboratory experimental-analytical aspects of blunt, subsonic probe behavior.

The experimental techniques associated with rocket-borne probes are well established. The application of particle collection theory to the data recorded by the probes, however, is required in order to predict atmospheric properties. The probes are flown as a means of obtaining number densities of the constituents in the particular region being studied. The current collected by the probe in response to applied voltage is scaled, transmitted, and catalogued. Appropriate

equations with assumed averaged properties of the medium are applied before the number densities are obtained. Burkhard (9) has suggested that the use of hybrid computer techniques would alleviate the data reduction problem by reducing the time required for reduction and by providing an increase in accuracy that is lost in any hand reduction process.

In order to study the response of probes for use in space, some laboratory experiments involving flowing plasmas have been conducted (10-18). The cylindrical Langmuir probe (10) has been widely used as the primary diagnostic tool in collisionless plasma ($\lambda_{s-n} \gg r_p$) research. There is a major difference, however, between the use of electrostatic probes for these collisionless plasma flow studies and their use as lower ionosphere diagnostic probes. In the lower ionosphere, rocket-borne electrostatic probes collect particles from a highly collisional plasma ($\lambda_{s-n} \leq r_p$) with an applied electric field operating in a region of free diffusion. The electrostatic probe flows that have been studied in laboratory plasmas serve to model reentry (hypersonic) flows that are highly ionized and have a large bias voltage so that they are influenced by ambipolar diffusion, and the space charge field (sheath) dominates the collection region. While such laboratory experiments are a means for predicting the effects that the flow velocity of the plasma will have on the response of one specific operating range for electrostatic probes, to date there has been no reported laboratory evaluation of electrostatic devices in flowing plasma that model D-region probe flows of interest here.

Research conducted on the response of electrostatic probes in flowing plasmas has dealt with some of the effects of flow on electron temperature and density, probe potential distribution, and plasma potential as related to ion and electron currents collected. Dunn and Lordi (11) made electron temperature measurements with cylindrical Langmuir probes in the collisionless ($\lambda_{s-n} \gg r_p$) and transition ($\lambda_{s-n} \simeq r_p$) regimes of a plasma produced in a shock tunnel. They found that the deduced electron temperatures were independent of the probes radius and end effects. Sonin (13) and Smetana and Iachetta (14) found that in a collisionless plasma the electron temperature indicated by cylindrical Langmuir probes was independent of the probe's orientation with respect to the flow velocity direction. More recently, Segall and Koopman (15) have studied the flow effects on indicated electron temperature in a laser produced collisionless plasma. Generally, they found that the indicated value of electron temperature in flowing plasma was higher than in the static plasma. From such results, it can be concluded that the electron temperature as determined from standard techniques using the slope of the logarithm of the electron current plotted as a function of applied probe voltage, provides an upper limit on temperature measured in a flowing plasma.

The effects of plasma flow on the indicated plasma potential was considered by Heatly (16). He found that the plasma potential may not be clearly recognized from the current-voltage characteristics. The current conducted by the probe at the plasma potential will be greater than the thermal current to the probe in the stationary plasma. Sonin (13) considered what effects the orientation of the probe would have on

the indicated plasma potential. It was found that the plasma potential as identified by a "knee" in the characteristic, is altered when the positively biased probe's orientation is changed with respect to the flow direction.

The potential distribution about the probe in a flowing collisionless plasma was considered by Laframboise (17) and Heatly (16). Heatly found that because of the imposed flow velocity, the effective cross sectional area of the sheath around a cylindrical probe is distorted from a circular shape. However, if the probe is positioned perpendicular to the flow direction the sheath will have a bilateral symmetry and the distortion of the potential field can be avoided. Heatly also concluded that, in principle, the response from the probe can be treated as if it were in a stationary plasma. More recently, Laframboise found that if the cylindrical probe is positioned parallel with the flow direction it will respond as if it were a stationary plasma when the mean free paths of the species being collected are larger than the probe's radius (17).

Regarding saturation, Segall and Koopman (15) found that when using cylindrical Langmuir probes, the electron current did not saturate. A nearly linear increase in the probe current with applied voltage was obtained, while the same probes did show saturation in the stationary plasma. It was concluded that the shielding effect of the sheath is lost due to the flow velocity. As a related observation, Iachetta and Smetana (14) found that the electron current is independent of the velocity of the plasma when the flow velocity is less than the particle random speed.

Jakubowski (18) and Sonin (12) both studied the effects that plasma velocity has on the conducted ion current. It was found that the maximum ion current is conducted when the probe is positioned parallel with the flow direction. As the orientation of the probe is changed with respect to the flow direction, the ion current decreases.

The studies of electrostatic probes in flowing plasmas discussed above give a general indication of the unresolved nature of the effects of flow velocity on the response of electrostatic probes. Some specific regimes of operation such as for collisionless particle collection, are fairly well understood and this can aid in understanding the response of lower ionosphere, collisional rocket-borne probes. The studies noted have dealt with strongly ionized plasmas and mostly with ion current collection. The intent of the present work is to provide an experimental verification of the response of electrostatic probes in a weakly ionized flow as experienced by rocket-borne probes descending through the highly collisional D-region of the ionosphere. Electron collection is of primary interest, and is used to allow correct determination of electron density from the response of the probes.

1.2   Objectives

In this work the flow over a D-region rocket-borne blunt probe will be simulated in collisional, continuum regimes in a laboratory experiment. Subsonic and supersonic flows are modeled in order to simulate the probe's flight conditions through the D-region. The D-region parameters are scaled to provide an alternative means of understanding the formation and dynamics of D-region probe flows. It is

one objective of this research to show that the response from the rocket-borne blunt probe can be correctly evaluated in a controlled D-region flow experiment.

The blunt probe theory was originally developed by Hale and Hoult (4) for subsonic rocket-borne probes. Sonin (19) provided an alternative interpretation and extended the theory to include supersonic probes. Both theories were based on the concept of particle convection in the zero space charge limit. Until recently, these were the only relevant theories which related the current conducted by the ionospheric probes to the ambient charged particle density for blunt probe flow. A new theory for electron collection has been outlined by Lai (2). This theory is developed for subsonic blunt probes and is based on a dominant mobility concept in the zero space charge limit. Not one of the above theories for the operation of an electrostatic blunt probe has been substantiated by controlled experimental results. On that basis, the interpretation of D-region data from subsonic and supersonically flown probes clearly needs further study. The present work will help identify the appropriate theory for the interpretation of blunt probe data by allowing comparison of appropriately determined electron density and temperature of the plasma with that determined from blunt probe data interpreted by each of these available theories for parameter ranges appropriate for full-sized D-region rocket-borne probes.

1.3   Method of Investigation

To obtain a properly modeled experiment, some plasma and probe properties were scaled by two orders of magnitude. The relevant flow parameters include the Reynolds number, Knudsen number and Mach number. The Reynolds number is given by

$$R_n = \frac{nmUD_p}{\mu} \qquad (1.3.1)$$

where n is the neutral concentration, m is the mass, U is the flow velocity, D_p is the probe diameter, and μ is the viscosity. The Knudsen number is given by

$$K_n = \frac{1}{n\sigma r_p} \qquad (1.3.2)$$

where σ is the collision cross section. The Mach number is given by

$$M_n = \frac{U}{(\gamma RT)^{1/2}} \qquad (1.3.3)$$

where γ is the ratio of specific heats, R is the gas constant, and T is the gas (heavy particle) temperature. In the D-region the Reynolds number for a 10 cm diameter probe, descending subsonically, ranges from about 4.1 at 90 km to 724 at 40 km, and about 110 at 90 km to 6.4×10^4 at 40 km for a supersonically descending probe. The electron Knudsen number varies from about 9 at 90 km to 8×10^{-3} at 40 km. The Mach numbers are about 0.3 and 2 for the subsonic and supersonic flight conditions, respectively, and were determined by using the average descending velocities of the probe through the D-region.

Equivalence of the flow parameters was reproduced by scaling the neutral concentration and probe diameter; the neutral density was scaled up by two orders of magnitude while the probe diameter was

scaled down by two orders of magnitude. By reproducing the correct

flow velocities and ambient temperature, the D-region flow parameters

were reproduced. Without this scaling, an excessive volume flow rate

of about 4 $m^3 sec^{-1}$ would be required by a pumping system for full scale

models. It was, therefore, desirable to scale the experiment by reduc-

ing the physical size while retaining the order of magnitude of the flow

parameters.

A glow discharge (20) was used to produce a weakly ionized plasma.

The glow discharge is characterized by a gas (heavy particle) tempera-

ture on the order of 300°K and an electron density on the order of

$10^8 cm^{-3}$. The degree of ionization in a glow discharge is on the order

of 10^{-14}. The proper D-region electron temperature and density was

achieved by allowing the discharge to flow through baffles, into a

nozzle, and into the test chamber. The ionization in the plasma enter-

ing the test chamber was controlled by the baffle system which lengthens

the path of the flow, allowing electron temperature and density to

relax to desired values. The plasma source was controlled by varying

the electrode configuration and power levels.

An impact pressure probe (21) was used to obtain impact pressure

measurements at the exit of the nozzles. These measurements describe

the characteristics of the flow field in the discharge jet.

The cylindrical Langmuir probe (10) has been widely used to

obtain electron temperatures and particle number densities in colli-

sionless laboratory plasmas. This type of probe consists of one or

more metallic electrodes with a large aspect ratio, ℓD_p^{-1}, which when

inserted into a plasma and biased relative to it, enables the local

properties of the plasma to be accurately determined when operated in the collisionless regime. Because the theory of its operation and the procedure for its use are well understood (22), it was used in this work to accurately establish the plasma characteristics in the test jet.

A scaled version of Hale's rocket-borne blunt probe (23) was also used to obtain standard current-voltage data indicative of the electron temperature and particle number densities. The data from the scaled blunt probe will be correlated with the data from the actual rocket-borne D-region probe. The validity of the plasma properties deduced from rocket-borne data will be determined by a comparison of the magnitudes of the exact plasma number densities and temperatures with those determined from the various techniques using the current-voltage characteristics in the laboratory experiment.

CHAPTER II

EXPERIMENTAL APPARATUS AND TEST CONDITIONS

2.1 Flow Scaling

The reproduction in the laboratory experiment of the flow about a descending D-region blunt probe requires the viscous (R_n), compressibility (M_n), and rarefraction (K_n) parameters to equal those in the ionosphere. The mass flow rate through the internal flow system must be controlled to produce the desired flow conditions over the scaled probe in the laboratory system, as

$$\dot{m} = 0.785 \text{ nmUD} \tag{2.1.1}$$

where m is the mass of the average gas particles. Excessive mass flow rates on the order of 8 gsec^{-1} would be required for a full-size model to be tested. By reducing the geometric size of the experiment, large reductions of mass and volume flow rate can be achieved because $\dot{m} \sim nD^2$. A reduction in size by one order of magnitude along with an increase in density by one order of magnitude, results in a lower mass flow rate of one order of magnitude, while the volume flow rate, $\dot{V}$, required by the pumping system is reduced by two orders of magnitude, as

$$\dot{V} = 0.785 \text{ UD}^2 \tag{2.1.2}$$

Since $K_n \sim (nD_p)^{-1}$ and $R_n \sim nD_p$, similarity of test and flight parameters is insured when the flow velocities, temperatures, and the product $n \times D_p$ (cm^{-2}) is the same in the actual and scaled flows. In this experiment the blunt probe diameter was reduced from 10 cm to 0.1 cm, and the gas density was scaled up by two orders of magnitude. This

scaling resulted in lower mass flow rates by two orders of magnitude and a reduction in the steady state volume flow rate by four orders of magnitude.

2.2 Apparatus and Evaluation of Alternative Plasma Sources

2.2.1 Introduction - Electrical Discharge and Test Chamber

In order to simulate the weak ionosphere plasma, the production of a low temperature and low density plasma was needed in this experiment. Various electrical discharge configurations for obtaining a low temperature and density plasma were tested before the glow discharge source with cross flow was established as the appropriate plasma source. The temperature and number density of charged particles was controlled by the geometry of the electrodes and a baffle system for the flow. The alternative techniques considered will be discussed in section 2.2.4.

A glow discharge is produced by the conduction of low-level current (mA) through a low density (mT) gas. The discharge is generally comprised of interelectrode regions, dark spaces, and a uniform positive column. The transport of electrons and ions in the gas are the primary processes which maintain the discharge. Ionization, excitation, recombination, attachment and dissociation, and the absorption and emission of photons are the processes which are involved in the total physical phenomena of the self-maintained glow discharge (20).

In the laboratory experiment, electrostatic probe measurements in the stationary glow configuration were made in the postive column. The positive column is characterized by a low gas (heavy particle) temperature on the order of $300°K$ and an electron density on the order of

10^8 cm^{-3}. This region of discharge extends from the Faraday dark space near the cathode to the anode glow. It is a quasi-neutral plasma $(n_i = n_e)$ which has been studied by standard Langmuir probe techniques (24).

In general, in the discharge configuration with cross-flow super-imposed, no such definable regions occured in the glow discharge. The electron concentrations in each definable static region were found to be mixed together. As the resulting ionized flow progressed from the discharge chamber into a baffle and accelerating nozzle, the concentration of electrons was also altered by the processes of diffusion to the walls and recombination. The control of the electron density was achieved by the geometry of the electrodes and the baffle system. The specific electrode configuration will be discussed in section 2.2.4 and the baffle system will be discussed in sections 2.3 and 2.4.

The circuit for the glow discharge is shown in Figure 2.1. It is comprised of a variable DC power supply and load resistor. As will be established in section 2.2.4, 28 mA was chosen as the appropriate working discharge current. The compatible voltage applied to the system was found to be a function of the operating pressure in the flow; it varied from 500 V to 1500 V. A 1000 Ω, 200 W load resistor was used in series with the power supply to insure a stable discharge (24).

Figure 2.2 presents a schematic of the experimental facility: glow discharge chamber, traversing mechanism, and test chamber. The test chamber was a standard 15 cm internal diameter pyrex cross. The discharge chamber was initially designed so that various types of plasma

Variable DC
Power Supply

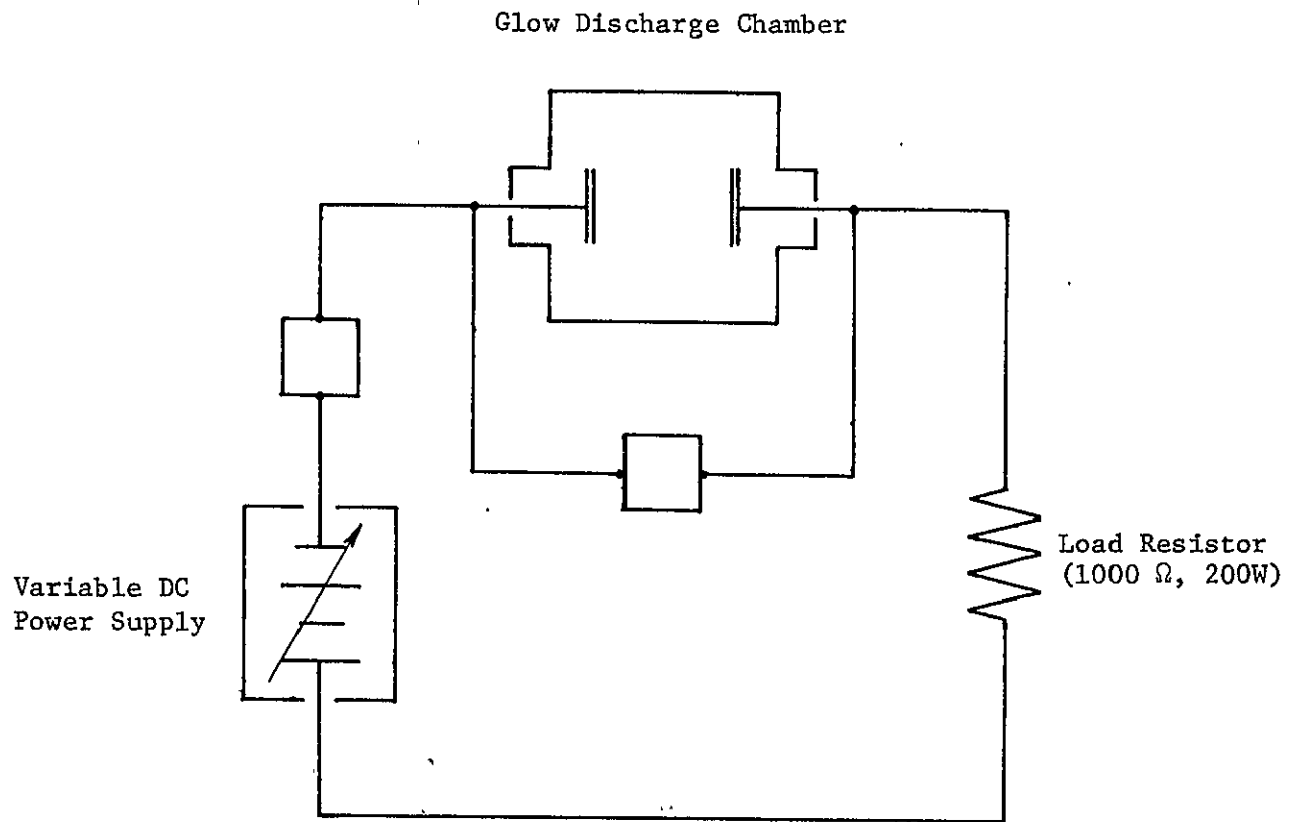Load Resistor
(1000 Ω, 200W)

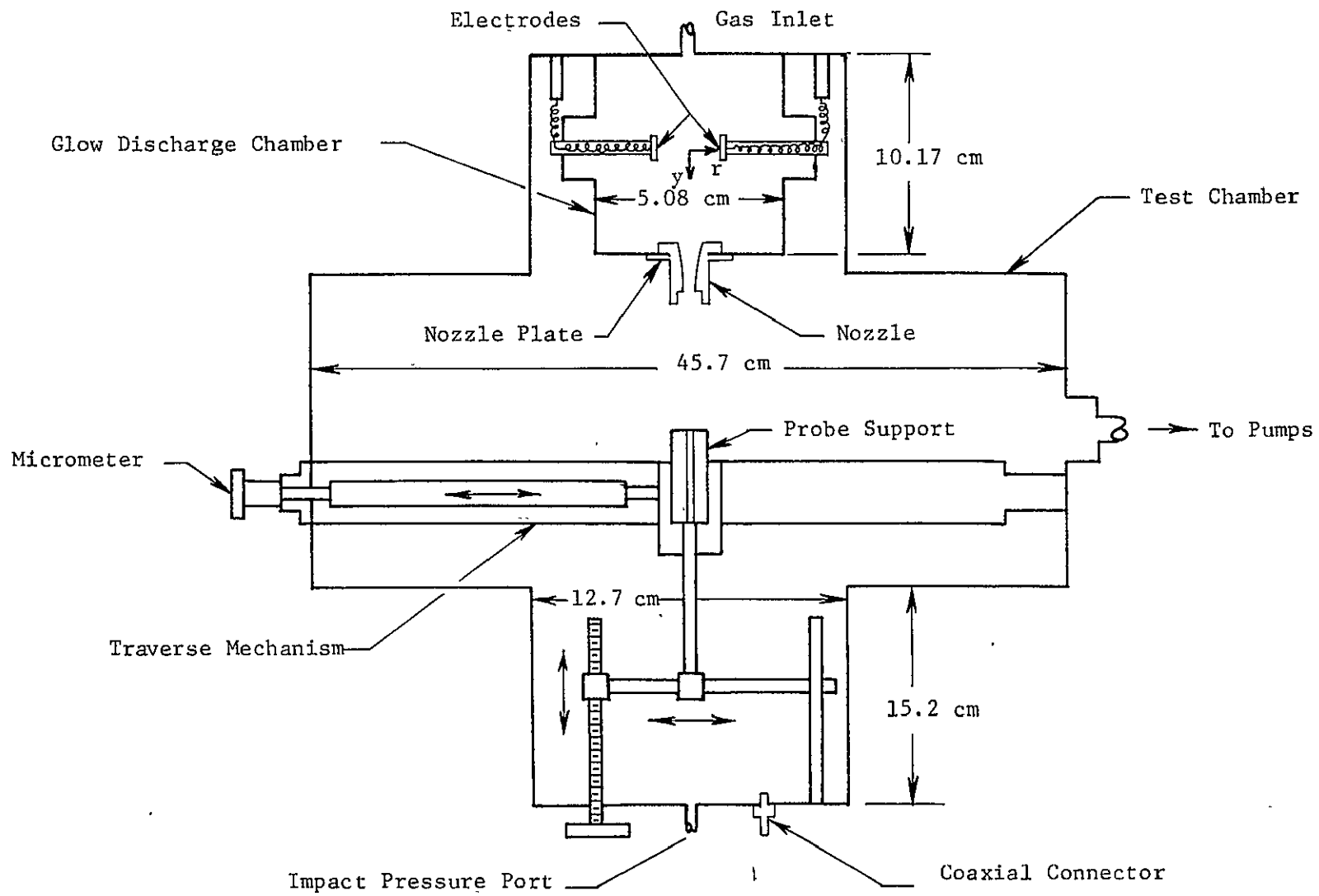Figure 2.1   Glow Discharge Circuit

Figure 2.2 Experimental Facility

sources could be emplaced in the pressure-isolated discharge chamber. The rectangular discharge chamber was fabricated from plexiglass, as low temperature plasma sources were originally envisioned; the electrical discharge was along a lateral axis and the neutral gas flowed along a longitudinal axis. A steady state flow system was developed. After ionization by the glow discharge, the gas was accelerated by a fitted subsonic or supersonic nozzle which allowed flow into the test chamber, which had a fixed pressure. The test station was located at the exit plane of the nozzle.

The traversing mechanism enabled the diagnostic probes to be moved with considerable precision across and along the discharge jet. It was made primarily of plexiglass components and was supported by two side plates in the test chamber cross-arms. An integral precision micrometer allowed accurate positioning of the probes across the discharge jet to within 0.01 mm.

The low density plasma jet streaming from the exhaust nozzles, flowed into the test chamber; probes were positioned in an axial orientation. The end plates of the test chamber were made of plexiglass. The aft end plate supported the glow discharge chamber. The forward end plate was used for electrical and pressure connections. The side plates also supported the 5 cm diameter vacuum pumping inlet.

2.2.2 Pumping System and Pressure Measuring Instruments

The low density, steady state volume flow rates were achieved by a tandem connection of two Welch 1397B (8.5×10^{-3} m^{3}sec^{-1}) mechanical pumps at a 5 cm internal diameter "T" junction. They were operated simultaneously and controlled through a common gate valve. The test

chamber was connected to the pumping system by heavy rubber tubing with a 5 cm internal diameter. The rubber tubing was connected to a cold trap which was mounted on the gate valve and pumps. This configuration is shown in Figure 2.3. Rubber tubing was also used to connect the pumps to the common linkage on the gate valve. This prevented vibrations associated with the vacuum pumps from being transmitted to the test chamber.

Two types of gauges were used for static pressure measurement. A Pirani vacuum gauge (0 to 2 Torr) was used for the scaled lower pressure range (0.09 to 0.16 Torr, 90 km)and a Wallace and Tiernan gauge (0 to 50 Torr) for the scaled higher pressure range (0.4 to 4 Torr, 70 km and 80 km). The Pirani gauge is a thermal conductivity vacuum instrument. The Wallace and Tiernan is a mechanical vacuum gauge. Both of these give direct pressure indications. They were calibrated with a McLeod mercury manometer. The connecting arrangement for these pressure instruments is also shown in Figure 2.3.

Impact pressure measurements in the discharge jet were made with a standard right circular cylinder impact probe; this instrument will be discussed in section 3.1. In the subsonic flow configuration, the impact probe was connected to a Granville-Phillips capacitance manometer. This manometer is a differential pressure instrument of high sensitivity; it gave pressure readings relative to the reference static pressure in the test chamber to within 0.001 mm Hg. In the supersonic flow configuration, the impact pressure probe was connected to a Cole-Parmer micrometric mercury manometer. This instrument also gave differential pressure readings; it was sensitive to within 0.05 mm Hg.
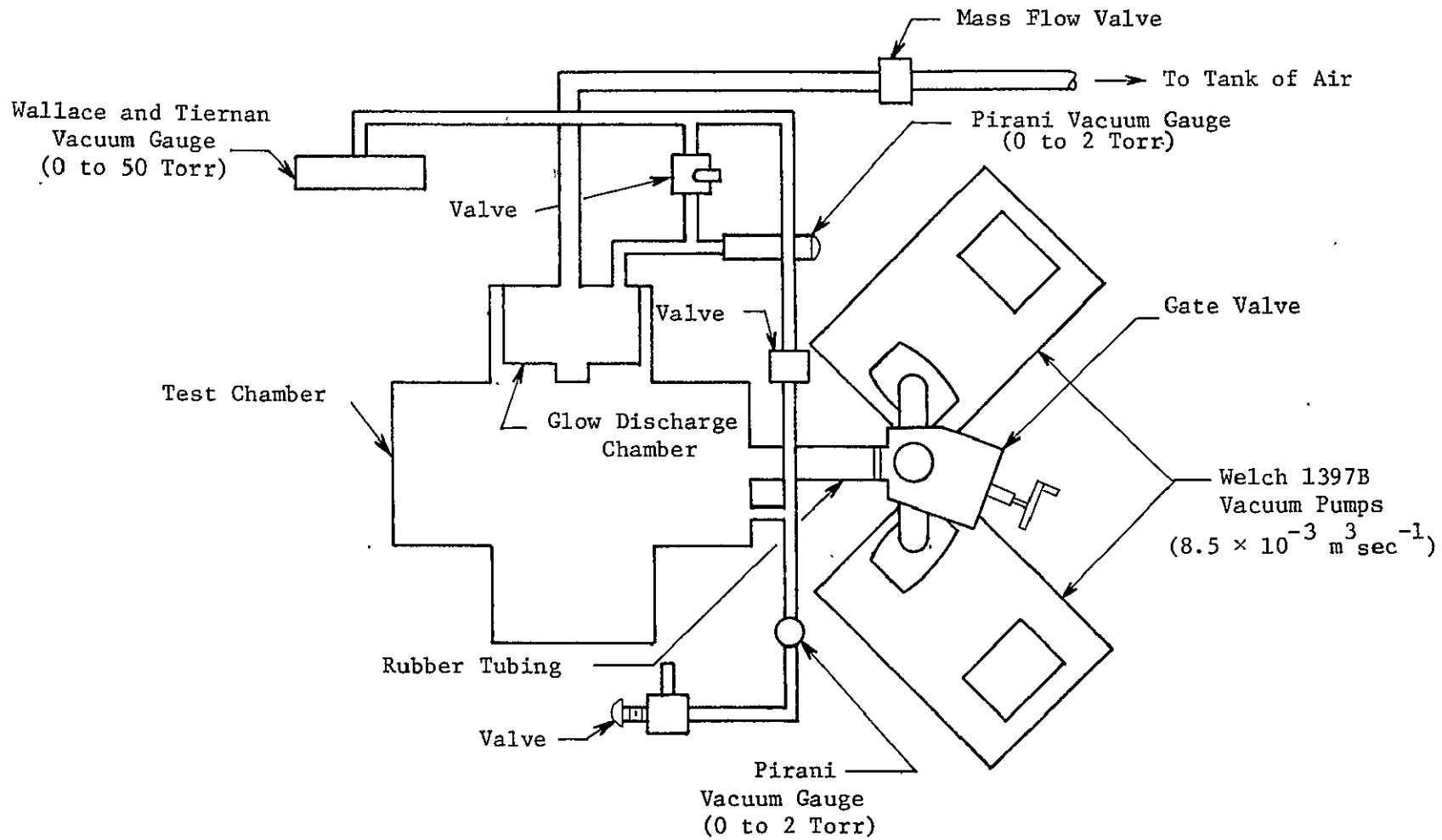
Figure 2.3 Pumping and Pressure Measuring System for Experimental Facility

The impact probe was also connected to a supplementary Welch 1400 $(3.5 \times 10^{-4} \, \text{m}^3\text{sec}^{-1})$ mechanical pump to help evacuate the impact probe prior to initiating a given series of data runs. When the static pressure in the probe and test chamber were equal the pump was closed, allowing the probe to respond to the impact pressure from the discharge jet. This arrangement is shown in Figure 2.4.

2.2.3 The Subsonic and Supersonic Nozzles

Both nozzles were designed for a constant volume flow rate of $1.18 \times 10^{-2} \, \text{m}^3\text{sec}^{-1}$. The ambient gas (heavy particle) temperature was maintained at room temperature (300°K) while the discharge pressure was adjusted for a specific operating condition. The neutral gas entered the discharge chamber through a choked orifice; the pumping system induced the steady state flow through the system. The exit area of the nozzles was determined by matching the mass flow rate entering the discharge chamber with the mass flow rate entering the test chamber. The continuity equation for this condition is

$$\rho_o \, U_o \, A_o = \rho_E \, U_E \, A_E \qquad (2.2.1)$$

where A is the cross sectional area and the subscripts o and E denote the entrance condition into the choked orifice and entrance condition (jet exit) into the test chamber, respectively. The predetermined conditions entering the choked orifice (P_o and T_o) and the specified scaled test conditions (P_E, ρ_E, T_E and U_E) enabled the exit areas of the nozzles to be determined. From Eq. (2.2.1) and the perfect gas law ($P = \rho RT$), the exit areas of the nozzles were determined by
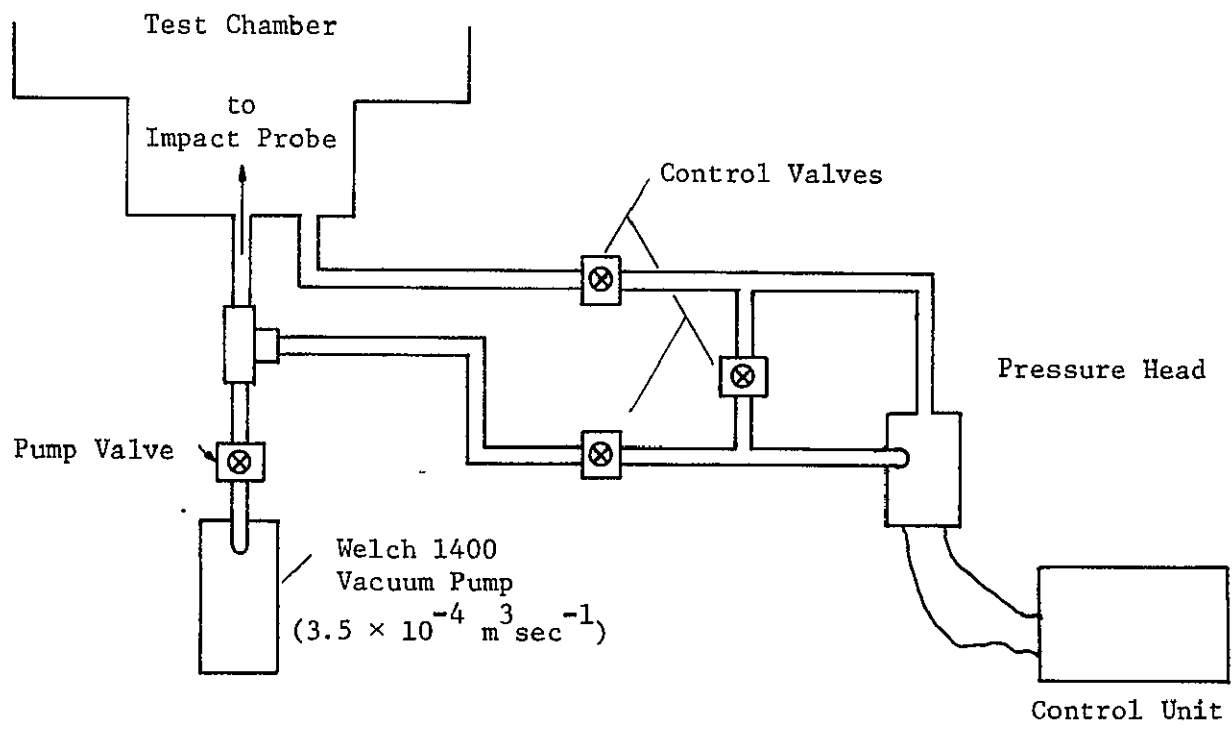
Figure 2.4   Impact Pressure Sensing System

$$A_E = \frac{T_E P_o \dot{V}}{T_o P_E U_E}$$

(2.2.2)

where $\dot{V} = U_o A_o$, the constant volume flow rate.

The exit diameter of the subsonic nozzle was 1.2 cm and was designed for the representative, average flow Mach number of a desending rocket-borne probe, $M_n = 0.3$. The nozzle was machined from plexiglass and polished smooth. The entrance of the nozzle was 3.18 cm diameter. The subsonic nozzle was found to produce the expected flow field and core region; this is further considered in section 4.2. The nozzle profile is shown in Figure 2.5A.

An exit diameter of 6 mm for the supersonic nozzle was designed to produce a representative, average Mach number, $M_n = 2$. The throat diameter was 4.3 mm. The supersonic nozzle was also machined from plexiglass and polished smooth. It was designed with a conical diverging section with a half angle of 10 degrees. The supersonic nozzle is shown in Figure 2.5B. The impact pressure profiles from the subsonic and supersonic nozzles will be discussed in Chapter IV.

The external design of the nozzles permitted each to be interchanged easily for a specific test run. The nozzles were attached through the nozzle plate which was fastened to the glow discharge chamber.

2.2.4 Low Temperature Plasma Sources

Several electrical heating methods were tested before the glow discharge techniques was accepted as the optimum plasma source for low temperature and low number density plasma of ionosphere interest. The
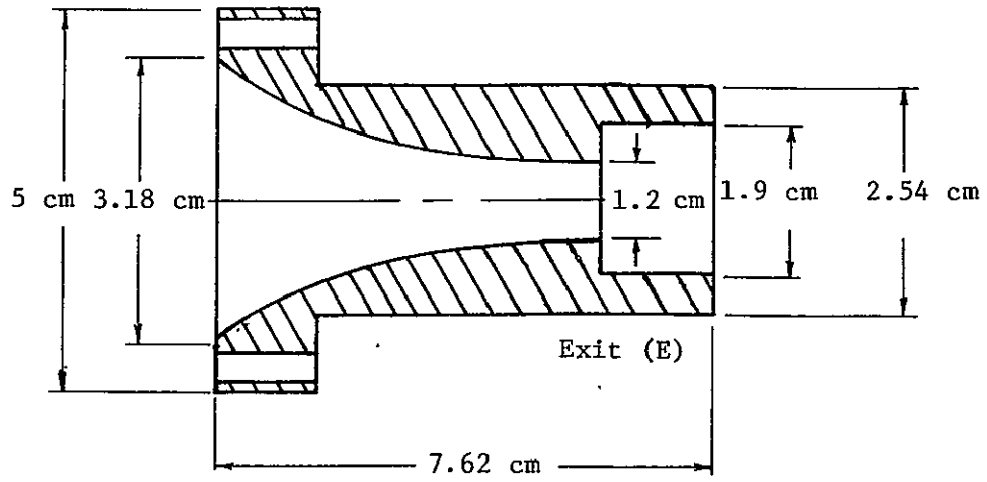
(A) Subsonic
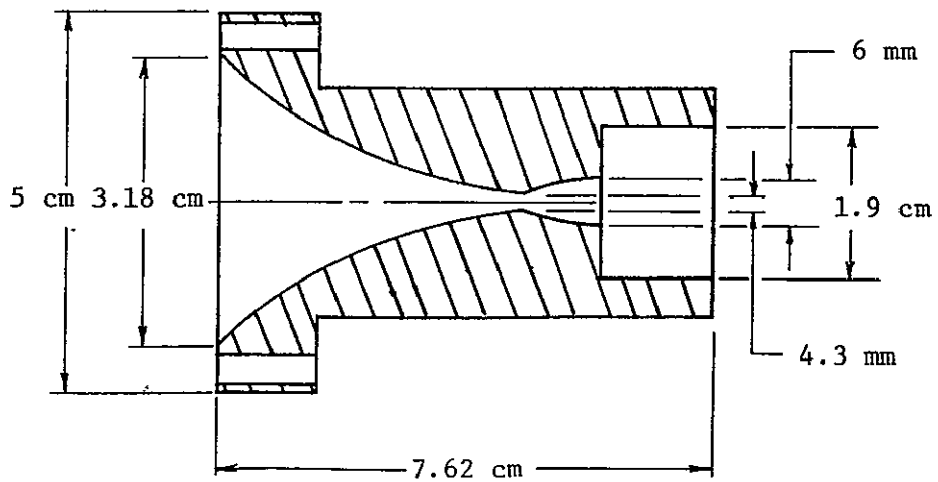
(B) Supersonic

Figure 2.5 Flow Nozzles

tests were conducted in the subsonic flow configuration. A double

Langmuir probe with 0.25 mm diameter tungsten filaments, discussed in

section 3.2, was used as the basic diagnostic tool for determining the

order of magnitude of the electron density and temperature in the

source plasma.

With simple, plane electrodes, shown in Figure 2.6A, and using a

5 mA discharge current, the electron temperature and number density range

were established to be on the order of 10^5°K and 10^7 cm^{-3}, respectively.

Electron temperatures and number densities were determined for various

values of discharge current by the logarithmic plot method described

by Johnson and Malter (25). A first variation examined the effects due

to an increase of the glow discharge current. By increasing the dis-

charge current from 5 mA to 30 mA, the order of magnitude of the

electron temperature decreased from 10^5°K to 10^4°K while the order of

the electron density increased from 10^7 cm^{-3} to 10^8 cm^{-3}. Persson (26),

and Bunting and Heikkila (27) have used discharge currents of 28 mA to

achieve electron temperatures on the order of 10^2°K. As a result of

their findings and the tests conducted, a discharge current of 28 mA

was chosen as the working glow discharge current. One and two cathode

systems were also compared. This arrangement of the cathode-anode

systems is also shown in Figure 2.6. The indicated electron tempera-

tures were found to be lower for the one cathode - one anode system.

The second variation evaluated the effects of a point anode and

plane cathode configuration, as shown in Figure 2.7. The glow dis-

charge is maintained by the flow of electrons emitted by the cathode

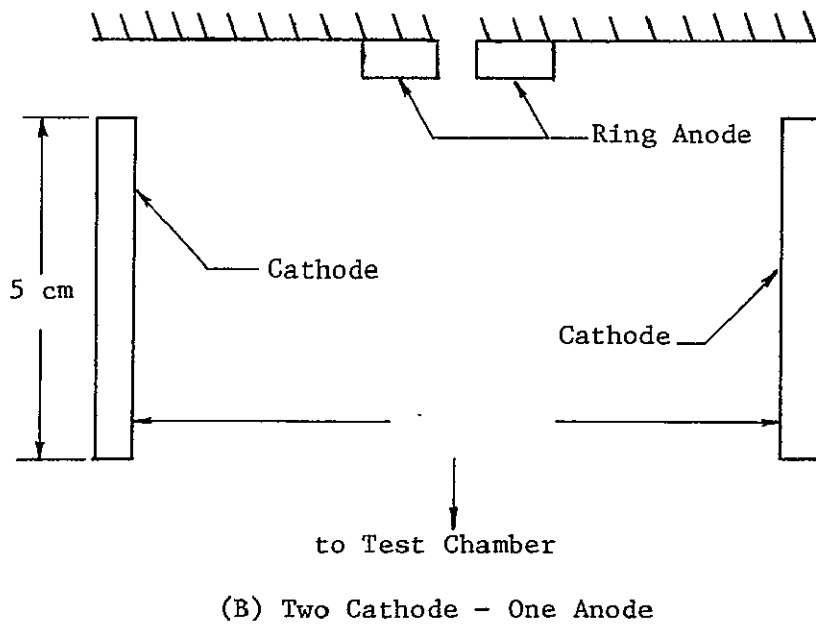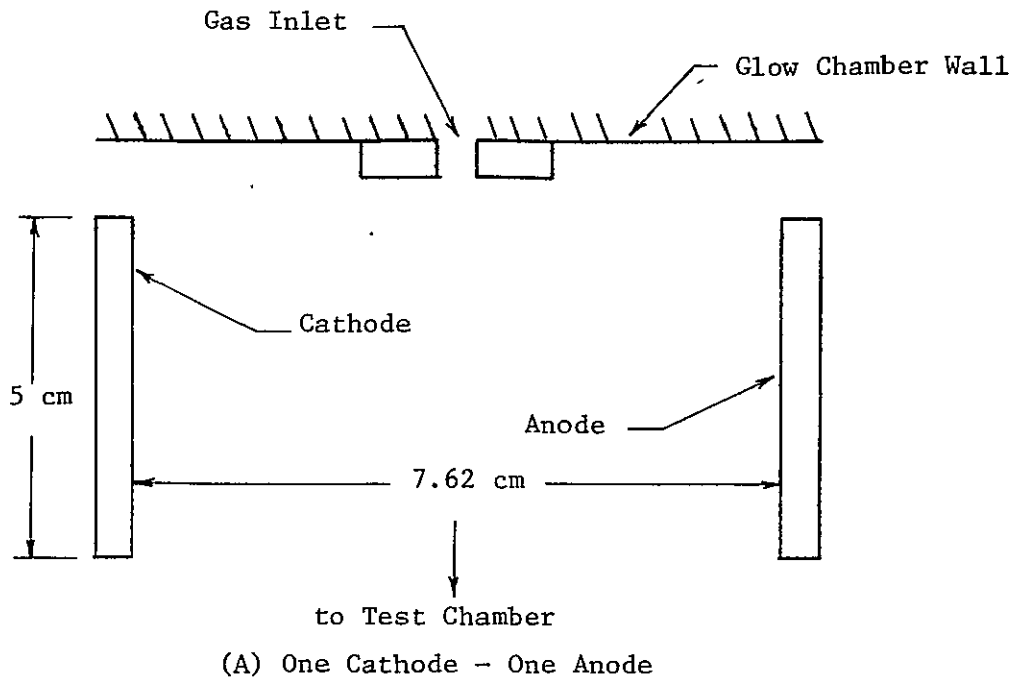upon bombardment by ions from the anode. The point anode discharge
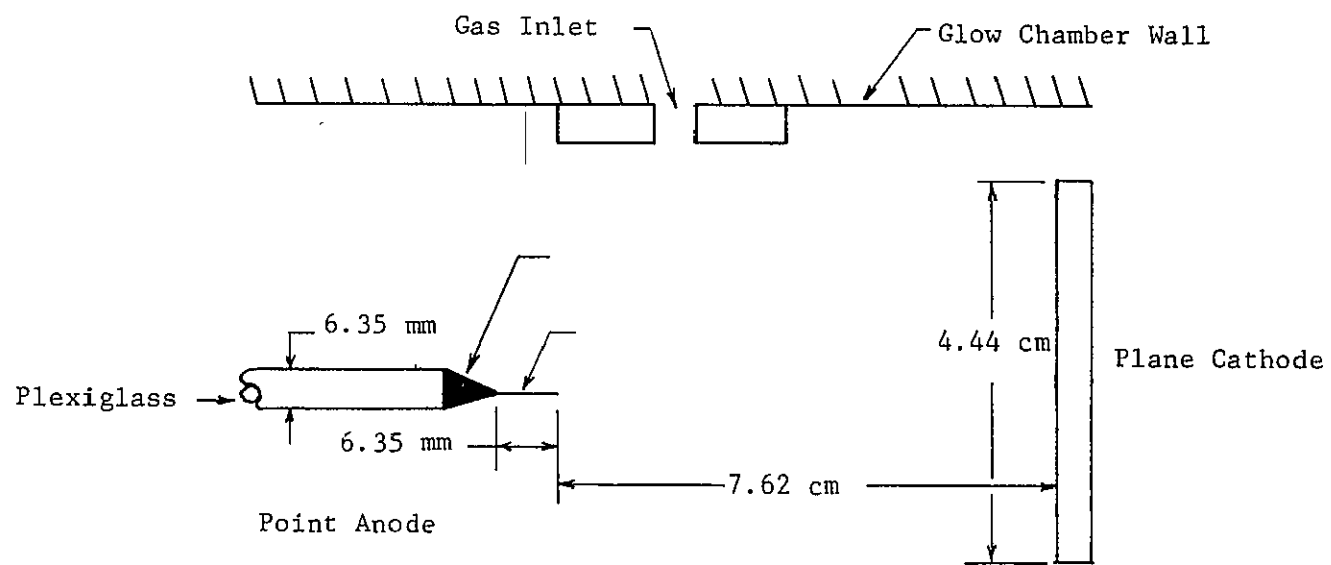
Figure 2.6 Glow Discharge System

Figure 2.7 Point Anode Discharge System

system was developed to minimize the ion bombardment at the cathode for a given discharge current. The anode was constructed from tungsten wire, 0.25 mm in diameter and 6.35 mm long. The cathode was machined from aluminum stock. It was 4.44 cm in diameter and 6.35 mm thick. The electrodes were separated by a 7.62 cm gap. The resulting electron temperature was found to be on the order of 10^4°K.

A ring cathode and ring anode configuration was also tested to determine if the electron temperature of the ionized flow could be reduced by permitting the plasma to flow through the cathode. The aluminum cathode with a hole through the axis was located at the entrance of the nozzle. A brass anode was located opposite the cathode; this is shown in Figure 2.8. Electron temperatures of order 10^4°K were obtained.

Because the electron temperatures were being reduced by only one order of magnitude by these previously described techniques, alternative methods of producing a cool, weak plasma were considered. A resistance heating technique (28) and a non-self-sustaining discharge technique (34) were tried in an attempt to produce a low temperature plasma of order 10^2°K.

Resistance heating is characterized by large currents (3-5 A) through a separate filament circuit and small voltages (6V). Three variations of this technique were tested. The configurations are shown in Figure 2.9. The first variation utilized a coiled tungsten wire filament, 0.25 mm in diameter. The coil was 6.35 mm in diameter and 7.62 cm long (30.5 cm uncoiled). The second variation utilized a straight piece of tungsten wire, 0.25 mm in diameter and 7.62 cm long.

Glow Chamber
Wall

Gas Inlet

Ring Anode (Brass)

7.62 cm

Ring Cathode (Aluminum)

Glow Chamber Wall

Subsonic Nozzle
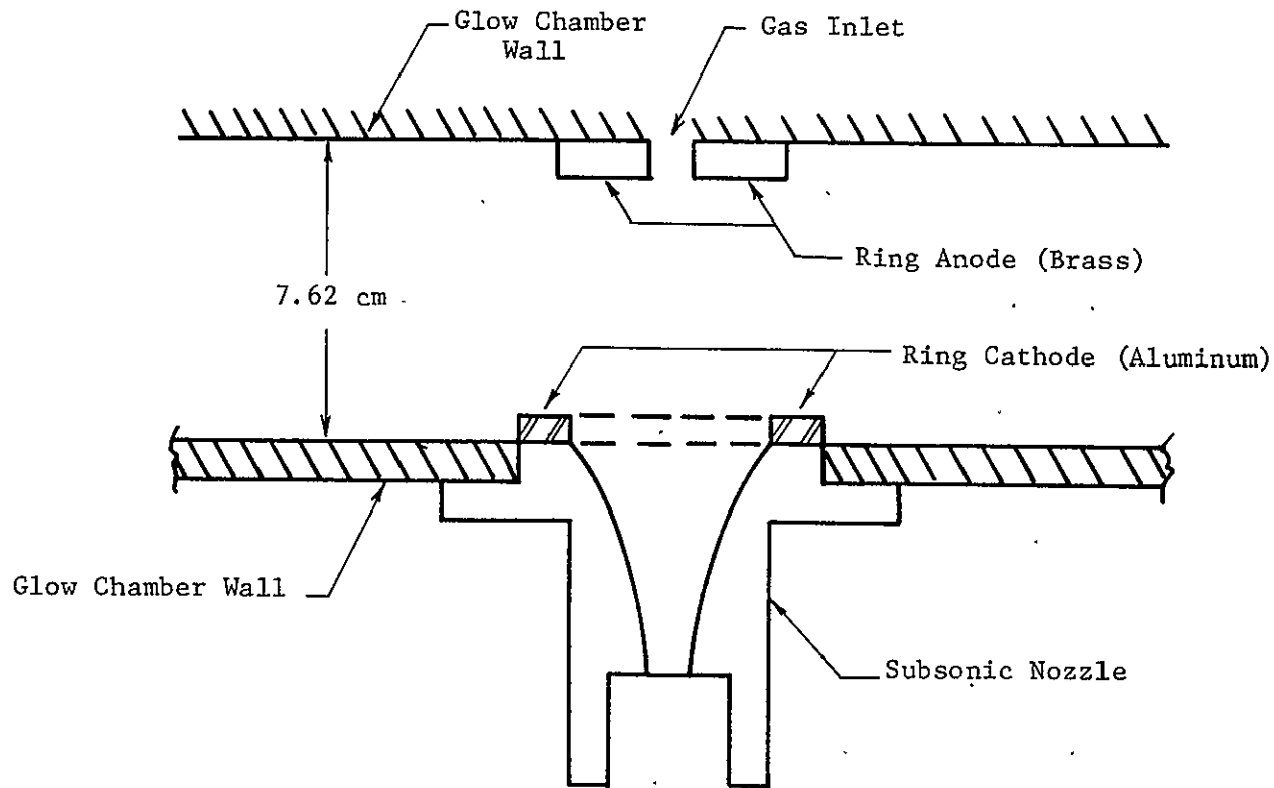
Figure 2.8   Ring Anode and Cathode Discharge System

Coiled Tungsten Wire, 0.25 mm Dia.

— 6.35 mm Dia., 7.62 cm Long

— 0.25 mm Dia. Tungsten Wire, 7.62 cm Long
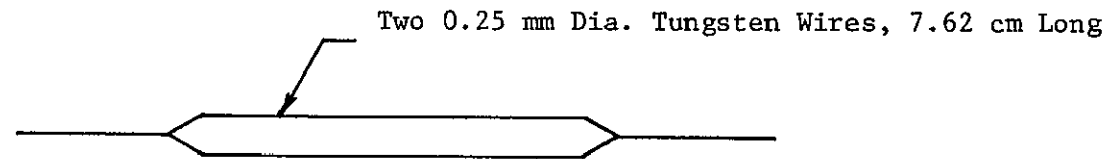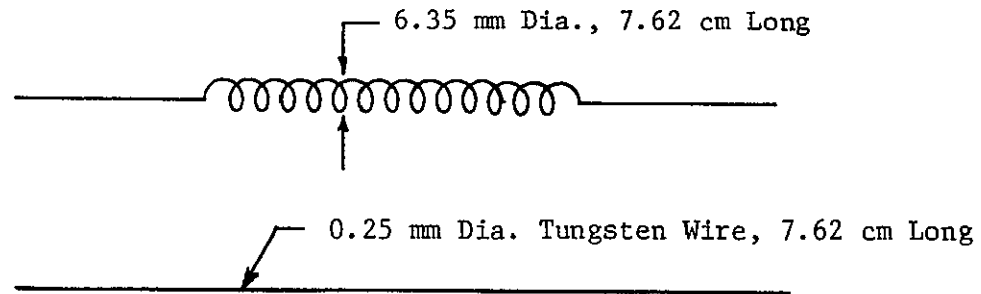
Two 0.25 mm Dia. Tungsten Wires, 7.62 cm Long

Figure 2.9 Resistance Heating Filaments

The third variation consisted of two pieces of 0.25 mm diameter tungsten wire, also 7.62 cm long. Each of these filaments broke when the necessary current level was maintained for extended periods of time ($\simeq 15$ min.), and current saturation as indicated by the Langmuir probe was not achieved. This appears to be explainable, as the applied current to the filaments constantly "boiled" off electrons; so as the applied positive probe potential was increased, electrons were continually drawn to the probe and therefore, the saturation level of the probe continually increased. To eliminate this effect the non-self-sustaining discharge was tested. This discharge is characterized by the emittance of electrons due to irradiation (24). For a specific operating voltage, all of the electrons emitted by the cathode are drawn to the anode. Increasing the voltage beyond this operating point does not result in further emittance. As the positive probe potential is increased, it draws electrons from a limited source and therefore, for a continual increase in probe potential a saturation level should be reached.

Figure 2.10 shows the two variations of the non-self-sustaining discharge technique that were tried. The first utilized a single loop of tungsten wire, 0.25 mm in diameter and 1.9 cm long as an ionization source for a high voltage anode. The second variation used the heater filament from a power pentode 6BK5 (29), and a high voltage anode. Both of these filaments also broke when the current was maintained for a continuous heating period of approximately 15 minutes, but current saturation could still not be achieved.

Since the resistance heating and non-self-sustaining discharge techniques did not reduce the magnitude of the electron temperature, a

Glow Chamber Wall   Gas Inlet

Single Coil
Tungsten Wire
0.25 mm Dia.

1.9 cm

Plane Anode

7.62 cm

5 cm

(A) Plane Anode and Coiled Tungsten Filament

6BK5 Pentode
Heater Filiment

Plane Anode
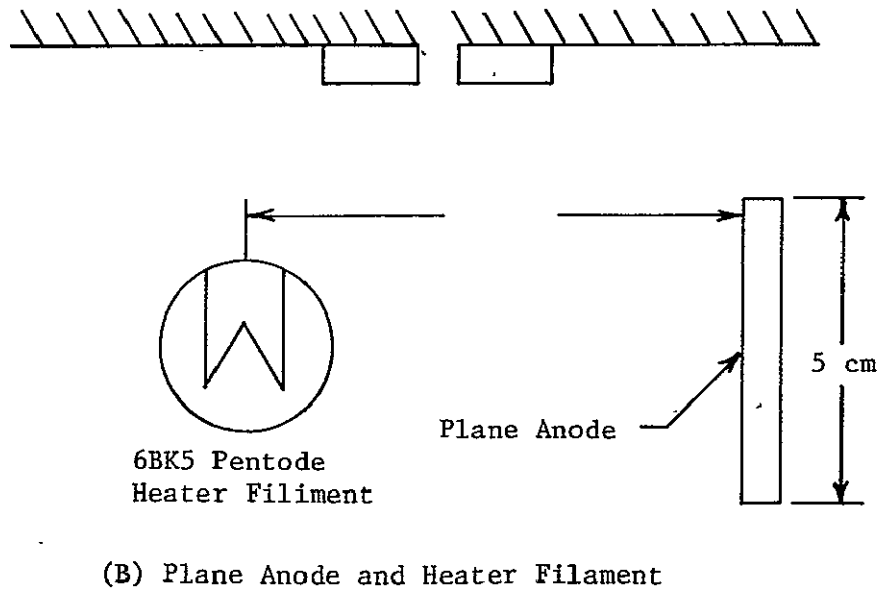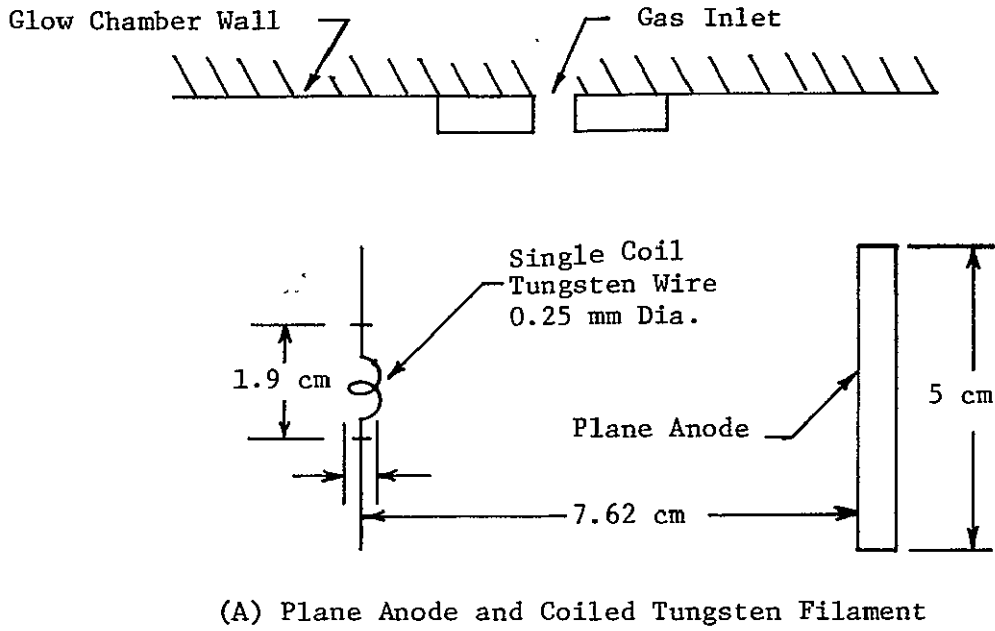
5 cm

(B) Plane Anode and Heater Filament

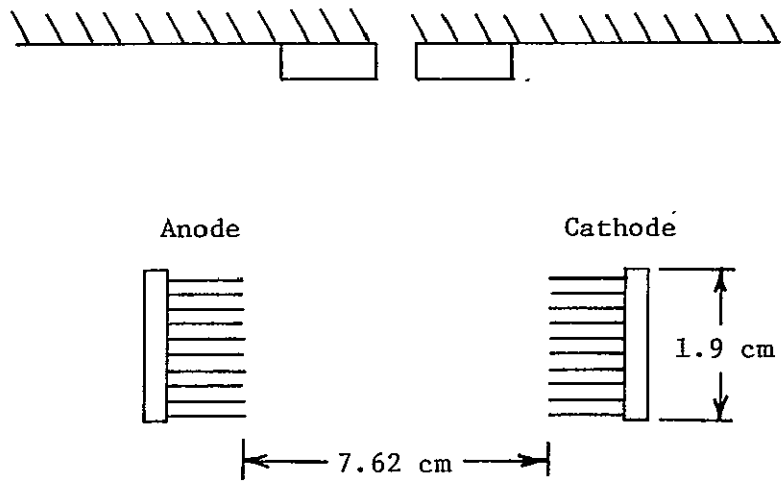Figure 2.10   Non-Self-Sustaining Discharge Systems

brush electrode system (26) was designed in an attempt to achieve current saturation and a lower electron temperature. Brush electrodes are known for producing a well defined negative glow with electron temperatures on the order of 10^2°K (26). One brush anode - one brush cathode, and two brush cathodes - one ring anode arrangements were tested. These configurations are shown in Figure 2.11. The brush electrodes were constructed from 0.25 mm diameter tungsten wire filaments, 1.6 cm long. Each brush electrode consisted of 50 tungsten filaments which were epoxied to a stainless steel base plate, 1.9 cm in diameter. A negative glow was obtained, extending out about three cathode diameters from each cathode, but the discharge was erratic and oscillatory. Because of the unstable nature of the discharge, current measurements could not be taken and the technique was abandoned.

The flow heating experiment was returned to the original glow discharge configuration but with an alteration to smaller electrodes insulated on all but the forward facing surfaces. The electrodes were reduced to a 2.5 cm diameter. They were insulated with a 2.3 mm layer of epoxy everywhere but their front surface and covered with plexiglass tubing, as shown in Figure 2.12A. The plexiglass was used to confine the plasma. The resulting discharge was stable but still produced electron temperatures of order 10^4°K.

A further variation of this configuration was made by using a 2.5 cm diameter cathode and a 4.67 mm diameter anode. Both electrodes were machined from aluminum stock. These electrodes were separated by a 2.5 cm gap.

Glow Chamber Wall ⌐   ⌐ Gas Inlet

Ring Anode

1.9 cm

Cathode |◄──── 7.62 cm ────►| Cathode
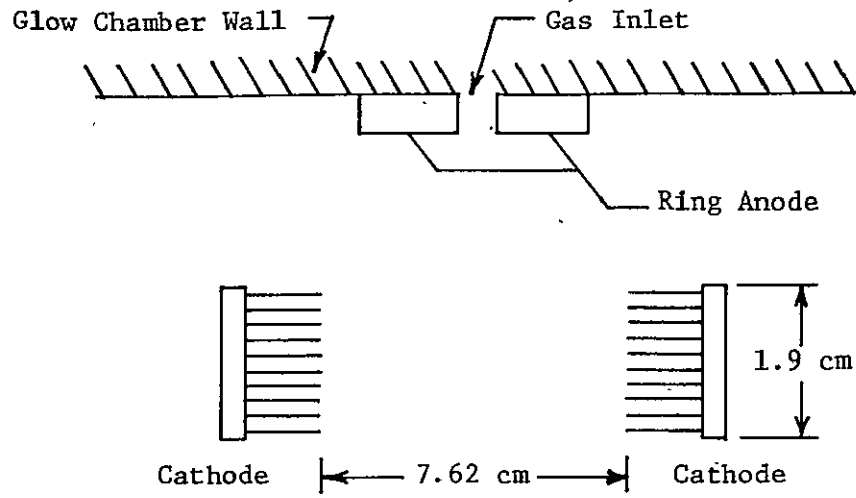
(A) Two Brush Cathode - One Ring Anode

Anode   Cathode

1.9 cm

|◄──── 7.62 cm ────►|

(B) One Brush Anode - One Brush Cathode

Figure 2.11   Brush Electrode Systems

Glow Chamber Wall ⎤   ⎡─Gas Inlet

2.5 cm ── 2.5 cm

2.3 mm Epoxy

2.5 cm

3.65 cm

7.62 cm

Anode   └─ 3.18 mm   .Cathode
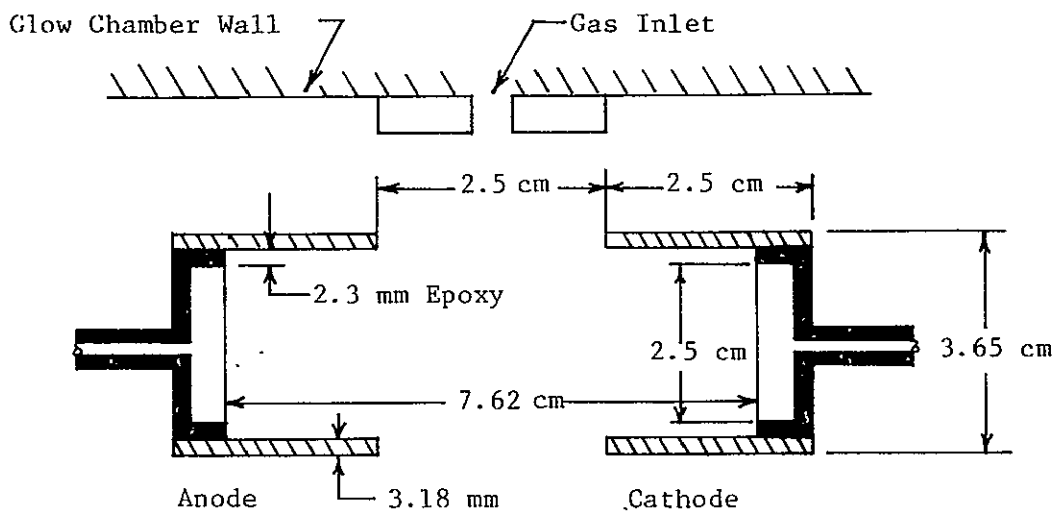
(A) Small, Insulated Electrodes

4.6 mm Dia.

2.5 cm Cathode

6.35 mm ─┘ Anode   2.5 cm

3 Phase Baffle

Glow Chamber Wall ──┐

Subsonic Nozzle
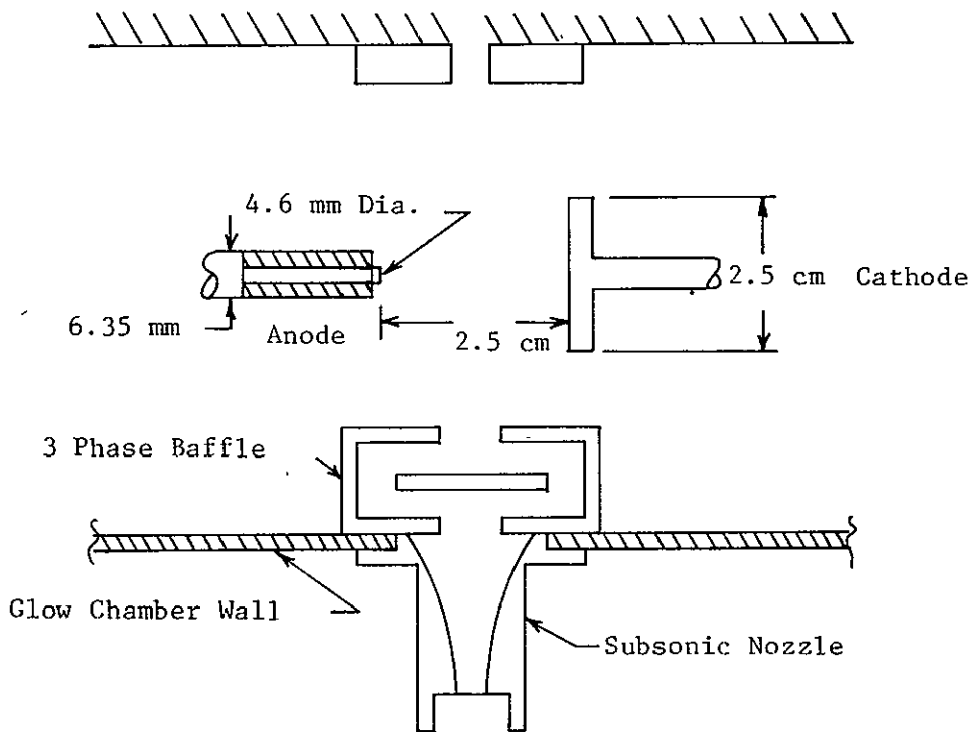
(B) Small Electrodes with Three Phase Baffle

Figure 2.12   Glow Discharge Systems

A basic difficulty arose when the Langmuir probe was grounded in any way. The ground caused the glow discharge to form between the anode and probe, this increasing the conducted current by 1 mA and distorting the local plasma properties. To prevent this the probe bias was made to float with the plasma as reference by employing DC battery operated power supplies.

In order to further reduce the temperature and density, this discharge system was operated in conjunction with a baffle system, shown in Figure 2.12B. The baffle system was positioned at the entrance of the nozzle; two and three phase baffles were used. The baffles also helped prevent the probe from being an active part of the glow circuit and helped suppress the electron concentration and temperature values. With the addition of the baffle system, the current levels sensed by the probes in the jet were reduced from 10^{-6}A to 10^{-9}A. The resulting electron temperatures were found to be on the order of 10^{2}°K. The electron number densities indicated in the jet varied from 10^{1} cm^{-3} to 10^{4} cm^{-3}; depending on the operating pressure. As a result of the achievement of satisfactory test conditions, this electrode configuration and baffle system were used for the production and control of the low temperature laboratory plasma.

2.3 Experimental Conditions

The simulation of D-region probe flows as discussed above, required some properties to be scaled by two orders of magnitude. With these scaled values, the test conditions in the experimental configuration were determined. With the introduction of baffles and different electrode geometries discussed above, the production of an appropriate

plasma was achieved. However, the available pumping apparatus for this experimental work did prove to limit the altitudes which the modeled flow could simulate.

Table 2 presents the scaled experimental conditions for the D-region. The table lists the test conditions for all of the altitudes of interest in the D-region (40 km to 90 km). It includes parameters for the glow discharge chamber and test chamber, specifically: the mass flow rates, $\dot{m}$, static and stagnation pressures, P_E, P_o, densities, ρ_E, and the baffle and electrode configurations.

The required mass flow rates for the steady state flow configuration were determined from the specified volume flow rate; the volume flow rate is characteristic of the pumping system. The two Welch 1397B vacuum pumps each has a volume flow rate of $8.5 \times 10^{-3} \text{ m}^3\text{sec}^{-1}$. Their combined volume flow rates were reduced in the calculations by 30 percent to account for mechanical and flow losses. With an effective volume flow rate of $1.18 \times 10^{-2} \text{ m}^3\text{sec}^{-1}$, the D-region probe flows that could be simulated were at altitudes to 70 km, 80 km, and '90 km.

The electron number densities and temperatures were controlled by the baffle system; two and three phase baffles were used and are shown in Figure 2.13. The baffles were machined from plexiglass and positioned at the entrance of the nozzle. In the subsonic flow configuration the two phase baffle was used at the 70 km and 80 km altitudes. The three phase baffle was employed for the 90 km altitude. In the supersonic flow configuration, no baffles were required to control the temperature or densities of the plasma.

Table 2: Scaled Experimental Conditions

| M_n	ALT (km)	$\dot{m}$ (g sec^{-1})	ρ_E (g cm^{-3})	P_o (Glow) (Torr)	P_E (Torr)	Electrode Configuration	Baffle Configuration
0.3	40	3.90	1.30×10^{-3}	1.89×10^2	1.78×10^2	Not Tested	Not Tested
	50	1.08	3.68×10^{-4}	5.25×10^1	4.95×10^1	Not Tested	Not Tested
	60	3.10×10^{-1}	9.20×10^{-5}	1.81×10^1	1.42×10^1	Not Tested	Not Tested
	70	8.75×10^{-2}	2.14×10^{-5}	4.14	3.89	Lg. Anode	2 - Phase
	80	1.76×10^{-2}	4.32×10^{-6}	8.54×10^{-1}	8.00×10^{-1}	Sm. Anode	2 - Phase
	90	3.68×10^{-3}	7.50×10^{-7}	1.68×10^{-1}	1.58×10^{-1}	Sm. Anode	3 - Phase
2.0	40	3.90	2.36×10^{-3}	7.88×10^2	1.00×10^2	Not Tested	Not Tested
	50	1.08	6.50×10^{-4}	2.19×10^2	2.80×10^1	Not Tested	Not Tested
	60	3.10×10^{-1}	1.60×10^{-4}	6.25×10^1	7.85	Not Tested	Not Tested
	70	8.75×10^{-2}	3.78×10^{-5}	1.75×10^1	2.25	Lg. Anode	No Baffle
	80	1.76×10^{-2}	7.35×10^{-6}	3.54	4.55×10^{-1}	Sm. Anode	No Baffle
	90	3.68×10^{-3}	1.33×10^{-6}	7.24×10^{-1}	9.30×10^{-2}	Sm. Anode	No Baffle

Table 2: Scaled Experimental Conditions (continued)

M_n	ALT (km)	n_n (cm^{-3}) Glow	λ_{e-n} (cm) Glow	λ_{n-n} (cm) Glow	n_n (cm^{-3}) Exit	λ_{e-n} (cm) Exit	λ_{n-n} (cm) Exit
0.3	40	7.5×10^{18}	7.65×10^{-4}	3.06×10^{-5}	7.2×10^{18}	8.0×10^{-4}	3.2×10^{-5}
	50	2.09×10^{18}	3.06×10^{-3}	7.84×10^{-5}	2.0×10^{18}	3.2×10^{-3}	8.2×10^{-5}
	60	5.95×10^{17}	1.14×10^{-2}	2.3×10^{-4}	5.7×10^{17}	1.2×10^{-2}	2.4×10^{-4}
	70	1.68×10^{17}	4.01×10^{-2}	7.84×10^{-4}	1.61×10^{17}	4.2×10^{-2}	8.2×10^{-4}
	80	3.38×10^{16}	1.9×10^{-1}	5.35×10^{-3}	3.24×10^{16}	2.0×10^{-1}	5.6×10^{-3}
	90	6.68×10^{15}	8.6×10^{-1}	1.9×10^{-2}	6.4×10^{15}	9.0×10^{-1}	2.0×10^{-2}
2.0	40	7.5×10^{18}	7.65×10^{-4}	3.06×10^{-5}	1.47×10^{18}	3.9×10^{-3}	1.56×10^{-4}
	50	2.09×10^{18}	3.06×10^{-3}	7.84×10^{-5}	4.1×10^{17}	1.56×10^{-2}	4.0×10^{-4}
	60	5.95×10^{17}	1.14×10^{-2}	2.3×10^{-4}	1.16×10^{17}	5.8×10^{-2}	1.17×10^{-3}
	70	1.68×10^{17}	4.01×10^{-2}	7.84×10^{-4}	3.24×10^{16}	5.8×10^{-2}	4.0×10^{-3}
	80	3.38×10^{16}	1.9×10^{-1}	5.35×10^{-3}	6.6×10^{15}	2.0×10^{-1}	2.7×10^{-2}
	90	6.68×10^{15}	8.6×10^{-1}	1.9×10^{-2}	1.3×10^{15}	9.69×10^{-1}	9.69×10^{-1}
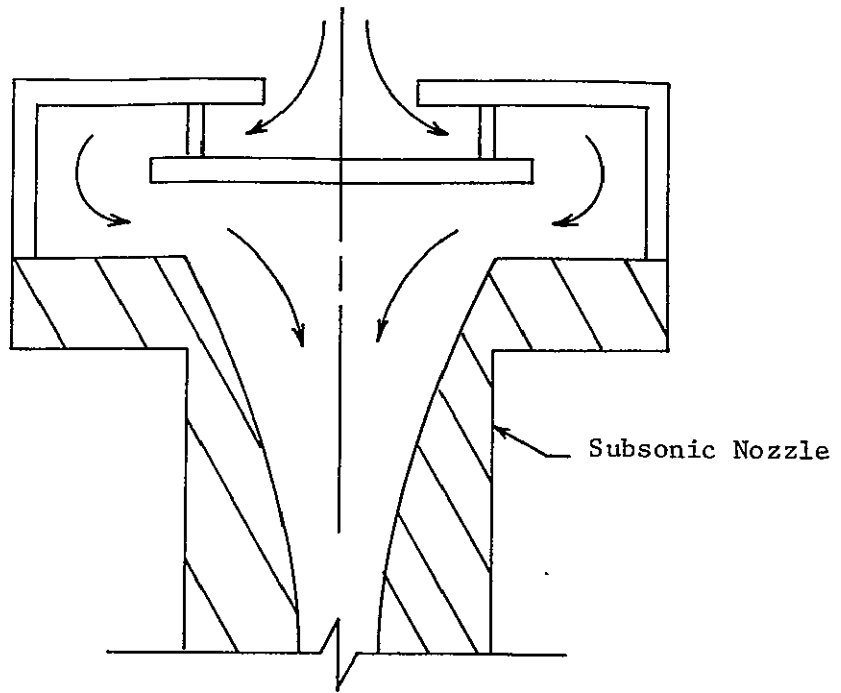
(A) Two Phase Baffle
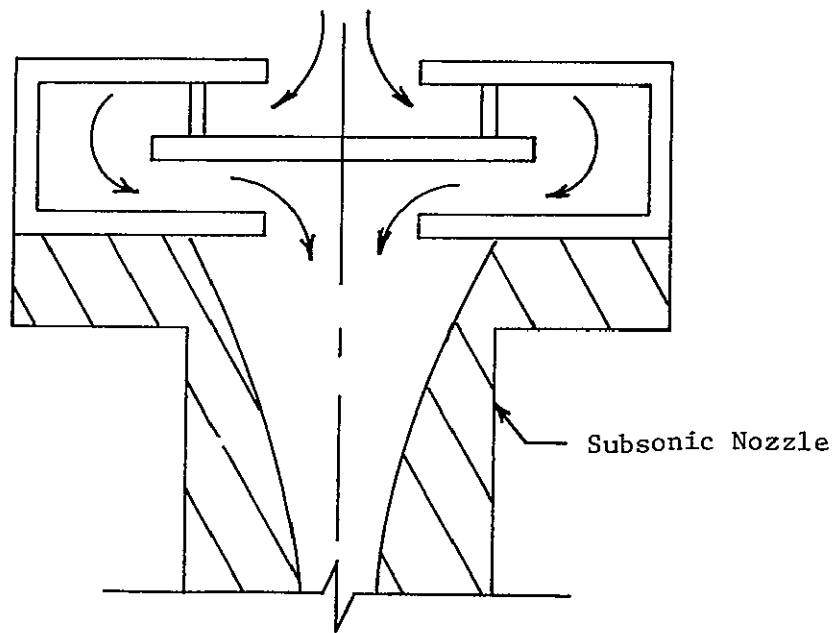

(B) Three Phase Baffle

Figure 2.13 Baffle Systems

The electrode configurations used for the production of the scaled plasma are shown in Figure 2.14. At the 80 km and 90 km altitudes the electrode configuration consisted of the 4.76 mm diameter anode and the 2.5 cm diameter cathode. The electrodes were separated by a 2.5 cm gap. At the 70 km altitude, 2.5 cm diameter electrodes were used, also separated by a 2.5 cm gap. Since the amount of source ionization is reduced by the higher chamber pressure, the larger anode was employed at the 70 km altitude to increase the order of magnitude of the electron number density, and accordingly reduce the magnitude of the Debye length.

2.4 Baffle System Effect on the Recombination Process

The electron concentration at the exit plane of the nozzle was controlled by the baffle system, as the baffles lengthened the path of plasma travel from the source and increased the flow time, thus allowing the recombination process to progress. The electron loss mechanisms involve diffusion to the walls and recombination. For purposes of analysis, it is here assumed that the plasma is recombination – controlled from the source condition in the discharge chamber. The diffusion to the walls, followed by surface neutralization, is presumed to be a negligible loss mechanism on the basis of surface to volume estimates. The resultant electron density at the exit plane of the nozzle will then be accounted for by an effective, average recombination coefficient (30).

First, for the ionization processes, it can be shown that the gas flow in the discharge chamber remained long enough to achieve equilibrium with the entire volume of plasma before entering the baffle
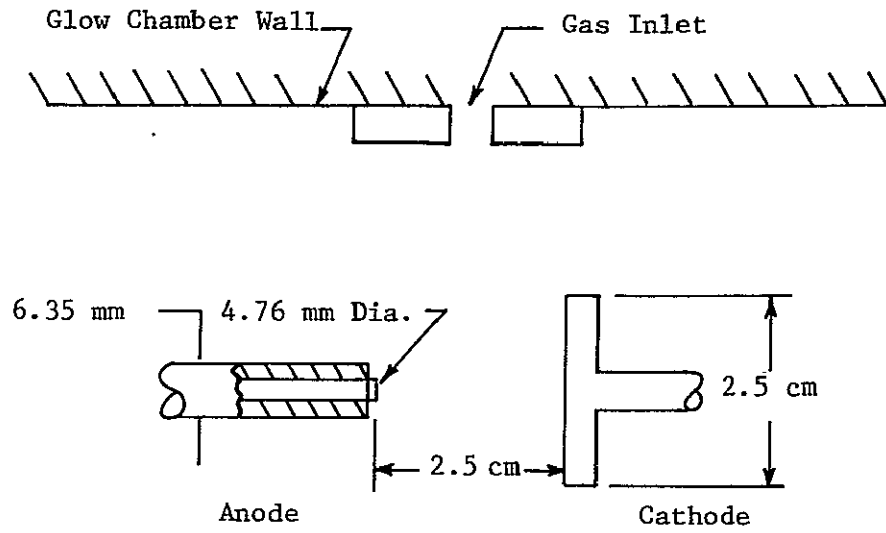
(A) Electrodes for 80 km and 90 km Altitudes
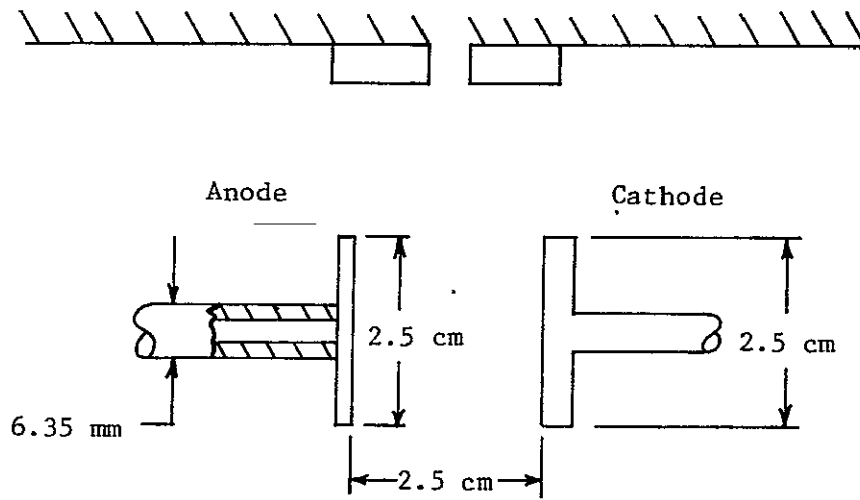
(B) Electrodes for 70 km Altitudes

Figure 2.14   Glow Discharge Test Configurations

system. The time required for ionization of the gas entering the discharge chamber can be expressed as the inverse of the electron-neutral collision frequency, as

$$t \doteq \frac{1}{n\sigma\bar{c}}$$

where n is the neutral particle density, σ is the cross section for ionization, and $\bar{c}$ is the mean (thermal) velocity of the electrons. Taking a lower limit on density at 10^{16} cm^{-3}, $\sigma \simeq 10^{-15}$ for electron-nitrogen ionization at 1 eV (30) and $\bar{c} = 7 \times 10^{7}$ cm sec^{-1} at 1 eV, a value of $t = 10^{-7}$ sec is indicated. Clearly, the cold gas input to the discharge chamber will quickly reach equilibrium with the local plasma. Second, for the recombination, the baffles increased the path of the flow without increasing the velocity. The gas in the discharge chamber flows at 6.1 cm sec^{-1} in the subsonic case and at 16.8 cm sec^{-1} in the supersonic case; these velocities were taken as average, constants through the baffle system. The time for the flow through the nozzles was on the order of 10^{-3} sec. The time for the flow through the discharge chamber and baffles was about 6 sec for the subsonic case and about 2 sec for the supersonic case. These relatively long times in the steady state flow system allowed recombination to proceed to a limiting state. The electron density recombination in the test flow will be further discussed in section 5.4.2, relative to specific data.

CHAPTER III

DIAGNOSTIC DEVICES

3.1 Impact Pressure Probe

An impact pressure probe (21) was used to determine the properties of the flow field in the test jet. The nature of the response from an impact pressure probe depends on its design. There are three basic types of response errors that arise with an impact pressure probe, which can be minimized by a carefully designed probe; these will now be considered.

The first error is related to the ratio of probe diameter to discharge jet diameter. This ratio should be made small so that the probe measures localized impact pressure. The impact probe employed here was designed with a diameter that was only 2 percent of the subsonic jet diameter and 4 percent of the supersonic jet diameter, thus minimizing the extent error.

The second error is related to the ratio of probe length to probe diameter. When slip or transitional flow conditions exist within the probe, the boundary layer growth can affect the pressure response (31). The slip flow regime occurs for Knudsen numbers within the range $0.01 < K_n R_n^{-1/2} < 3$ (32). For the subsonic jet flow, a slip condition occured within the impact probe at the scaled 70 km and 80 km conditions. At the scaled 90 km condition, transitional flow occured within the probe. In the supersonic jet flow, transitional flow occured within the probe at the scaled 80 km and 90 km altitudes, while the slip flow condition occured at the scaled 70 km altitude. Rogers et al. (31)

point out that the length to diameter ratio should be larger than about 20 for the slip and transitional flow conditions so that the errors resulting from this geometry would be negligible. This impact pressure probe was designed with a length to diameter ratio of 32.

The third type of error is related to viscous effects due to the flow within the probe. The extent of viscous corrections to the impact pressure probe response depends on the specific flow conditions, as previously discussed. The viscous corrections could be minimized by designing a probe with an internal diameter which would allow the flow to attain the free molecular flow condition, $K_n R_n^{-1/2} > 3$ (32). This condition, however, was not reached by the flow within the probe. Viscous corrections required for the slip and transitional flow regimes were obtained by Eq. (4.2.1) for subsonic flow and by Eq. (4.3.1) for supersonic flow. It was found that the corrections were less than 2 percent for the subsonic flow case, while no viscous corrections were required in the supersonic flow configuration. The response from the impact probe will be further discussed in Chapter IV.

The impact pressure probe was designed so that the above errors in response would be minimal. It was constructed from 0.5 mm outside diameter, 0.25 mm inside diameter, stainless steel hypodermic tubing, 1.62 cm long. The hypodermic tubing was epoxied into a 6.35 mm outside diameter brass sleave. The brass sleeve was epoxied into a 6.35 mm outside diameter brass tube which was electrically insulated by pyrex tubing, 8 mm in diameter. The inlet (sensing) end of the probe had an external chamfer of 10 degrees. The length of hypodermic tubing extending from the brass sleeve to the chamfer tip is 8 mm. The probe

was connected to the Cole-Parmer and Granville-Phillips pressure measuring instruments through 6.35 mm outside diameter copper tubing. The impact pressure probe configuration is shown in Figure 3.1.

3.2   Langmuir Double Probe

The unique design of the Langmuir double probe (10) was developed to facilitate the removal and replacement of the electrode filaments. This alleviated the need to construct an entirely new probe when the filaments became contaminated by deposits from the discharge during each use.   The configuration is shown in Figure 3.2. The probe consisted of removable electrode filaments within a permanently epoxied housing; the filament used was made of tungsten wire, 0.25 mm in diameter.

The electrode filaments were mounted in 0.8 mm outside diameter, 0.4 mm inside diameter stainless steel hypodermic tubing. Each tube was filled with Hysol K16 conductive epoxy after which the tungsten filaments were inserted. Hysol 1C white epoxy was placed over the interface of the filament and stainless steel tubing forming a conical shape as it cured. The epoxy cone was 3 mm in length and 1.6 mm in diameter at its base.

The filament housing was formed from a Hysol 1C white epoxy mold. The mold was machined into a conical shape, 4.76 mm in diameter at the front and 8 mm in diameter at the base. Two stainless steel hypodermic tubes, 1.2 mm outside diameter and 1.6 cm long were placed through the center of the cone and epoxied in place. Each tube was insulated with two layers of Scotch No. 74 mylar tape, 0.05 mm thick. The hypodermic tubing was connected to RG 174 coaxial cable. The coaxial cable was
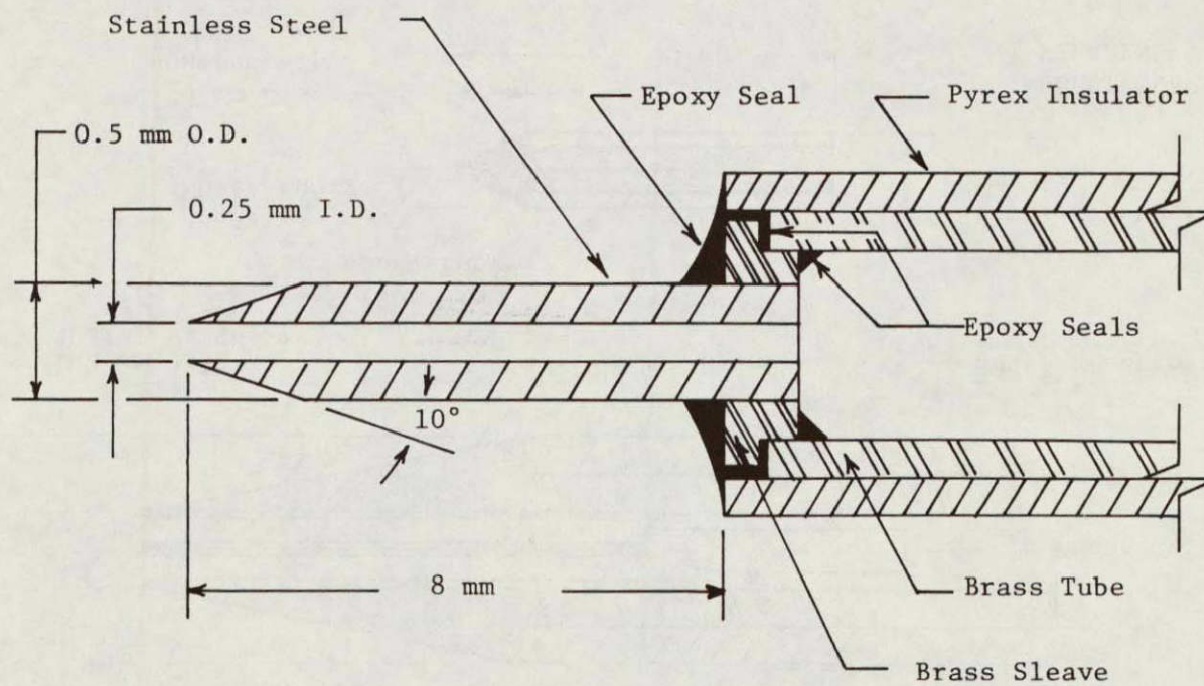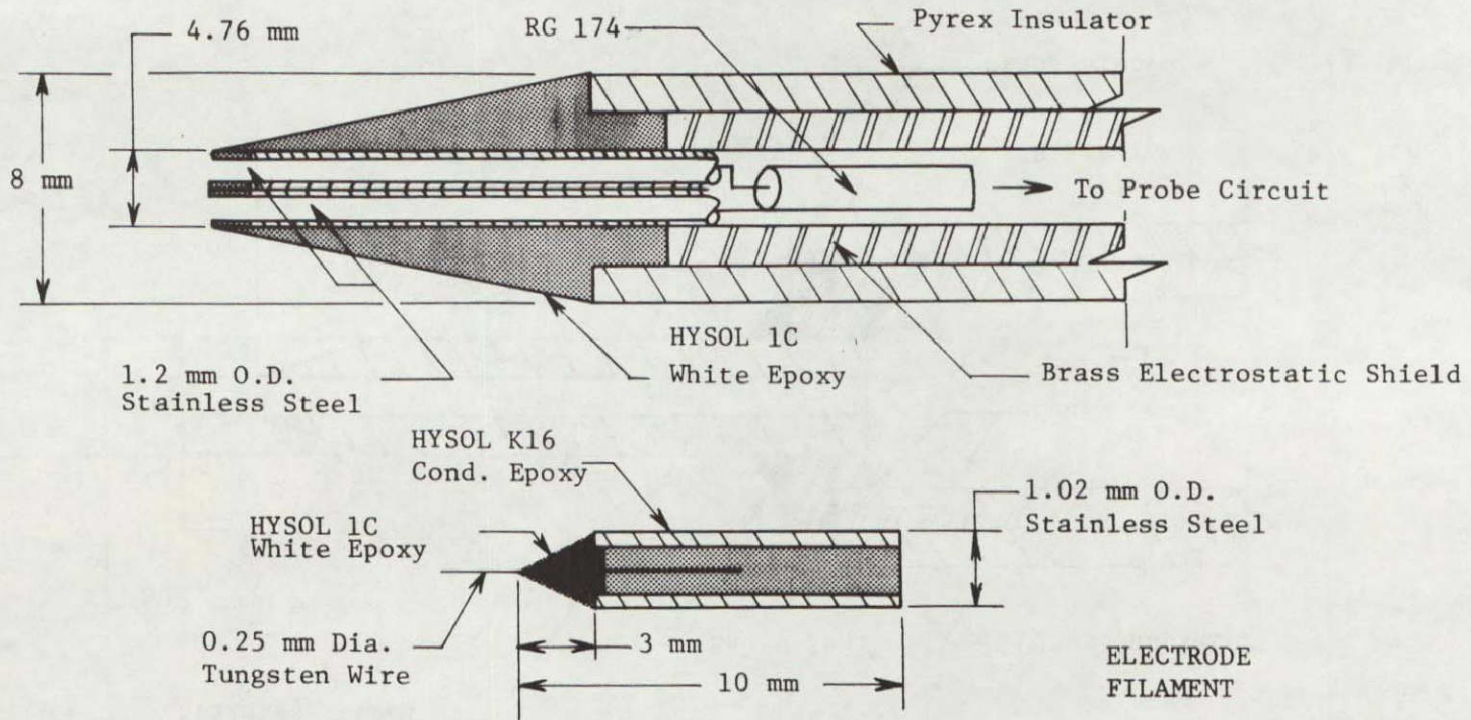
Figure 3.1   Impact Pressure Probe

HOUSING

Figure 3.2   Double Langmuir Probe

placed through a 6.35 mm outside diameter brass tube which acted as an electrostatic shield (33). An 8 mm outside diameter pyrex tube was fitted over the brass shield, insulating the unit. The pyrex and brass tubing was permanently epoxied to the filament housing, forming a vacuum seal. When the electrode filaments were inserted into the filament housing the separation distance between them was 2 mm. To minimize the end effects (7) in the plasma flow configuration, each tungsten filament was made 4 mm long.

Figure 3.3 shows the circuit used for the Langmuir probe. The circuit suggested by Johnson and Malter (25) permits the potential between the electrodes to float with respect to the plasma. The circuit used in this work consisted of a variable DC power supply, Keithley 602 electrometer and a Dynamics 501 millivoltmeter. The electrometer used for the recording of the current, and the millivoltmeter used for precise voltage settings, were both DC battery powered, allowing the system to float.

The current conducted by the probe will indicate the correct plasma parameters only when the potential difference between the electrodes is floating with the plasma as reference. When the reference is grounded, the glow discharge forms between the anode and probe, because the resistance between the probe and anode is less than between the cathode and anode. The grounded reference then causes the current to increase by 1 mA. This excessive current was found to clearly distort the plasma parameters being measured.

Before every test run it was found necessary to insure that the electrode filaments were carefully cleaned. This was done by first

To Probe

Variable DC Power
Supply

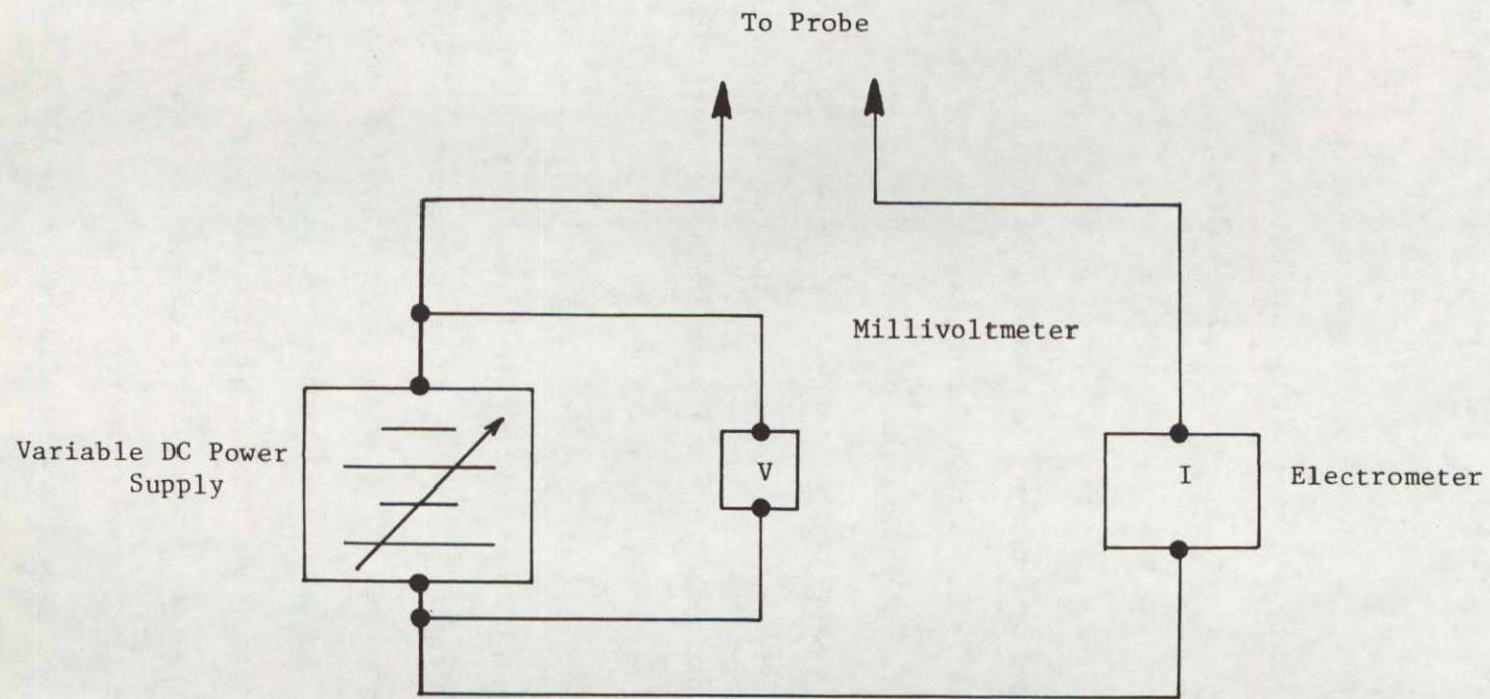Millivoltmeter

V

I   Electrometer

Figure 3.3   Circuit for Langmuir and Blunt Probes

flushing the filaments with acetone so as to insure that all dust and oil deposits had been removed. Second, after the probe was under vacuum at about 1 Torr, 10 mA of current was applied across the filaments for 15 sec intervals. This procedure was repeated until all spurious deposits were removed from the surface, as indicated by the soft-glow between the two filaments.

The cleanliness of the probe was important in influencing the quality and reproducibility of the current-voltage characteristic through the active collecting area of each filament (34). After every test run the electrode filaments were removed from the filament housing and replaced with new ones.

3.3 Scaled Rocket-Borne D-Region Electrostatic Blunt Probe

A scaled electrostatic blunt probe was designed and fabricated to simulate the rocket-borne D-region probes used by Hale (23). The blunt probe was scaled down by two orders of magnitude. It is shown in Figure 3.4A. The probe consisted of a 0.25 mm diameter tungsten wire with its end surface functioning as the collector disc. The wire was wrapped on its side with five layers of Scotch No. 74 mylar tape; this forms the insulator ring between the collector disc and guard ring. A 1 mm outside diameter, 0.75 mm inside diameter stainless steel hypodermic tube formed the guard ring for the probe. The guard ring was insulated with two layers of mylar tape leaving only the front end of the probe electrically conducting. The return electrode was formed by a 1.6 mm outside diameter, 1.35 mm inside diameter stainless steel hypodermic tube. The return electrode was 1 mm long and was positioned 3 mm from the front end of the probe. The collector disc,
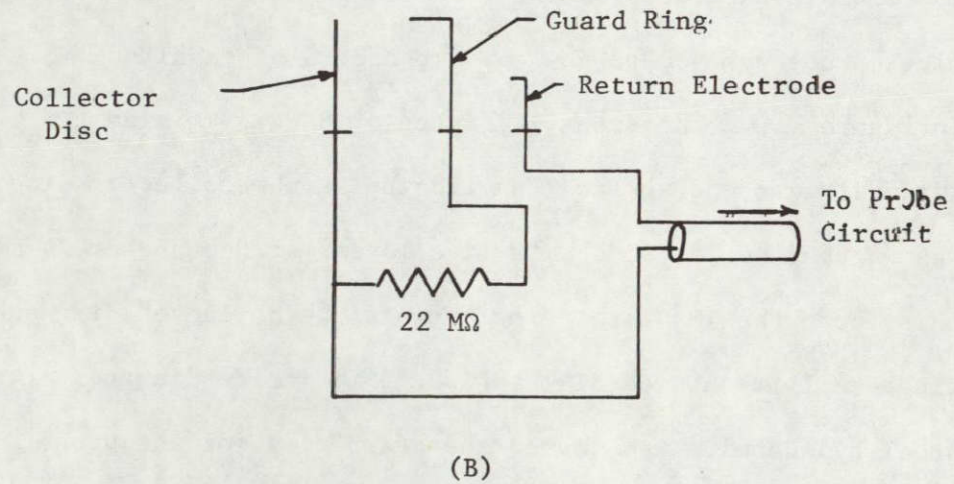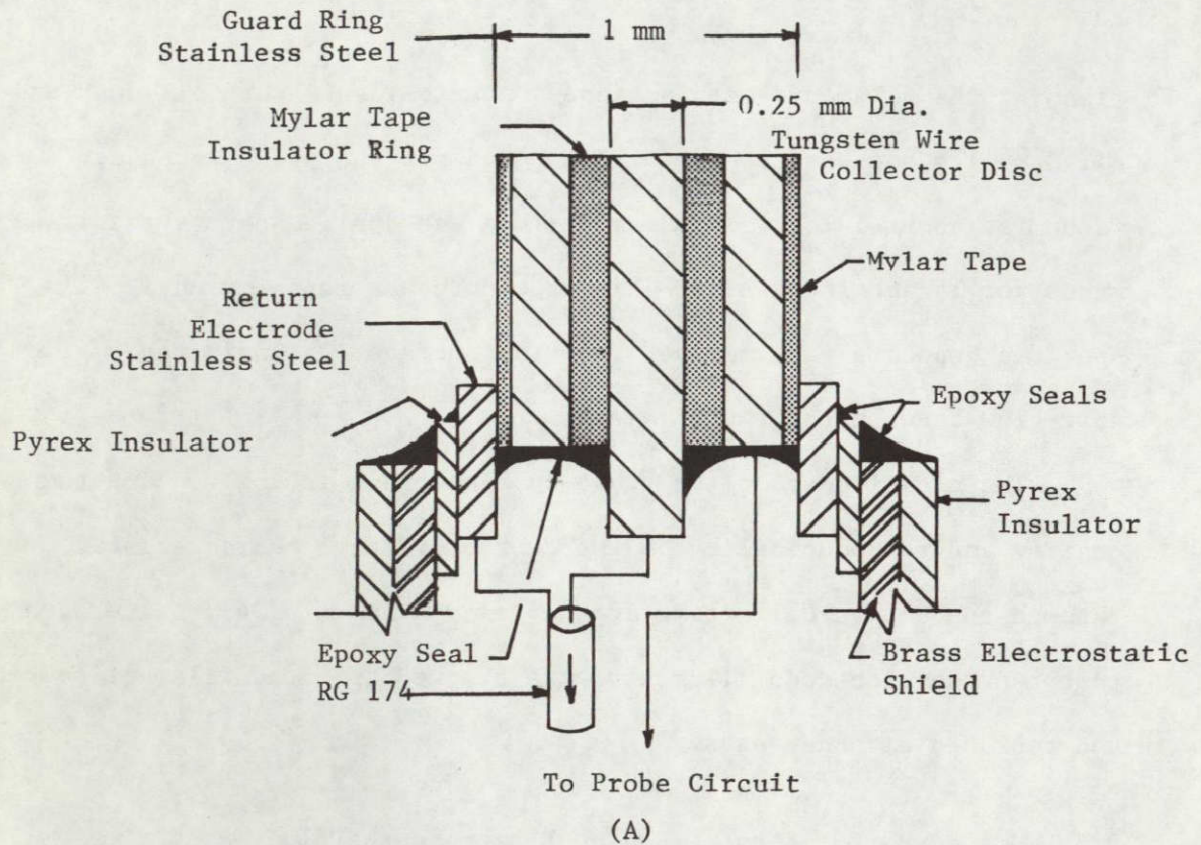
Figure 3.4   Blunt Prove System
(A) Blunt Probe   (B) Probe System Circuit

guard ring and return electrode were each connected to No. 24 copper wire which was insulated with heavy formvar. The copper leads from the guard ring and collector disc were connected to RG 174 coaxial cable. The copper wire from the return electrode formed the third lead in the circuit for the probe system. The coaxial cable and third lead passed through a 4 mm outside diameter brass electrostatic shield which was epoxied to a 2.4 mm outside diameter pyrex tube. This pyrex tube was epoxied to the return electrode forming a vacuum seal. The brass tubing was insulated with pyrex tubing which ran the length of the probe. The pyrex and brass tubing were epoxied together forming another vacuum seal.

Figure 3.4B shows the circuit for the blunt probe system. The collector disc was biased relative to the return electrode as in the Langmuir double-probe system. No current will be drawn through the guard ring due to the 22 MΩ resistor between the collector disc and guard ring. The guard ring will, however, assume the same potential as the collector disc. The floating circuit for the blunt probe is the same circuit used for the Langmuir probe.

The blunt probe was cleaned before every test run. The front end of the probe was first rubbed smooth with No. 500-A silicon carbide paper. Acetone and carbon tetrachloride were then used to clean the collector disc, guard ring, and return electrode.

CHAPTER IV

EXPERIMENTAL CHARACTERISTICS OF THE PLASMA JET TEST FLOW

4.1 Introduction

The test flow was produced by metering room temperature purified air through a choked orifice feed line into a glow discharge chamber which allowed passage through a nozzle into a low pressure test chamber. The gas pressure in the glow discharge chamber was adjusted to a value required to obtain the desired test conditions at the exit plane of the nozzle. The scaled D-region conditions therefore set glow and test chamber pressures, and both being related to the desired flow through the nozzles. The pressures in the test chamber were those corresponding to the scaled D-region values.

An impact pressure probe was used to identify the flow field properties in the test jet. The open-ended type of probe was employed because it is easy to construct and with proper design the viscous corrections would be less than 1 percent down to a Reynolds number of about 25 (21). The probe was initially positioned at the exit plane of each nozzle.

4.2 Subsonic Flow

The subsonic nozzle was designed to produce a Mach number on the order of 0.3. This condition represents the average descending velocity of a rocket-borne blunt probe (100 m sec^{-1}) through the D-region of the ionosphere.

The flow-field patterns from the nozzle were found to be characteristic of low density flow in a round, free jet (21). The flow at

the exit plane of the nozzle was found to be uniform and parallel. The mixing region of the jet was found to extend about four nozzle diameters downstream of the exit plane. Within this region there is a shearing layer between the ambient test chamber gas and the jet flow; in this shear layer the turbulent intensity and Reynolds stress are maximum. The shearing layer reduces the kinetic energy in the flow field. Downstream of the mixing region there is an adjustment region where the flow decays in a turbulent state (31).

The Reynolds number for the flow within the 0.5 mm diameter impact pressure probe required only very small viscous corrections to the impact data. The Reynolds number values were 2.4 at 90 km, 14 at 80 km and 69 at 70 km. The viscous corrections are expressed by the ratio of the measured impact pressure (P_i) to the impact pressure under free molecular flow conditions (P_{ideal}) which is given by (21)

$$\frac{P_i}{P_{ideal}} = \frac{\gamma M_n^2 C_\mu}{2} + 1 \qquad (4.2.1)$$

where C_μ is a pressure coefficient parameter; it is determined for each Reynolds number from the experimental curve given by Enkenhus (21). The values for the viscous corrections are 1.13 at 90 km, 1.02 at 80 km and 1.0 at 70 km. These corrections are less than 2 percent for the subsonic flow condition.

The jet flow field was determined by measuring the impact pressure in the discharge jet relative to the static pressure in the test chamber ($P_i - P$). Measurements were made along the centerline and across the exit plane of the nozzle. Figure 4.1 is representative of the impact pressure profiles obtained across the exit plane of the
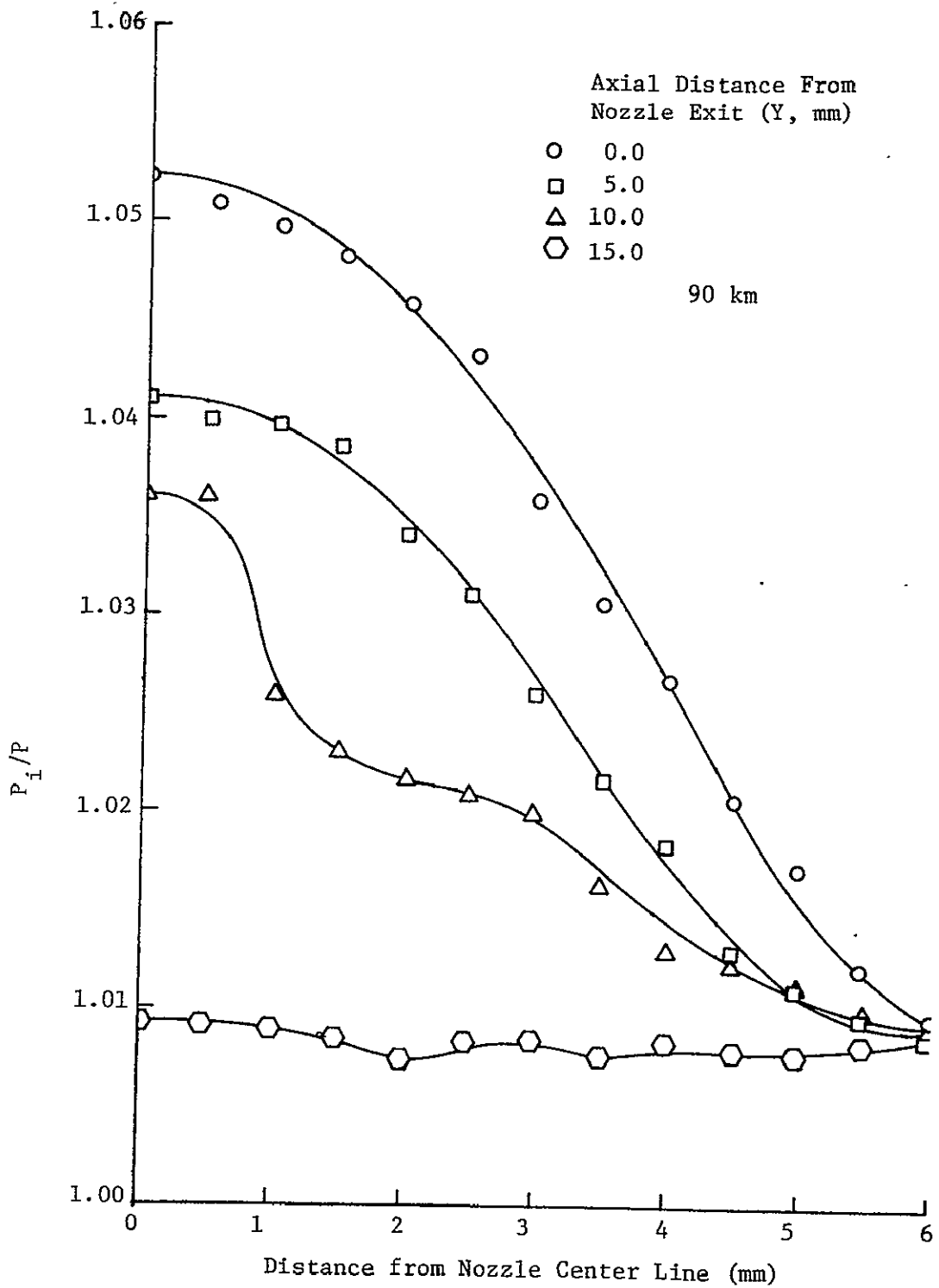
Figure 4.1   Radial Distribution of Impact Pressure for Subsonic
Nozzle Flow

nozzle and at positions downstream of the exit. Pressure is nondimensionalized with the test chamber static pressure to indicate a typical response for the D-region under subsonic flow conditions. The decay of the impact pressure across the exit plane indicates the effect of the shearing layer on the flow. The turbulent decay of the flow dominates the field beyond about 10 mm from the exit plane of the nozzle.

Mach number distributions were determined from the ratio of impact to static pressure as (21)

$$M_n = \left[\left(\frac{P_{ideal}}{P} - 1\right)\frac{2}{\gamma}\right]^{1/2} \tag{4.2.2}$$

where it is assumed that the flow decays isentropically. The centerline Mach number at the exit plane of the nozzle was found to be 0.27, which is within 10 percent of the intended value. Figure 4.2 shows the decay of the Mach number across the exit plane of the subsonic nozzle flow. The jet can be seen to possess a fairly uniform core region of about 3 mm in diameter at the exit of the plane of the nozzle.

4.3 Supersonic Flow

The supersonic nozzle was designed to produce a centerline Mach number of about 2 in the test jet. Rocket-borne probes utilized by other researchers (5,6) typically ascend supersonically through the ionosphere and descend without a parachute drag system, thus reaching large supersonic velocities. A Mach number of 2 is taken as representative of the flow field that such a probe will experience in its passage through the D-region.
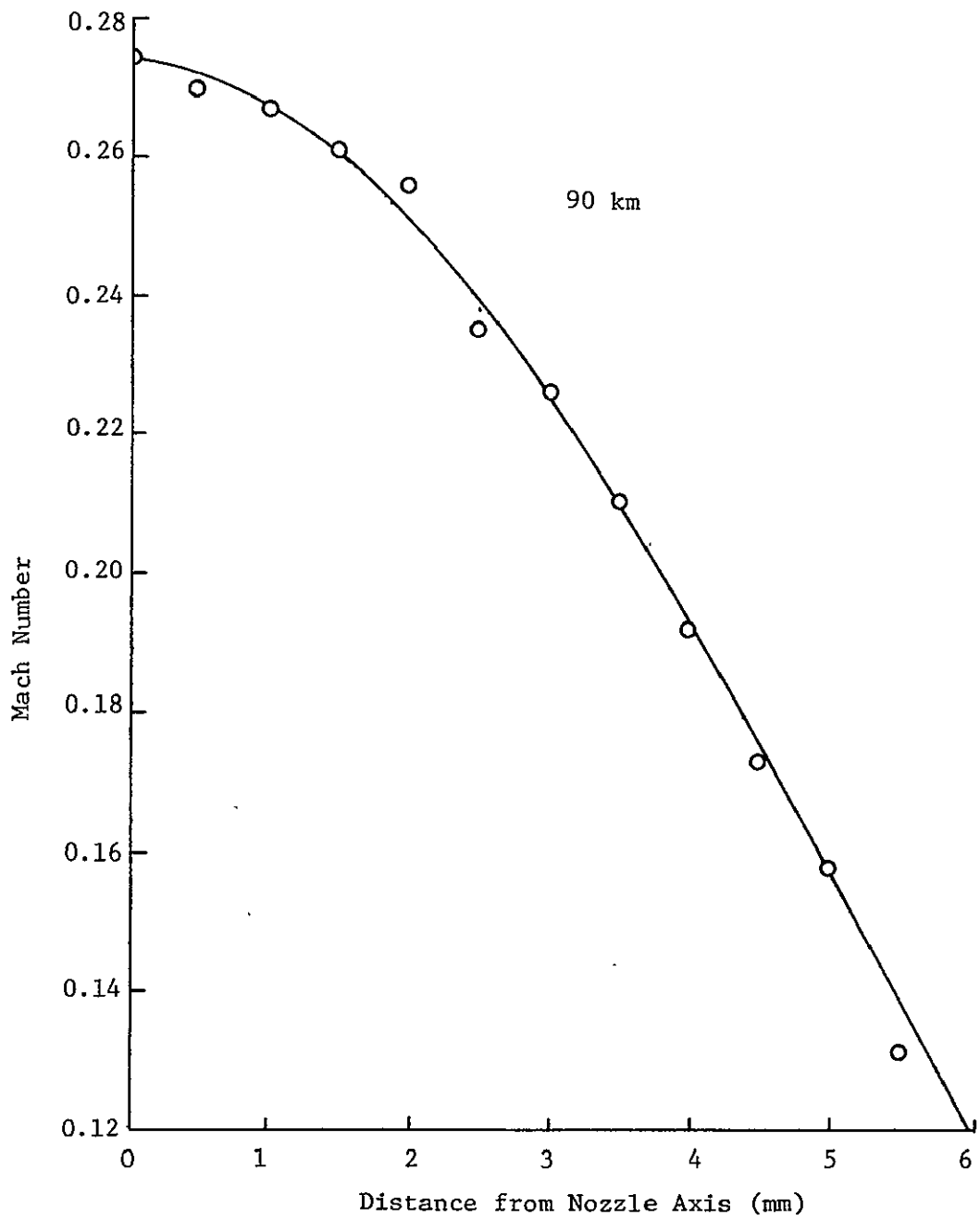
Figure 4.2   Mach Number Distribution across Exit Plane
of Subsonic Nozzle

The scaled laboratory experiment utilized a test jet with flow field patterns from the supersonic nozzle that are once again basically characteristic of low density flow from round, free jets. In the supersonic flow test configuration in the present case, the static pressure ratio across the jet-background interface is equal to 1 and therefore compression or expansion zones are not present near the exit of the nozzle. Abramovich (36) points out that the near field jet behavior is independent of the flow velocity and temperature when compression zones are not formed at the exit of the nozzle. Under such a condition the flow characteristics from the supersonic nozzle will be similar to that for a subsonic jet. Compression zones will form away from the nozzle exit when the static pressure ratio across the jet boundary increases above the unity value (35).

The viscous effects in nozzle flow and in the impact pressure probe response are determined to be negligible on the basis of flow Reynolds number. Relative to the former, the smallest value of the nozzle Reynolds number based on the sonic throat conditions is about 140. Ashkenas and Sherman (37) point out that the viscous effects from the growth of the boundary layer at the throat should therefore be small. Relative to the latter, the viscous effects on the impact pressure probe response are negligible for Reynolds numbers above about 20 (21). The Reynolds numbers are found to be 33 at 90 km, 183 at 80 km and 942 at 70 km. Therefore, no viscous corrections were necessary for the supersonic flow configuration.

The radial impact pressure profiles were determined in the same manner as for the subsonic flow configuration. Figure 4.3 shows a
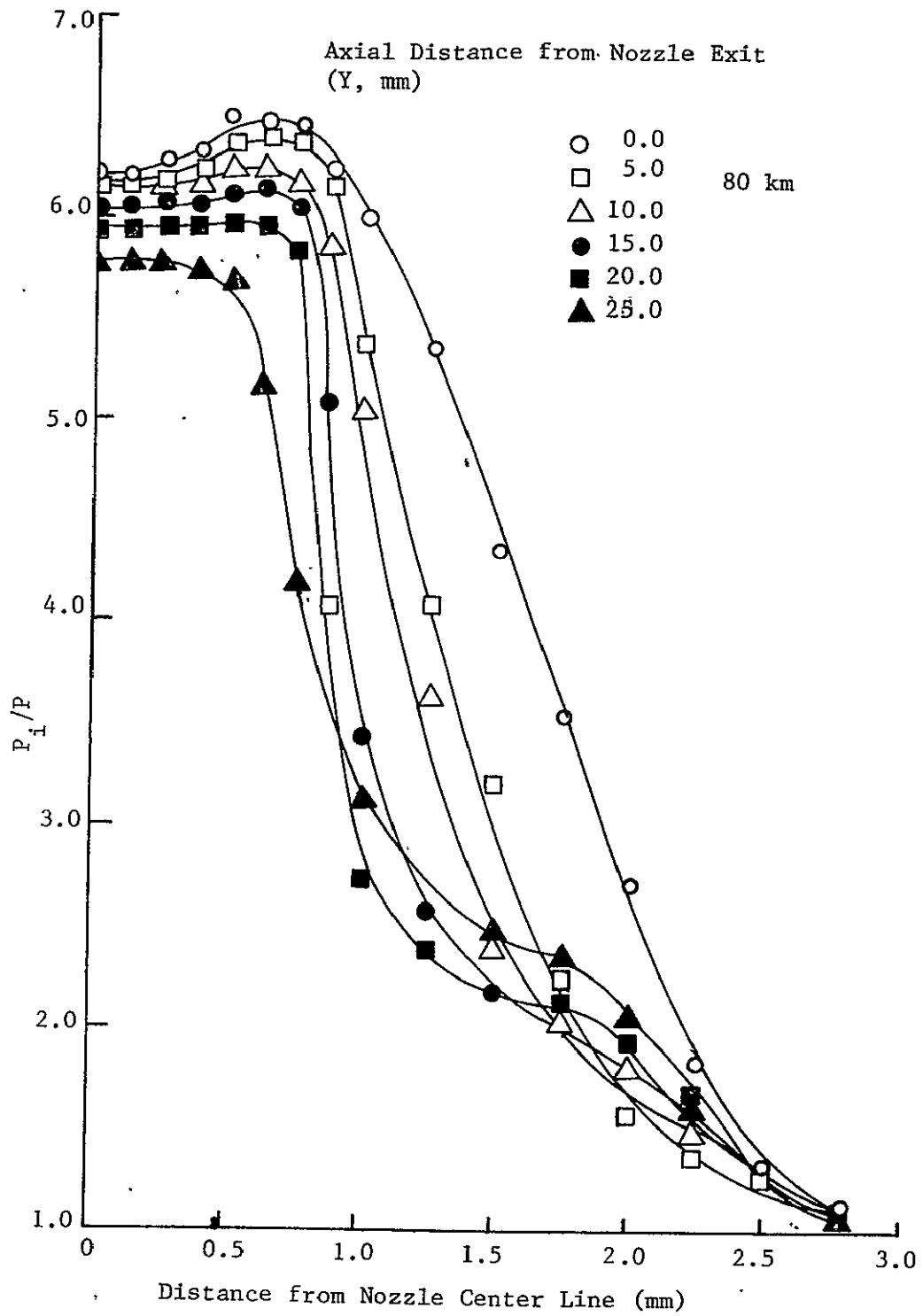
Figure 4.3 Radial Distribution of Impact Pressure for
Supersonic Nozzle Flow

representative impact pressure profile across the exit plane and at subsequent positions downstream of the exit. As the radial distance from the nozzle axis is varied, the impact pressure is found to peak at $r_n \simeq 1$ mm. As the axial position downstream is increased, the peak value is found to decrease relative to the centerline pressure, an effect compatible with decreasing Reynolds number. The dissipation of kinetic energy in the mixing region between the potential core and jet boundary causes the location of the peaks to move radially inward toward the nozzle axis as the axial distance increases (31).

Mach number distributions were determined from the ratio of static and impact pressure by the Rayleigh formula (35), which is given as

$$\frac{P_i}{P} = [M_n^2 \ (\frac{\gamma + 1}{2})]^{\frac{\gamma}{\gamma - 1}} \ [\frac{2\gamma}{\gamma + 1} M_n^2 - \frac{\gamma - 1}{\gamma + 1}]^{\frac{-1}{\gamma - 1}} . \qquad (4.3.1)$$

For a ratio of the specific heats, $\gamma = 1.4$, the form of the equation for the Mach number is

$$M_n = 0.78 \ (\frac{P_i}{P})^{0.47} \qquad (4.3.2)$$

The centerline Mach number is found to be 2.1, which is within 5 percent of the intended value. Figure 4.4 shows the decay of the Mach number across the exit plane of the supersonic nozzle; it indicates a core region of about 1.5 mm in diameter at the exit plane of the nozzle as determined from the distance between the impact pressure peaks. Figure 4.5 shows the axial distribution of the Mach number from the exit plane. The Mach number is found to increase downstream until the region where compression zones are formed, about 2 mm; this is due to the increase in the local static pressure ratio because of viscous interactions.
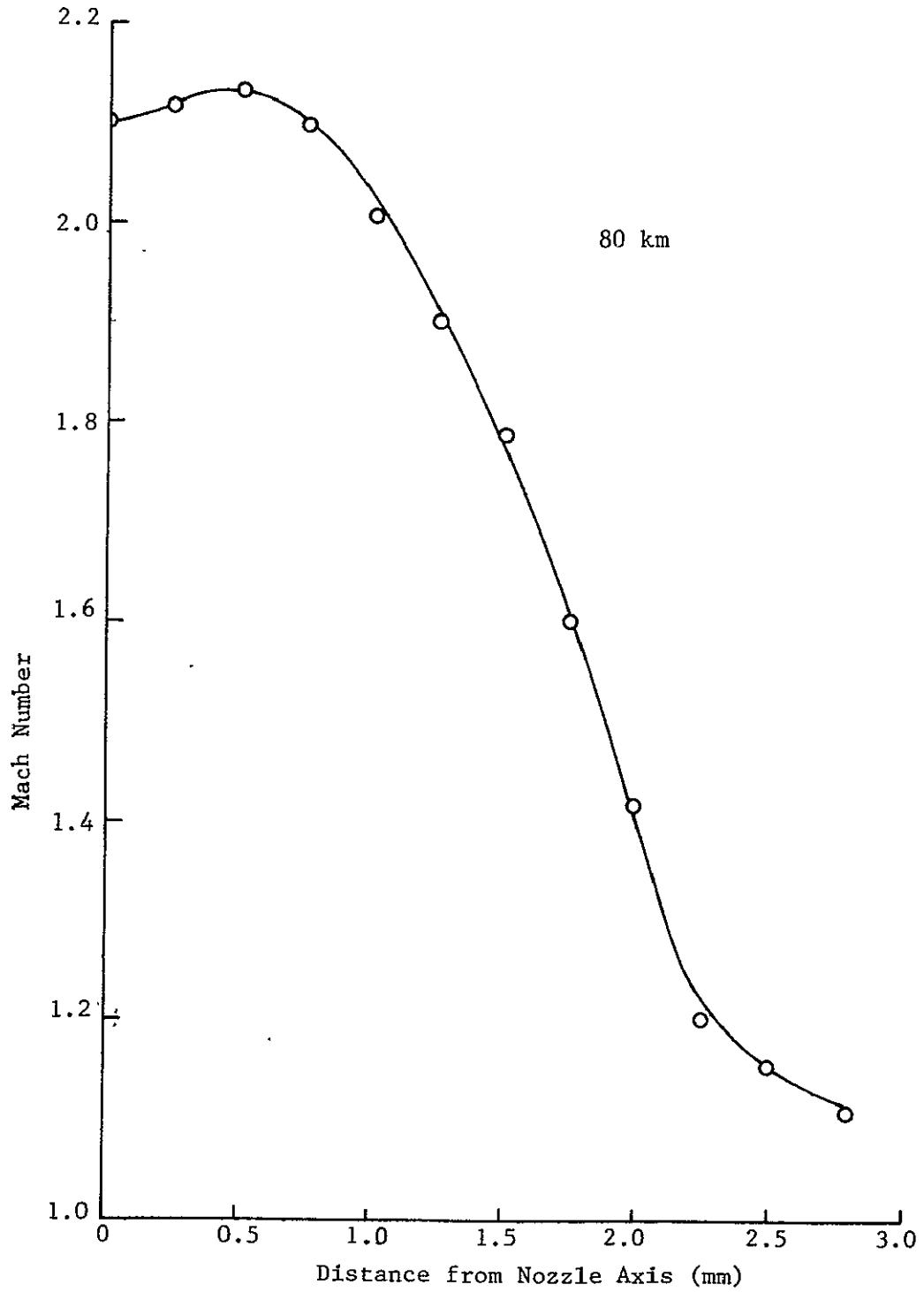
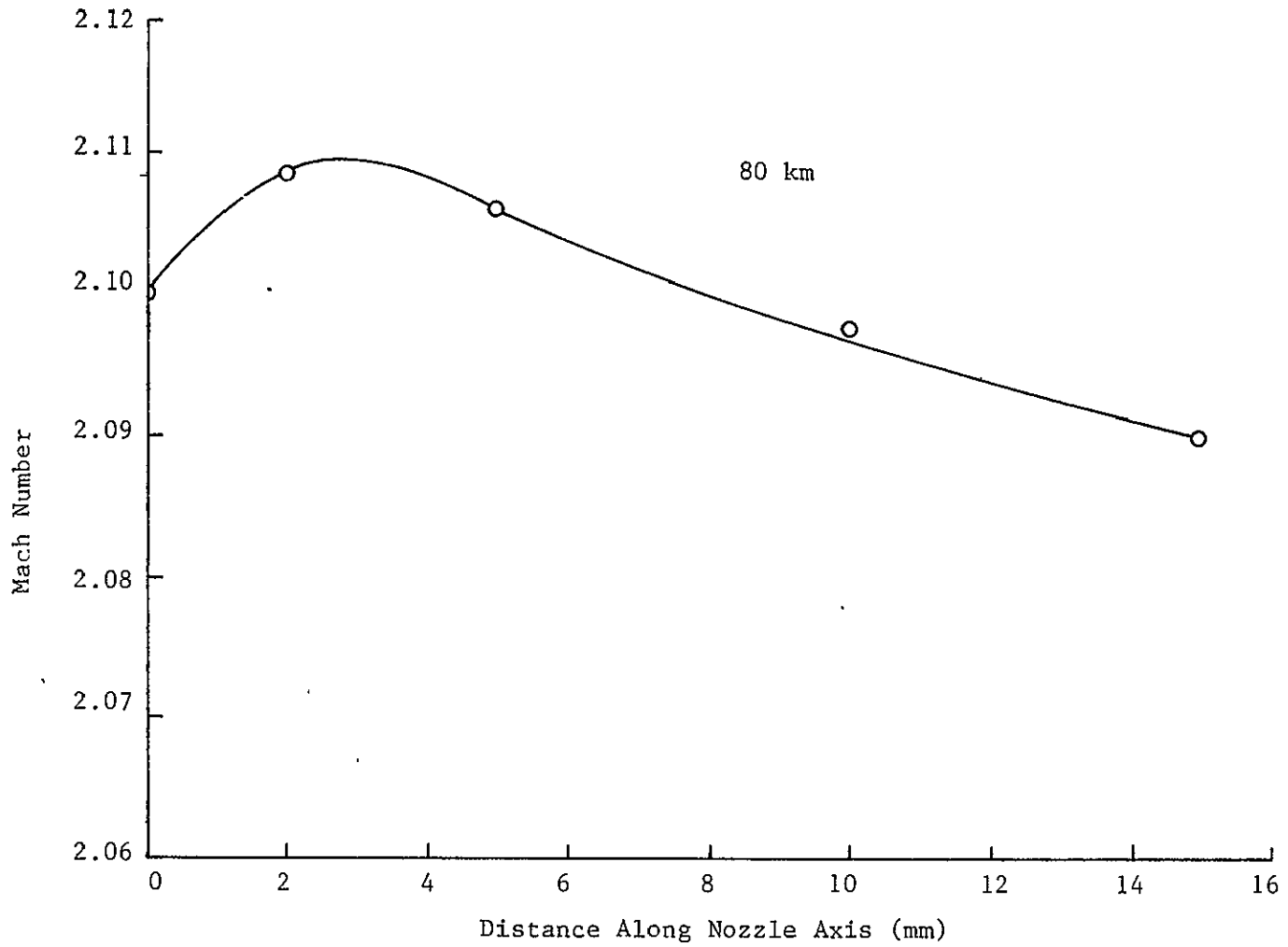Figure 4.4   Mach Number Distribution Across Exit Plane
of Supersonic Nozzle

Figure 4.5   Mach Number Distribution Along Supersonic Jet Axis
Downstream from Exit Plane

In Figure 4.5,the gradual decrease of the Mach number is observed as the distance from the exit plane of the nozzle increases beyond 2 mm.

CHAPTER V

ANALYSIS OF EXPERIMENTAL DATA AND COMPARISON

WITH ROCKET-BORNE BLUNT PROBE DATA

5.1   Introduction

The experimental flow facility was used to produce accurately

scaled D-region probe flows. The cylindrical double Langmuir and blunt

probes were both used to obtain current-voltage data from which electron

temperatures and number densities of the weakly ionized plasma were

evaluated. Data from the test runs are presented and will be evaluated

by employing appropriate continuum, transitional, or collisionless

diagnostic probe theories for specific operating regimes. The specific

probe theory most valid for the reduction and interpretation of the data

is determined by the plasma-probe interaction phenomena. The relevance

of each of the probe theories is dependent upon knowing the degree of

interaction between the plasma electrical and fluid mechanical properties,

as related to the probe size. The plasma-probe regime will be delineated

for each test condition.

Reference values of the plasma electron temperatures and densities

are determined by double Langmuir probe diagnostics, whose accuracy will

be established relative to the probe theories. Comparison of the raw

data obtained by the Langmuir and blunt probes, and reduced plasma

properties determined from available diagnostic probe theories, will

enable the several relevant blunt probe theories to be evaluated under

carefully controlled experimental conditions. Again, since the theory

of the collisionless and transitional Langmuir probe is well understood

(7, 22), the reduced plasma properties derived from the cylindrical

double Langmuir·probe will be used as reference to indicate the validity of the blunt probe reduction procedures. Evaluation of ionosphere data recorded with rocket-borne blunt probes will also be made.

5.2   Criteria Related to Application of Particle Collection Theories

Collisions between particles provide a most fundamental influence on the current conducted to a probe and therefore the indicated temperature and density of the plasma. These interactions among neutral particles, ions, and electrons provide a number of possible collisional parameter scales within the plasma. The probe theories that have been formulated are clearly dependent upon an understanding of the internal collisional structure of the plasma. Specifically, when an electrostatic probe is inserted into a plasma and biased relative to it, collisions between particles within the effective collection layer of the probe determine the exact state of the plasma-probe interaction, such that the probe may be in a continuum interaction with respect to one particle (e.g., ions) while in a collisionless regime with respect to another type of particle (e.g., electrons). Such criteria for the validity of any specific theory must then be examined.

In order for a collisionless probe theory to accurately describe electron collection within the collection layer of the probe, two criteria must be met. The first criterion is a function of the degree of ionization in the plasma and is related to the number of particles in a Debye cube, $n\lambda_D^3$ (12). When $n\lambda_D^3 \gg 1$, electrons are free to move within the effective collection layer of the probe without encountering collisions between ions or neutral particles. This is a physical constraint on the structure of the collection layer immediately

adjacent to the probe surface and may be represented by (12)

$$(0.329) \ \frac{T_e^3}{n_e} \ \gg 1 \qquad (c.g.s.) \tag{5.2.1}$$

for electron collection, where T_e is the electron temperature and n_e is the electron number density. Eq. (5.2.1) was derived from the Debye length, λ_D, a basic parameter that indicates the thickness of the effective collection layer adjacent to the probe; it is given by (2)

$$\lambda_D = \left[\frac{kT_e}{4\pi e^2 n_e} \right]^{1/2} , \qquad (c.g.s.) \tag{5.2.2}$$

where k is the Boltzman constant.

A second criterion specifies the collision state of the plasma-probe interaction for specific particle species being collected. When a probe collects one particular species, the average distance between collisions of that particle and a neutral particle must be large compared to the probe size, r_p. This reduces the possibility of collisions in the region near the probe surface. This criterion is represented by (12)

$$\frac{\lambda_{s-n}}{r_p} \ \gg 1 \tag{5.2.3}$$

where λ_{s-n} is the mean free path between a neutral particle and the attracted species, and r_p is the probe radius.

When both the above criteria are not satisfied, collisionless probe theory is not valid. Transitional ($\lambda_{s-n} \geq r_p$) and continuum ($\lambda_{s-n} < r_p$) probe theories which account for the increasing effect of collisions between particles within λ_D, must then be applied to explain the plasma behavior as influenced by any surface fluid interaction layer(s) and electrical interaction layer(s) in the near field of the probe.

The plasma-probe interaction problem may be further complicated by the mere presence of the probe. In the electrostatic probe theories which will be discussed, the probe acts as a sink for the charged particles and so is itself a cause for perturbation in the plasma. Particles are collected with the assumption that the probe, through surface recombination processes, is a perfect absorber of charged particles. Once a particle is collected by the probe as current, it is removed from the problem. The degree of perturbation arises from the size of the probe and the magnitude of the conducted current. If the current collected is small compared to the current which maintains the plasma, it can be neglected as a disturbance source (12). This was experimentally considered in a case (12) where the glow discharge current was maintained at mA, while the conducted probe current was less than 10^{-9} A; in that situation, the current conducted by the probe could be ignored as a source of plasma disturbance.

5.3 Review of Particle Collection Theories

Various electrostatic probe theories are used to evaluate the relationship between ambient plasma conditions and the current-voltage

response of the probe, including the effect of field-fluid structure of the plasma during the collection. When a probe is biased at a potential, V_d, relative to the potential of the plasma, V_p, the attracted particles are influenced by the resulting electrical fields, and so will move relative to the ambient plasma where the particles are generally assumed to have a Maxwellian velocity distribution.

Random particle motion, mobility, and diffusion processes control the convective motion of the attracted particles through distinctly different layers in the near field of the probe. Specific layers can be defined as being dominated by one or more of these processes. When the attracted particles reach the surface of the probe they are absorbed by surface recombination and surface diffusion processes, thus satisfying the zero density boundary condition at the probe's surface. In a collisionless plasma, the dominant feature involves attracted particles with an equilibrium random kinetic flux at a distance of one mean free path from the probe's surface. In a continuum plasma, the probe size is the dominant scale length and particles are driven toward the probe in a field-diffusion process by the nondimensional probe potential, $\varphi_d = eV_d \, (kT_e)^{-1}$. Both collisionless and collisional probe regimes involve the concept of a "sheath", or electrically perturbed region in the general sense, near the probe's surface; this region can be envisioned as extending outward from the physical collecting surface to create an effective, displaced particle collection surface. Distinctly different from the "probe" or "flow" condition, a sheath may be collisionless, transitional, or collisional (7). The mathematical formulation of this "sheath" region ultimately must match the ambient

plasma conditions on one side with the zero density surface condition on the other side.

The standard and specific definition of a sheath (7) is: that region near the probe's surface where charge separation ($n_e \neq n_i$) cannot be neglected, and the particle motion is determined by the magnitude of the positive or negative bias of the probe and the extent of the plasma-probe interaction condition. Under steady state conditions the flux of particles through the sheath to the probe is constant, and the rate at which the attracted particles are absorbed by the probe is balanced by the rate at which charge particles enter the sheath region. In the sheath, charge neutrality ($n_e = n_i$) does not hold, and the distribution of charged particles is the dominant feature of this region. Particle density and motion must be consistent with the local, altered electric field. Some standard, basic solutions are well known (11, 27).

Generally, electric field generated by the collector-plasma potential difference extends into the plasma away from the probe, and is diminished by the plasma within a characteristic length which is a function of the electron temperature and number density. Under certain conditions, this effective screening distance is found to be the Debye length, λ_D, represented by Eq. (5.2.2). The formulation of a value for screening distance was examined in the specific sense by Lai (2), where it was pointed out that the standard, physical interpretation of λ_D as an indicator of a sheath thickness is only valid for $\phi_d \ll 1$. Further, the Debye ratio, $r_p \lambda_D^{-1}$ (7), indicates the extent of charge particle saturation within the sheath region (2).

When $r_p \gg \lambda_D$ (thin sheath), the paths of the attracted particles to the probe are straight and intersect the probe perpendicular to the collection surface. For a thick sheath, $r_p \ll \lambda_D$, the trajectory of the particles will converge toward the probe and those particles intersecting the collection surface will be collected as current. Thus, in the collisionless thick sheath limit, $\lambda_D \to \infty$, the current conducted by the probe will be over estimated relative to the current collected through a thin sheath (7). However, if $\lambda_{s-n} \ll \lambda_D$ the number of attracted particles reaching the probe surface is decreased by the effect of charge particle collisions within the sheath region (33).

The collisionless plasma-probe interaction state (collisionless probe and collisionless sheath) is described by the orbital-motion-limit (7). The current conducted in this regime is that due to attracted particles that pass through a collisionless sheath and are not prevented by potential barriers from reaching the probe. This current is a function of energy and angular momentum considerations (7). In the one dimensional central-force problem relating the trajectory of the particles to the current collected by the probe, the potential energy, E_p (r, Ω), of the attracted particles in the collisionless regime is related to their radial velocity, v_r, and local electrical potential, and is given by (7)

$$E_p \ (r, \ \Omega) = Z \ \psi(r) + \frac{\Omega^2}{2mr^2} \tag{5.3.1}$$

where Ω is the angular momentum of the particles, Z is the charge on the particles, and $\psi(r)$ is the local particle potential. The potential

energy governs the radial motion of the particles. The total energy

of the particles, E, is not affected by the motion, and is given by (7)

$$E = \frac{mv_r^2}{2} + E_p(r, \Omega) \qquad (5.3.2)$$

The total magnitude of E and Ω together determine the path and

location of the particles relative to the probe's collection surface.

When $r_p \lambda_D^{-1} \neq o$, potential barriers will dominate $E_p(r, \Omega)$ and prohibit

certain particles from reaching the probe. Particles whose trajectory

is dominated by the magnitude of Ω will not be absorbed by the probe,

but will pass by it because of their trajectory. The particles whose

value of $E_p(r, \Omega)$ are sufficient to overcome the effect of Ω will enter

trapped orbits. In a steady state collisionless probe theory, Chung

et al., (7) point out that the procedure to determine the density of

these particles has not been formulated. However, Laframboise (17) has

found that the influence of particles in trapped orbits is not

important in the determination of the current collected by the probe.

The orbital-motion-limit is applicable when spherical or cylindrical

probes are used for collisionless particle collection. Chen (33)

points out that orbital-motions are not possible with plane probes

because of the probe's geometry; further, in that case the sheath size

is assumed constant after charge particle saturation, when V_d is larger

than V_p.

In general, the state of the plasma within a sheath (electrically

perturbed) region is determined by the relationship between the species

mean free path, λ_{s-n}, r_p, and λ_D. In the case when $\lambda_D \gg \lambda_{s-n} \gg r_p$,

collisions between charged particles occur within a sheath region, while a collisionless plasma exists with respect to the probe (7). The gas operating pressure, P, will serve to define λ_{s-n}, and along with other variables, λ_D, and so determine the degree of plasma-probe interaction and thus the collisional state within the sheath. Specifically, since $\lambda_{s-n} = (n\sigma_{s-n})^{-1}$ where σ_{s-n} is the species collision cross section, the number of collisions will increase with higher P and will prevent attracted particles from entering orbital (collisionless) motions in the near field of the probe. The magnitude of the electron density, n_e, electron temperature T_e and applied probe potential, V_d, determine the thickness of the sheath (electrically perturbed) region.

Chung et al., (7) review the many regimes of specific plasma-probe interactions and the relevant analytical schemes for stationary and flowing plasmas. The various operating regimes for electrostatic probes are discussed and the available diagnostic theories are formulated to interpret the probe's response within these regions. The review work includes the response and operation of Langmuir probes in transitional and collisionless plasmas. The use of Langmuir probes in continuum plasmas is also presented, but as discussed, the validity of the analysis in this regime is open to some question. In that work, primary consideration was given to ion particle collection. However, Lai (2) does present a specific electron collection diagnostic theory appropriate for blunt probes in the continuum regime of the ionosphere. Other blunt probe continuum theories have been developed by Hoult (38) and Sonin (19), as noted above; again, these theories were formulated primarily to explain ion collection.

To date none of these blunt probe theories have been substantiated in laboratory experiments appropriate for the lower ionosphere, D-region, which is of primary concern in this work.

The cylindrical double Langmuir probe operating in the collision-less and transitional regimes will be used in this work to determine the properties of the plasma produced in the flow facility. This probe consists of two relatively thin cylindrical ($r_p < \ell$) electrodes which, when biased, conduct a current, the magnitude of which will indicate the potential of the plasma, the onset of charge particle saturation, and hence, the appropriate values of electron temperature and number density. When this constraint, $\lambda_{s-n} \geq r_p$ is met, the Langmuir probe will function in a plasma-probe interaction condition which is collisionless or transitional, regimes which are well under-stood theoretically and experimentally (7, 22). Because of the well established collisionless and transitional operational procedures and evaluation schemes for the Langmuir probe, it was considered sufficiently reliable as a diagnostic tool to substantiate the state of the test plasma, in order to then be able to evaluate the response of the blunt probe for electron collection. Differences in response mechanisms between the blunt and cylindrical probes will require an indepth understanding of the difference in the collisionless and continuum theories formulated for each of these diagnostic probes.

The diagnostic theories developed for cylindrical collisionless probes, as outlined by Chung et al., (7), account for the formation of orbits by the attracted particles within the collection surface.

The most widely accepted and experimentally verified theory for
cylindrical collisionless probes was formulated by Laframboise (17).
This theory was formulated single probes and for the range, $r_p \lambda_D^{-1} \geq 1$,
and has been well established as the primary comparative theory for the
particle collection processes in collisionless plasmas, where the
possibility of orbits formed by the attracted particles is most
prevalant.

The double probe method of diagnosing plasma properties was first
presented by Johnson and Malter (25); this analysis is appropriate for
collisionless probes with thin sheaths in static plasmas. A more
general development of double probe theory, including the effects
of thicker sheaths and the influence of applied potential on ion
current, has more recently been outlined (39). The work presented
there considered cases with $r_p \lambda_D^{-1} \geq 1$, variable temperature ratios,
and comparison of the results with those of Laframboise (17) for
similar conditions.

Chou et al., (40) have developed the most complete theory for
the operation of electrostatic single probe in the transitional plasma
regime. However, the work was quite detailed and did not permit a
form of the theory appropriate for simple interpretation of experimental
work (22). More recently, Talbot and Chou (41) have presented a
transitional regime analysis for saturation ion current to spherical and
cylindrical probes for the range $r_p \lambda_D^{-1} \geq 0$ which can be used to
interpret diagnostic results. Their theory has compared well with
experiments conducted by Kaegi and Chin (42), and Kirchhoff et al., (22).
The Talbot-Chou theory was developed for cylindrical single Langmuir

probes in a flowing plasma and describes the effects of collisions on ion and electron current collection.

While the saturation current for a single probe can be used to derive the plasma number density from double probe data, a specific formulation including the effects of collisions in the transition regime for double probes has been presented by Thornton (43). It should be noted that, generally, such thick sheath theories involve the definition of a sheath boundary and the evaluation of an effective collection surface area at that position (22, 41, 43). Further, it has also been noted (7, 22) that the double probe is less sensitive to collisional effects, distortion, and the analytical theories can be used with more confidence with double probes.

In the continuum plasma regime the effect of orbital trajectories is reduced because of the increase in charge-neutral collisions. A conprehensive discussion of the available theories for this regime is presented by Chung et al., (7) and a detailed discussion of direct interest is included in the work of Kiel (44). Once again there does appear to be a reasonably consistent analysis available when current-voltage data up to saturation is used for the determination of plasma properties. As one effort of interest Chung and Blankenship (45) have developed a continuum theory appropriate for flat plate double diagnostic interpretation; their theory has been experimentally verified in experiments by Chung (46).

The blunt probe geometry and relatively constant sheath size with an increasing probe potential, V_d', above plasma potential, V_p, will eliminate the formation of orbital trajectories of the attracted

particles (33). This major difference in the particle collection

process for blunt probes requires different diagnostic theories to

describe the motion and path of the collected particles. The

Child's Langmuir theory (47) was formulated to interpret the response

of highly biased plane probes in collisionless plasmas. This theory

can also provide a basic description of the electron collection

process $(V_d > V_p)$ for blunt probes in other, non-orbital regimes.

A new electron collection theory for subsonic continuum blunt probes

was outlined by Lai (2). As yet, however, no theory for electron

collection in flowing plasma has been validated by laboratory experi-

ments.

5.4 Determination of Plasma Properties Using the Double Langmuir Probe

5.4.1 Introduction

The cylindrical double Langmuir probe was used to define the

plasma properties in the static and flow configurations. From the

studies conducted in collisionless plasmas (10, 13), where the

Langmuir probe was used to determine the local properties of the plasma,

it was found that this diagnostic probe is dependable in securing

accurate and useful current-voltage data. A cylindrical geometry was

chosen for the probe because a large aspect ratio, $\ell D_p^{-1} \approx 16$, reduces

the influence of end effects on the response of the probe. The

double probe configuration was used because of the minimal disturbance

of the plasma and, as concluded by Kirchhoff et al., (22), the twin

electrode geometry is less sensitive to collisional effects than the

single electrode geometry and so would be more reliable in determining

the correct values of plasma temperature and density in the range of

operation. Johnson and Malter (25) have pointed out that the double

probe's electrical circuit allows the probe to function independently

of the plasma discharge system. As discussed in section 3.2, the

Langmuir probe circuit is not grounded, but floats with respect to the

discharge system, and thus conducts current unaffected by the potential

which maintains the plasma discharge. The electron number density and

temperature were determined with this probe and are the basic properties

in the ionized, scaled regimes.

In the static plasma configuration, the values of electron tempera-

ture and density were measured at positions between y = 1 cm to y = 4 cm

from the center of the flow discharge chamber. The y direction is defined

along the axis of the nozzles between the discharge chamber and the

test chamber (Fig. 2.2); the reference point (y = 0) corresponds to the

center of the glow column, or the intersection of the transverse axis

along which the electrodes are positioned (Fig. 2.2). Under static

conditions the probe current was so small that it could not be measured

in the test chamber, because the discharge chamber walls localized the

plasma distribution. In the subsonic and supersonic flow configurations,

the probe current was measured on the axis of the flow nozzle at the

exit plane, y = 8.5 cm from the center of the plasma source.

The precise interpretation of the data obtained with the Langmuir

probe requires the application, of diagnostic theories which are

appropriate for each operating regime. The equations which allow

electron temperature and number density to be determined from the raw

data are correctly applied only to specific collection regimes. As

discussed in section 5.3, the relationship between the collected

particle mean free path, λ_{s-n}, and λ_D and r_p determine the exact

operating regime of the probe with respect to the plasma. Raw data

was obtained for collisionless ($\lambda_{s-n} \gg r_p$), transitional ($\lambda_{s-n} \gtrsim r_p$),

and continuum ($\lambda_{s-n} < r_p$) plasma regimes. This data will be

presented and then analyzed relative to the specific operating regimes

where the probe was functioning.

5.4.2 Static Source Plasma

. The values of temperature and density for different altitudes of

interest in the D-region have been presented in Table 1. The scaled

values of discharge chamber pressure and number density and test (jet)

pressure and number density have been presented in Table 2; also, on

the basis of the approximation (24) that the glow discharge plasma will

have a cold ($T_i \approx 300^{\circ}K$) ion temperature and hot ($T_e \approx 1$ eV $\approx 10,000^{\circ}K$)

electron temperature, the mean free paths (λ_{e-n}, λ_{n-n}) presented in

Table 2 were estimated. The correct, specific method of reducing

double Langmuir probe data, comprised of current-voltage characteristics,

depends in detail on the relative magnitude of λ_{s-n}, λ_D, and r_p.

While the relationship of λ_{s-n} and r_p can be estimated by the above

method, the order of magnitude of λ_D requires values of n_e as well as

T_e for the different experimental positions and conditions. In order

to establish orders of magnitude for λ_D, an approximate evaluation

of n_e, T_e for all conditions by a standard collisionless double

probe analysis (25) will first applied to the experimental current-

voltage characteristics to be discussed.

Figure 5.1 presents typical current—voltage characteristics for the double Langmuir probe in the static plasma configuration for the scaled 90 km regime; the data is for four axial positions relative to the center of the glow discharge.

The current—voltage characteristics for the double Langmuir probe at three different source pressures that model the 70, 80 and 90 km altitudes are presented in Figure 5.2.

In general there is a well defined saturation region indicated by the "knee" in these figures. In Figure 5.1, the probe is moved away from the center of the plasma source and along the discharge chamber axis, the "knee" indication of saturation is seen to decrease; the reduced slopes and magnitudes of current conducted to the probe indicate that the electron density of the plasma in the discharge chamber decreases, while the temperature increases, with distance away from the center of the source. Also, relative to the data in Figure 5.2, some general comments can be made. In a glow discharge, ionization is caused by electron—neutral inelastic collisions, and as pressure is increased the mean free path is decreased, resulting in lower electron and ion densities. The reduced number of ions impinging on the cathode will also serve to decrease its effective electron emissions. This behavior would necessarily result in the anode collecting fewer electrons; in Figure 5.2 the electron current is seen to decrease from about 10^{-9}A to about 10^{-10}A with increasing discharge pressure. Figure 5.2 also demonstrates a decrease in the indicated degree of saturation with increase in the gas pressure; there is little indicated saturation for 70 km, while the 80 km data is anomalously high.
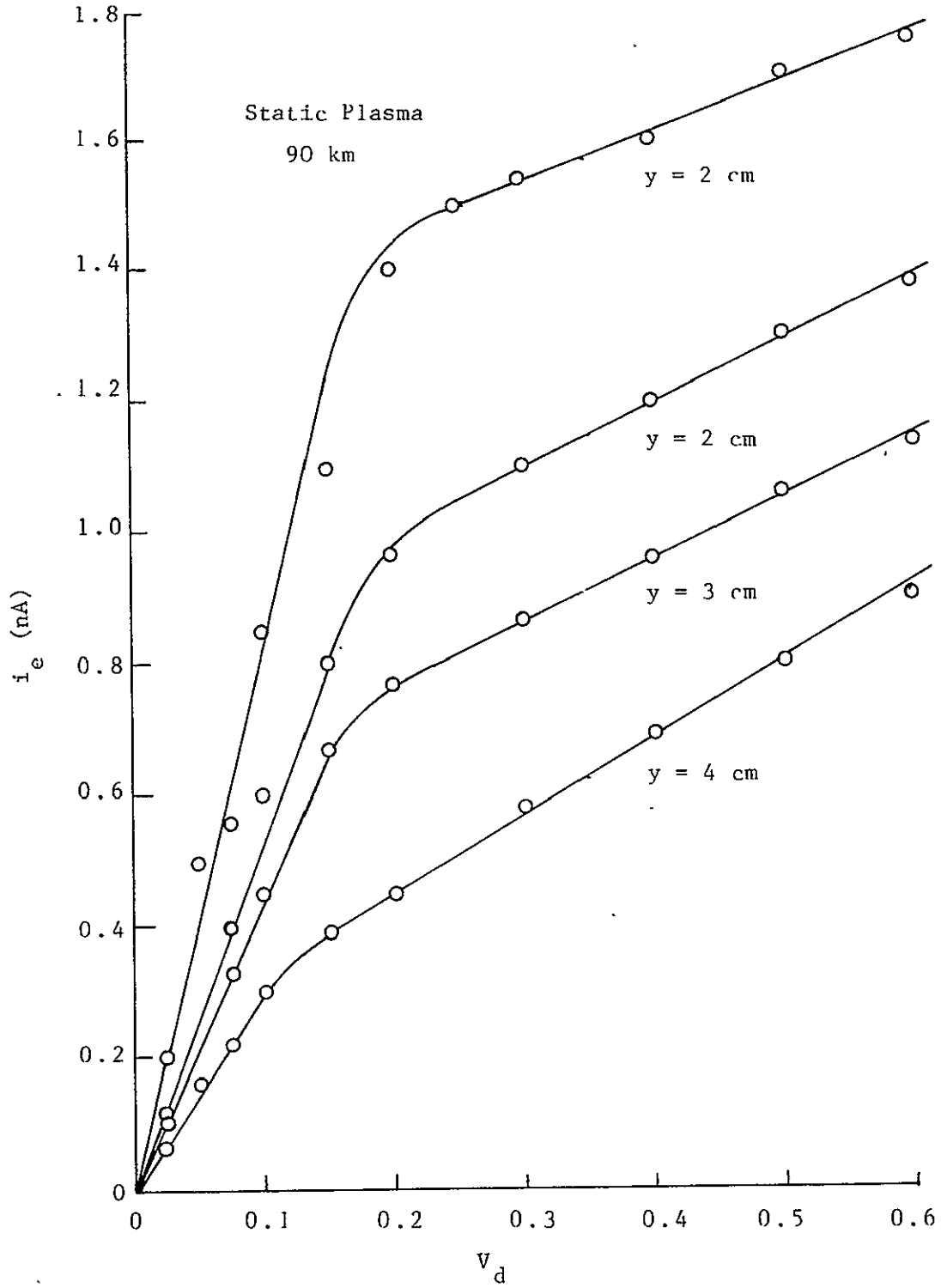
Figure 5.1   Double Probe Current-Voltage Characteristics
for Static Configuration
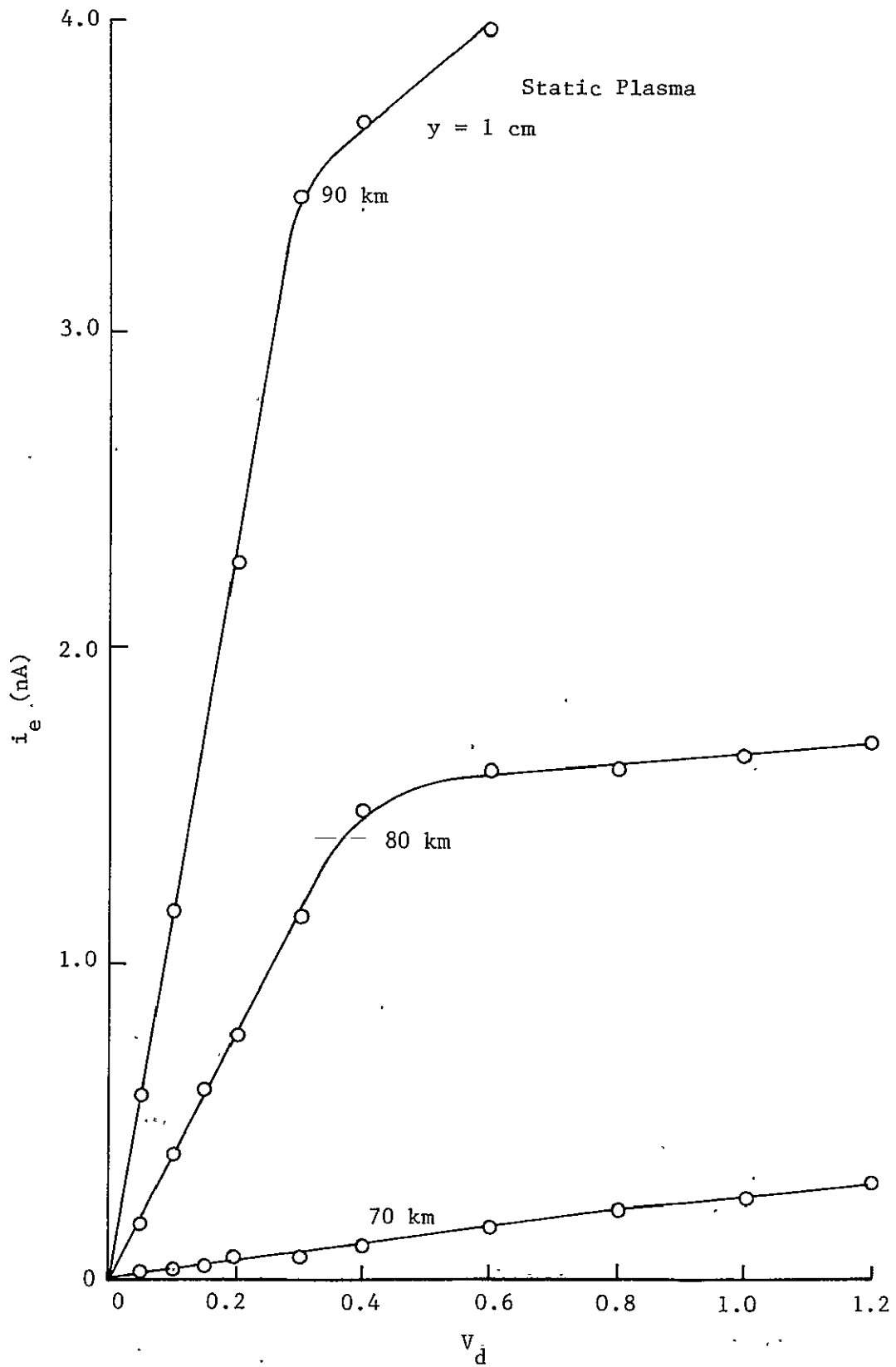
Figure 5.2 Double Probe Current-Voltage Characteristics
for the Static Plasma in the Discharge Chamber
for 70, 80 and 90 km Regimes

The collisionless double probe analysis formulated by Johnson
and Malter (25) was applied to the current-voltage data to obtain an
indication of the magnitude of n_e, T_e and thus λ_D. The electron
temperature was estimated from the formulation:

$$T_e = 1.16 \times 10^4 \; (\Delta V_d / \Delta \ln \Gamma) \qquad (5.4.1)$$

where Γ is a nondimensional current (25) conducted by the double probe.
The values of n_e were then determined from the relationship;

$$n_e = 4J/e\overline{U} \qquad (5.4.2)$$

where

$$J = 2 \; k \; T_e \; (\Delta I/\Delta V)_{V=0} / A_s e \qquad (5.4.3)$$

and

$$\overline{U} = (8 \; kT_e / T \; m_e)^{1/2} \qquad (5.4.4)$$

Equation (5.4.3) expresses the current conducted to the probe in
terms of the slope of the current-voltage characteristic before saturation
is reached.

Table 3 presents a summary of the approximate magnitudes of T_e,
n_e, λ_D, and λ_{e-n}, determined by using the method outlined above. Again,
the values presented are indicative of plasma within the glow discharge

Table 3: Approximate Properties in the Static Discharge Plasma

$$T_i \simeq 300^\circ K$$

Scaled ALT	Axial Displacement from center of electrode axis y = cm	T_e ($^\circ K$)	n_e (cm^{-3})	λ_D (mm)	λ_{e-n} (mm)
90	1	1160	1.04×10^4	6.51	2.6
	2	987	6.7×10^3	7.49	2.8
	3	748	5.25×10^3	7.36	3.13
	4	669	3.08×10^3	9.06	3.48
80	1	1857	1.23×10^3	2.4	0.442
	2	870	5.8×10^2	2.4	0.571
	3	1005	1.28×10^1	17.3	0.551
70	1	481	1.17×10^2	39.5	0.141
	2	446	8.08×10^1	46.8	0.163

chamber. No plasma properties were obtained outside the discharge chamber and in the nozzle, $y \geq 8.5$ cm, because with the static plasma the glow discharge chamber localized the plasma, resulting in indistinguishable probe signals at the nozzle exit.

The approximate magnitudes of n_e determined by Eq. (5.4.2) range from 10^4 cm^{-3} to 10^1 cm^{-3} as the Langmuir probe is moved axially away from the center of the glow discharge.and as the source pressures are increased to model the 90, 80 and 70 km altitudes. The values of T_e range from 10^{3}°K to 10^2 °K; the values of λ_D are of the order 10 mm. The mean free path between electrons and neutral particles are also presented in Table 3 to indicate the plasma-probe interaction domain.

Table 4 summarizes the relationships between r_p, λ_{e-n}, and the approximately determined λ_D. The operational regimes as outlined by Chung et al., (7) for the double Langmuir probe in the static glow discharge source plasma were concluded to be: collisionless $(\lambda_D > \lambda_{e-n} \gg r_p)$ at 90 km, transitional $(\lambda_D > \lambda_{e-n} \approx r_p)$ at 80 km and 70 km.

The approximate evaluation of the static source plasma has indicated the relative magnitudes of λ_{s-n}, T_e, n_e and λ_D. The standard collisionless double probe analysis (25) used to evaluate the data gives the appropriate operational domains. As indicated by the data the simulated 90 km altitude is collisionless while the 80 km and 70 km altitudes are transitional. Exact methods for evaluating double Langmuir probe data will now be applied to the data.

Table 4:   Plasma-Probe Interaction for Static Source Plasma

Scaled ALT (km)	λ_D (mm)		λ_{e-n} (mm)		λ_{n-n} (mm)	r_p (mm)	PROBE STATE
90	6.51	>	2.6	>	0.19	0.127	Collisionless
80	2.4	>	0.442	<	0.05	0.127	Transitional
70	39.5	>>	0.141	<	.01	0.127	Transitional

The most widely accepted and experimentally verified theory for cylindrical collisionless probes was formulated by Laframboise (17). The exact value of n_e in the scaled 90 km collisionless regime was obtained from a reported application of this theory; using the ion saturation current at the "knee" of the current-voltage characteristic by (48),

$$n_e = J_i \left[2\pi \, m_i/k \, T_e \right]^{\cdot 1/2} / \alpha_p \, e \, A_s \tag{5.4.5}$$

where

$$\alpha_p = f \left(r_p/\lambda_D, \, T_i/T_e \right) \tag{5.4.6}$$

and J_i is the ion saturation current. A_s is the surface area of the probe, V_p is the plasma potential and m_i and m_e are the mass of the ion and electron, respectively. From Laframboise (17), for $T_i/T_e \approx 0$, $r_p/\lambda_D \approx 0$, $\alpha_p \approx 2.5$. Eq. 5.4.5 was arranged in diagnostic form to simplify the data reduction process, and the electron number density was determined by the formulation

$$n_e = \frac{\left[2\pi \, m_i/kT_e \right]^{1/2}}{(2.5) \, e \, A_s} \, J_i \tag{5.4.7}$$

In the collisionless regime at 90 km, the electron temperature,

T_e, was determined from the slope of the logarithm of the electron

current, i_e, plotted as a function of the applied probe potential, V_d.

This technique was outlined by Johnson and Malter (25) for cylindrical

double Langmuir probes, and has been experimentally verified by microwave

techniques as reported by Graf (48). The values of T_e were determined

by

$$T_e' = \frac{e}{k} \left(\frac{\Delta V_p}{\Delta \ln i_e} \right) \tag{5.4.8}$$

where i_e is the electron current collected by the probe. For a

double Langmuir probe Eq. (5.4.8) is presented in diagnostic form

by Eq. (5.4.1).

The exact values of n_e and T_e obtained in the collisionless

plasma regime at 90 km are presented in Table 5 at the end of this

section. These values were obtained at probe positions varying from

$y = 1$ cm to $y = 4$ cm from the center of the source discharge. Values

of n_e range from 3.98×10^6 cm^{-3} to 8.9×10^3 cm^{-3}, respectively. The

values of T_e range from 1160 °K to 669 °K. Table 5 also presents

desired values of λ_D and λ_{e-n}; when these are compared with the probe

size, $r_p = 0.127$, reconfirm the collisionless and transitional plasma-

probe operation.

In the transitional condition at scaled 70 km and 80 km, the values

of n_e were obtained from the theory developed by Talbot and Chou (41).

As discussed in section 5.3, this transitional probe theory has been

substantiated in laboratory experiments over a range of conditions

from well-defined collisionless states into transitional plasma regimes. The relation for n_e developed by Talbot and Chou was presented in diagnostic form by Kirchhoff et al., (22), and is given by

$$(n_e)_{Trans} = (n_e)_{Col} \frac{\gamma^{-1}}{j_{i,\infty}{}^*} \qquad (5.4.9)$$

where $(n_e)_{Col}$ is the value of n_e evaluated under collisionless conditions, γ^{-1} is defined by Eq. (2) in Ref. (22), and $j_{i,\infty}{}^*$ is defined by Eq. (5) also in Ref. (22).

The values of T_e were determined in the transitional regime at 70 and 80 km by the diagnostic procedure formulated by Johnson and Malter (25), Eq. (5.4.1). As pointed out by Kirchhoff et al., (22) the electron temperature evaluated by Eq. (5.4.1) in the transitional regime should be adjusted by a correction factor. The modification, however, is less than a few percent. Thus a double probe analysis may be used to evaluate T_e in the transitional regime.

Table 5 at the end of this section presents the values of n_e, T_e, λ_D, and λ_{e-n} obtained in the transitional plasma regime. The data was obtained at probe positions from $y = 1$ cm to $y = 3$ cm from the center of the plasma source. The electron number density ranged from 3.6×10^3 cm^{-3} to 2.6×10^2 cm^{-3}. The electron temperature varied from 1857°K to 635°K. The magnitude of T_e, as indicated by the slope of the probe characteristics in the electron retarding region can be seen to decrease.

With the exact values of n_e and T_e in the source plasma established, values of λ_D can also be calculated. Table 5 presents the exact values of n_e, T_e and λ_D in the source plasma. As a point of interest,

indication of the virtual surface area for particle collection at λ_D can be made. In the scaled 90 km source plasma, the identification of saturation from the "knee" in the probe current-voltage characteristic was found to decrease as the probe was moved further from the plasma source. This was felt to be due to the field perturbed region increasing in thickness; λ_D can be seen to increase from 0.33 mm to 5.34 mm. Also, as the source plasma pressure was increased, the current-voltage characteristics evidenced a less definable saturation; this could be due to the larger perturbed thickness approximated by $\lambda_D = 16.5$ mm at 80 km and $\lambda_D = 34.8$ mm at 70 km. As pointed out by Chung et al., (7) convective effects in the thick sheath regions are relevant. The convection of ions and electrons into the large perturbed region of the probe necessitates larger applied potentials for saturation. As evidenced by the data the increased size of λ_D does require higher values of V_D.

Values of λ_{e-n} which indicate the extent of particle collisions, are presented in Table 5. The number of collisions between electrons and neutral particles increases with pressure because the neutral density increases from 6.4×10^{13} cm^{-3} at 90 km to 1.61×10^{15} at 70 km. The values of T_e remain of order $10^{2}°K$; this causes the collision cross section of the electrons, σ_{e-n}, to also remain of the same order. At 70 km, the resulting λ_{e-n} is 0.130 mm which is an order of magnitude smaller than in the collisionless 90 km regime, $\lambda_{e-n} = 2.6$ mm. The values of the non-dimensional probe potential, ϕ_d, and the degree of ionization, θ, are also presented in Table 5 for the source plasma.

Table 5: Properties in the Source Plasma Configuration

ALT (km)		T_e ($^\circ$K)	n_e (cm^{-3})	λ_D (mm)	λ_{e-n} (m-m)	φ_d	θ
90 km	y = 1 cm	1160	3.98×10^6	0.33	2.6	2.0	5.2×10^{-10}
	y = 2 cm	987	4.32×10^5	0.932	2.8	2.18	1.1×10^{-11}
	y = 3 cm	748	5.70×10^4	2.28	3.13	2.32	9.3×10^{-12}
	y = 4 cm	669	8.9×10^3	5.34	3.48	2.34	6.5×10^{-13}
80 km	y = 1 cm	1857	2.6×10^3	16.5	0.442	2.25	3.8×10^{-14}
	y = 2 cm	870	3.66×10^3	9.5	0.571	2.53	1.79×10^{-14}
	y = 3 cm	1005	3.40×10^3	3.35	0.551	2.19	3.96×10^{-16}
70 km	y = 1 cm	830	2.6×10^2	34.8	0.130	2:1	7.27×10^{-16}
	y = 2 cm	635	3.04×10^2	28.1	0.148	2.1	2.49×10^{-16}

5.4.3 Flowing Plasma Properties at the Test Station

As has been clearly established (7), flow can have a substantial effect on the collection of particles by an electrostatic probe. Again, the collection theories that have been developed were reviewed and classified by Chung et al., (7), and it will be emphasized here that most theories were developed to explain ion collection, not electron collection which is of primary interest in the present work. However, since the n_e determination from double probes involves ion saturation current, ion response must be given careful consideration in the double probe data interpretation.

One basic point to be recognized is the fact that the electron particle velocity, V_D, induced by the applied (probe) electric field, is the dominating velocity component in the electron collection process. Specifically, in the present experiments the subsonic flow velocity is 10^3 cm sec^{-1} and the supersonic flow velocity is 5×10^4 cm sec^{-1}; from the experimental field data and the drift velocity measurements presented by McDaniel (30), it was estimated that V_D was on the order of 10^6 cm sec^{-1} which is two orders of magnitude larger than the supersonic flow velocity and three orders of magnitude larger than the subsonic flow velocity. Also, from an analysis of thermal neutron, the electron arithmetic or average velocity (30) is of order 1×10^7 cm sec^{-1}. The thermal velocity estimate is four orders of magnitude larger than the subsonic flow velocity and three orders of magnitude larger than the supersonic flow velocity.

In this experiment, $T_i \approx 300°$K and the ion thermal velocity estimate (30) is 4×10^4 cm sec^{-1}. The ion flow velocity is two orders of

magnitude smaller than the electron particle velocity, V_D. Clearly, the electron drift velocity is the dominant velocity component of the plasma flow field of interest.

Since the particle dynamics are governed by the vector sum of the imposed flow velocity, U, and drift velocity, $_D$, and since the latter is so dominant, there is generally no violation of the basic assumptions of static plasma theories. Therefore the probe theories specifically formulated for static plasma diagnostics will be used to evaluate data in flowing plasma when $V_D >> U$.

The current voltage characteristics for the subsonic flow configuration are shown in Figure 5.3. In general, the electron saturation region is not as well defined as in stationary plasmas. A decrease in the conducted probe current at the test station relative to the static source could be expected; this decrease was noted to be from about 10^{-8}A to 10^{-11}A. Due to recombination and equilibration processes, the values of T_e and n_e at the test station are expected to be reduced relative to values in the discharge chamber.

Again, the Johnson-Malter double probe collisionless analysis (25) was first applied to obtain an indication of the magnitude of n_e, T_e and λ_D; Equations 5.4.1, 5.4.2 and 5.2.2 were utilized. Table 6 presents approximate plasma property values for the subsonic flow configuration.

The relationship between the Langmuir probe size, r_p, λ_D and λ_{e-n} again determines the specific plasma-probe operating domain. Table 7 presents a summary of these values. The approximate analysis
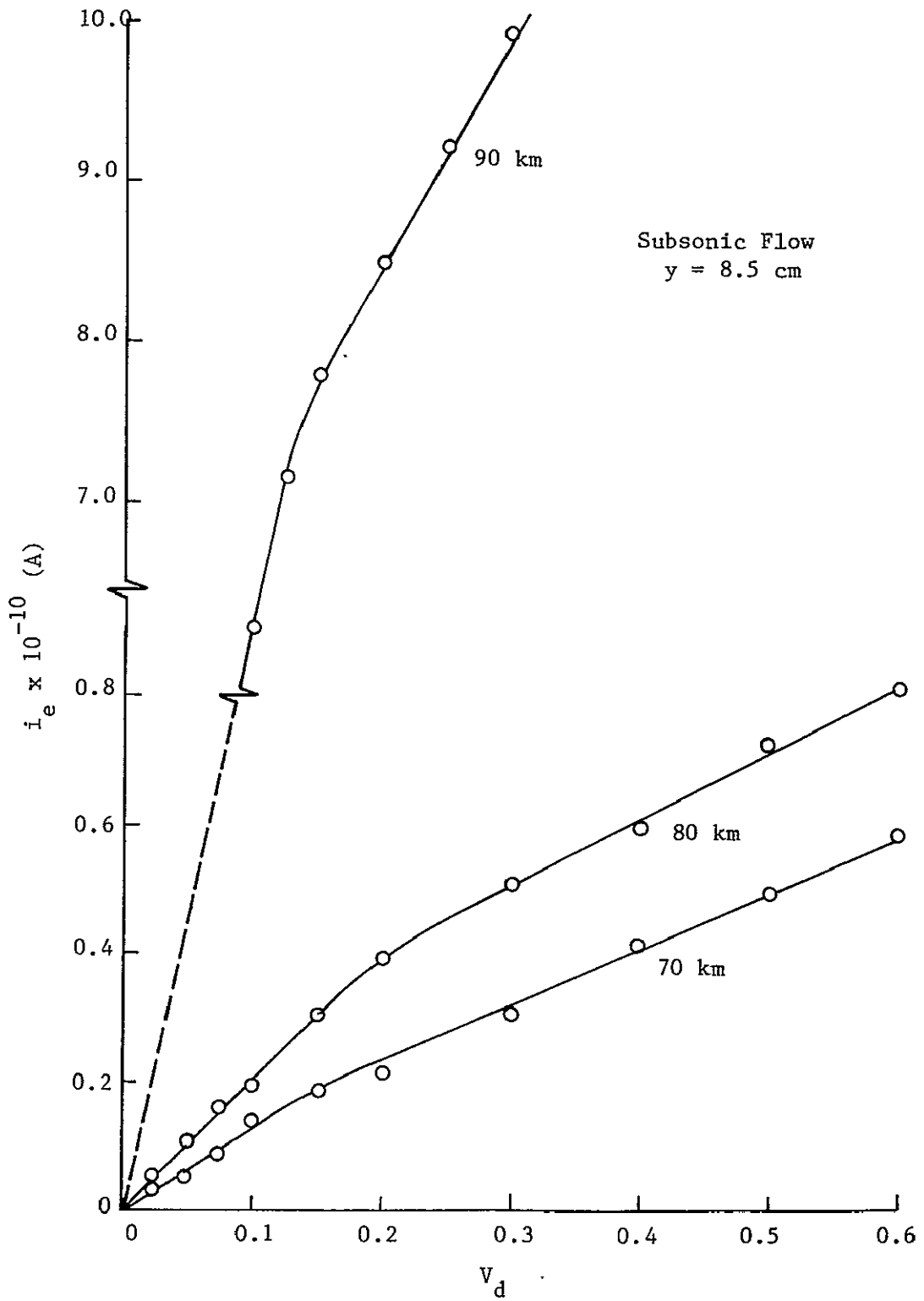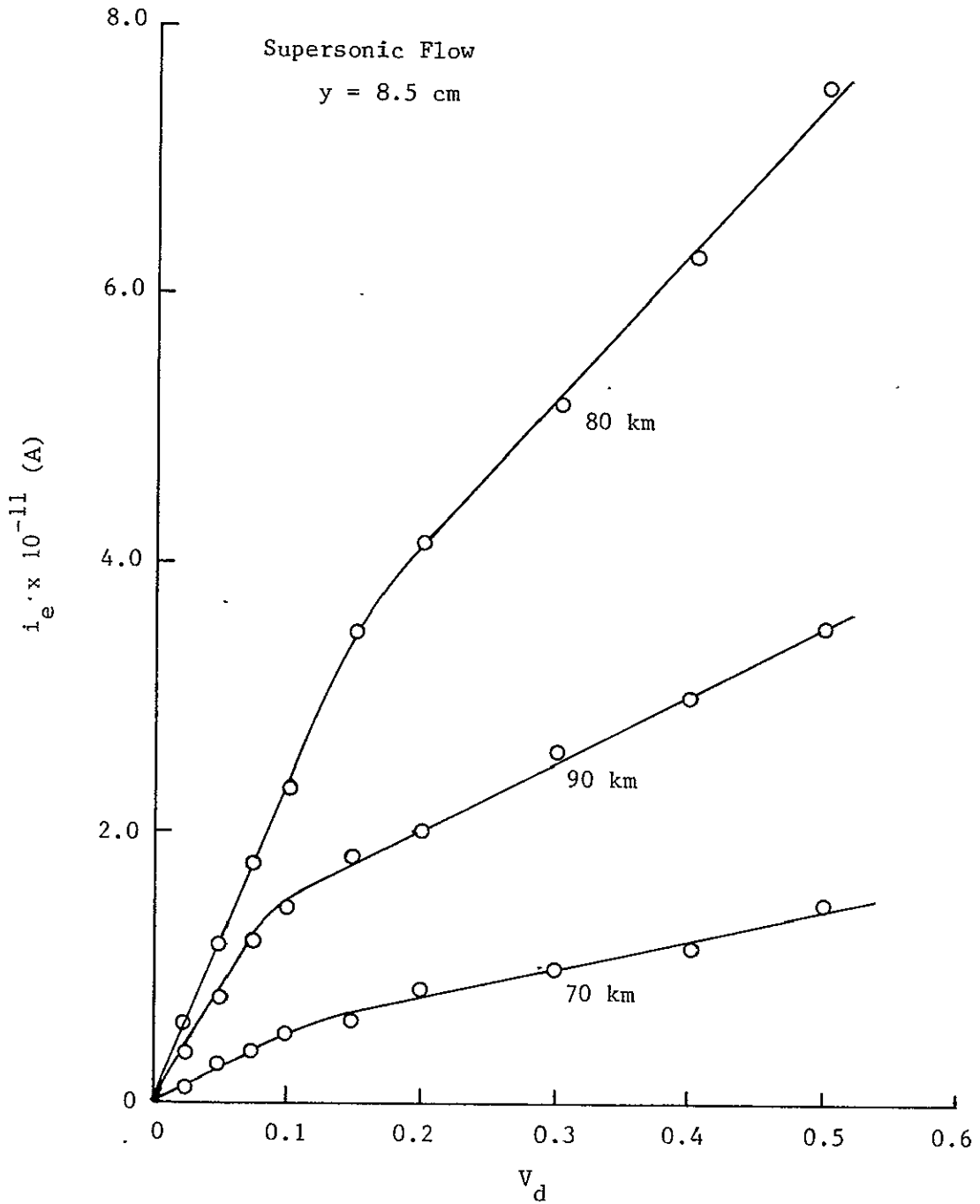
Figure 5.3   Double Probe Current-Voltage Characteristics
for Subsonic Flow in the 70, 80 and 90 km Regimes

Table 6: Approximate Plasma Properties with Subsonic Flow at Exit Station

$$T_i \quad 300^{\circ}K$$

ALT V_m	T_e $^{\circ}K$	n_e cm^{-3}	λ_D mm	λ_{e-n} mm
90	707	6.04×10^3	6.66	3.14
80	893	2.29×10^2	12.19	0.3088
70	439	6.75×10^1	49.75	0.168

Table 7: Plasma-Probe Interaction States in Subsonic Flowing Plasma

y = 8.5 cm

ALT	λ_D		λ_{e-n}		λ_{n-n}		r_p		PROBE STATE
km	mm		mm		mm		mm		
90	6.66	>	3.14	>	0.20	>	0.127		Collisionless
80	12.19	>>	0.3088	$\geq$	0.056	$\approx$	0.127		Transitional
70	49.75	>>	0.168	$\approx$	0.008	<	0.127		Transitional

of the plasma data in the test flow indicates that in the subsonic flow regime the plasma was collisionless ($\lambda_D > \lambda_{e-n} > r_p$) at 90 km, transitional ($\lambda_D \gg \lambda_{e-n} \geq r_p$) at 80 km, and transitional ($\lambda_D \gg \lambda_{e-n} \approx r_p$) at 70 km.

As discussed by Chung et al., (7) when all relevant Knudson numbers, $K_n \gg 1$, a cylindrical probe aligned with the flow direction will exhibit similar characteristics as a cylindrical probe in a static plasma. This condition does not hold, however, when $r_p \lambda_D^{-1} \ll 1$. An "end-effect" condition occurs when the sheath radius becomes larger than the probe radius. An aligned probe with the flowing plasma will collect particles through the lateral and end surfaces of the sheath area. If the flow velocity, $U \gg (k\, T_e\, m_i^{-1})^{1/2}$ or if the number of ion-ion collisions is not negligible, then a significant number of ions can reach the probe surface and cause a sharp peak in the measured ion current. As defined by Chung et al., (7),

$$T \equiv \left[k\, T_e\, m_i^{-1} \right]^{1/2} U^{-1}\, \ell\, \lambda_D^{-1} \qquad (5.4.10)$$

is the "end-effect" parameter; it is the following ratio: the product of the lateral sheath dimension (length) ℓ, and the transverse velocity, $(k\, T_e\, m_i^{-1})^{1/2}$, to the product of the end sheath dimension (thickness), λ_D, and the directed flow velocity, U. When $T \gg 1$ the end-effect on a cylindrical probe is negligible. When $T \leq 1$ the ion current will be greater than the orbital-motion limit value because of the increase in ions reaching the probe surface through the end of the sheath. Also,

the end-effect is associated with very small angular ranges, $\Delta \theta$, of the probe and flow directions; around $\theta = 0^{\circ}$.

As discussed earlier the alignment of the Langmuir probe was controlled in the test configuration by a traversing mechanism and micrometer. These devices were capable of accurately aligning the probe with the flow direction to within 2.5×10^{-3} cm. Therefore, with the probe directly aligned with the flow direction on ion current peak could be expected to occur in the recorded current data if the ion dynamic parameters are appropriate. Since the n_e values are determined from the ion saturation current, higher values of n_e indicated data could be expected with an active end-effect flow condition, than in the stationary plasma configuration.

In this experiment, the end effect parameters for the aligned cylindrical Langmuir double probe in the subsonic flow configuration were considered. The values, $r_p \lambda_D^{-1}$ range from 1.4×10^{-2} to 2.5×10^{-3}. However, the end-effect parameter, T, ranges from 23.2 at 90 km to 2.43 at 70 km and thus conditions generally satisfy the requirement that $T >> 1$ for the 90 km collisionless altitude of interest.

In the subsonic flow configuration an exact analysis of the plasma properties was determined from the diagnostic theories previously discussed in section 5.4.2. To reemphasize, the flow velocity, U, is not the dominant velocity component, therefore, the constraints on the basic static plasma theories have not been violated. Eqs.(5.4.5, 5.4.8 and 5.4.9) were used to evaluate the exact plasma properties in the subsonic flow configuration. In 5.4.5, $\alpha_p \simeq 2.7$ was used for $T_e/T_i = 1.3$, $r_p/\lambda_D \simeq 0$.

Table 8 presents the results of an analysis of plasma properties in the subsonic flow configuration; values for T_e, n_e, λ_D, λ_{e-n}, $\mathcal{Y}_d$ are given. The electron temperature ranges between 707°K and 893°K; these values are comparable to the values obtained in the static plasma configuration as presented in Table 5. The electron number densities are 9.66×10^4 cm^{-3} in the collisionless regime (90 km) and 9.48×10^1 cm^{-3} and 4.98×10^1 cm^{-3} in the transitional regimes at 80 km and 70 km, respectively. These values indicate a reduction in n_e, due to recombination, of about one order of magnitude from the static plasma values. The particle collection surface area, λ_D, can be seen to be of the same order of magnitude as in the static plasma, but at 90 km, λ_D is approximately half as small in the subsonic case, whereas at 80 km and 70 km, λ_D is approximately twice as large.

The current-voltage characteristics for the supersonic flow configuration are shown in Figure 5.4. In general, the saturation region is as well defined as in subsonic flow but not as well defined as in stationary plasma. The conducted probe current is further reduced by one order of magnitude from the subsonic flow values.

The Johnson-Malter double probe collisionless analysis (25) was again first applied to obtain an approximate indication of the magnitude of n_e, T_e and λ_D; equations 5.4.1, 5.4.2 and 5.2.2 were utilized. Table 9 presents approximate values for the supersonic flow configurations. Table 10 presents a summary of the plasma-probe operating domains. In the supersonic flow case the approximate double probe analysis indicates that at 80 and 90 km the flow was collisionless and transitional at 70 km.

Table 8: Plasma Properties in the Subsonic Flow Configuration

ALT	T_e	n_e	λ_{e-n}	λ_D	ϕ_d
km	$°K$	cm^{-3}	mm	mm	
90	707	9.66×10^4	3.14	1.668	2.3
80	893	9.48×10^1	0.3088	59.84	2.6
70	828	4.98×10^1	0.148	79.51	2.1

Figure 5.4   Double Probe Current-Voltage Characteristics for Supersonic Flow in the 70, 80 and 90 km Regimes

Table 9:   Approximate Plasma Properties with Supersonic Flow
at Exit Station

$$T_i \approx 300^\circ K$$

ALT	T_e	n_e	λ_D	λ_{e-n}
km	$^\circ K$	cm^{-3}	mm	mm
90	644	1.41×10^4	13.18	10.39
80	476	1.95×10^2	30.4	2.11
70	284	3.36×10^1	56.6	0.544

Table 10: Plasma-Probe Interaction States in Supersonic Flowing Plasma

$$y = 8.5 \text{ cm}$$

ALT	λ_D		λ_{e-n}		λ_{n-n}		r_p	PROBE STATE
km	mm		mm		mm		mm	
90	13.18	>	10.79	>	9.69	>>	0.127	Collisionless
80	30.4	>>	2.11	>	0.27	>	0.127	Transitional
70	56.6	>>	0.544	>	0.04	$\approx$	0.127	Transitional

In supersonic flow, the characteristics of a shock wave formed in front of an object depend upon the degree of rarefaction in the flow. The Knudsen number specifies the rarefaction and is the parameter on which the change from continuum behavior is based (32). The values of Knudsen number ($K_n \equiv \lambda_{nn}/r_p$) in the supersonic flow in front of the Langmuir probe elements are: 76.2, 2.12, .314 for 90, 80 and 70 km scaled conditions, respectively. The flow interaction can be concluded to be free molecular at 90 km, transition at 80 km, and slip flow at 70 km, scaled. Generally, the thickness of the shock wave transition region is on the order of one mean free path, λ_{nn}, and in continuum flow ($\lambda_{nn} \ll r_p$) the shock stand-off distance is on the order of the body radius, r_p (35). However, for flow at fixed Mach number, or Knudsen number increases, the thickness (δ_s) of the shock transition region increases and the shock position (Δ) forward of the body moves farther away from the body. Specifically, following McKenna (49), for $10^{-2} < K_n < 10^{0}, \delta_s = 5\,\lambda_{nn}$, and for $10^{-2} < K_n < 10^{1}$, $\Delta \approx .5\,r_B + 2\,\lambda_{nn}$. Accordingly at the scaled 90 km, $\Delta \approx 20$ mm while $\lambda_D = 13.18$ mm; at 80 km, $\Delta \approx .60$ mm and $\lambda_D \approx 30.4$ mm; at 70 km, $\Delta = .22$ mm and $\lambda_D = 56.6$ mm. Since the extrapolation at 90 km is not precise, it can be approximated at all conditions that the shock lies within the collecting surface and should not perturb the particle collection process. Accordingly, the calculation of free stream plasma conditions will be made assuming that temperature and density jumps occur in standard fashion across a shock wave, before particles reach the collecting surface. With a shock wave at $M = 2.0$, it can be presumed that it does not create further ionization in the plasma. The probe response is taken to represent the

M = 0.56 subsonic flow behind the shock, and calculation to account

for compression and heating by the shock wave were necessary to obtain

correct free stream properties.

The end-effect on the Langmuir double probe in the supersonic

flow configuration must be considered. Values for the end-effect

parameter, T , range from 0.046 at 90 km to 0.30 at 70 km. Also, the

parameter, $r_p \lambda_D^{-1} << 1$, ranged from 2.24 x 10^{-3} to 9.6 x 10^{-3}. There-

fore, values of n_e indicative data must be examined for enhanced currents

in this end-influenced flow condition as in the stationary plasma

configuration. When the detailed discussion in Hester and Sonin's work

(50 is considered, it can be seen that for large values of r there is

enhancement of collected ion current. However, an examination of the

results presented also indicate that for values of r << 1, there is

also no enhancement. Intuitively, this can be understood on the basis

of the fact that short length sheaths, even though thick, will have

little ability to alter ion trajectories and so gather larger numbers

of ions. In the present experiments with r = .046 at 90 km, the

one relevant collisionless state, there would appear to be little

likelihood of enhanced collection, and it will not be considered in

detail here.

Table 11 presents the values of T_e, n_e and λ_D calculated for

conditions in the supersonic flow configuration. The exact values of

T_e and n_e were determined by the appropriate diagnostic theory as

discussed in section 5.4.2. In the collisionless regimes n_e = 1.04 x 10^4

cm^{-3} and n_e = 5.26 x 10^1 cm^{-3} at 90 and 80 km, respectively. In the

trnasitional regime at 70 km, n_e = 7.8 cm^{-3}. The value of n_e at

Table 11: Plasma Properties in the Supersonic Flow Configuration

ALT	T_e	n_e	λ_D	λ_{e-n}	ϕ_d
km	$°K$	cm^{-3}	mm	mm	
90	340	2.91×10^3	6.66	14.0	1.9
80	269	5.26×10^1	44.10	2.7	3.6
70	268	7.8	114.67	0.707	4.3

70 km is above the 80 km value due to the larger anode employed in the scaled 70 km test; this was done so relevant values of n_e would be obtained. These values indicate a reduction in n_e from the static plasma, due to recombination, of about two orders of magnitude. The values of T_e were $340^\circ K$, $269^\circ K$ and $268^\circ K$ for the 90, 80 and 70 km conditions respectively.

The double Langmuir probe data presented and analyzed above will be compared with the blunt probe data to evaluate the blunt probe's operation and the analytical procedures. However, the double Langmuir probe reduced data will first be compared with other experiments. Figure 5.5 presents a comparison of data obtained from this experiment and the work by Dunn and Lordi (11) with the theoretical prediction in the orbital-motion-limit (collisionless regime) by Laframboise (17) for specific values of Debye ratio, $r_p \, \lambda_D^{-1}$ and nondimensional current density,

$$J_i \, (2\pi r \ell)^{-1} \, (e \, n_e \, ((k \, T_e) \, (2\pi m_i)^{-1})^{1/2}).$$

The work by Dunn and Lordi was conducted using single probes in nitrogen with Debye ratios about two orders of magnitude larger than the values obtained in this scaled D-region flow experiment. Hester and Sonin (50) indicated these data needed reduction for end flow enhancement. The figure shows that the transitional data falls further away from the theoretical values, while the collisionless data lies close to Laframboise's prediction. It can be seen, therefore, that the Langmuir probe data is relatively consistent with theory and experimental data obtained in other works.
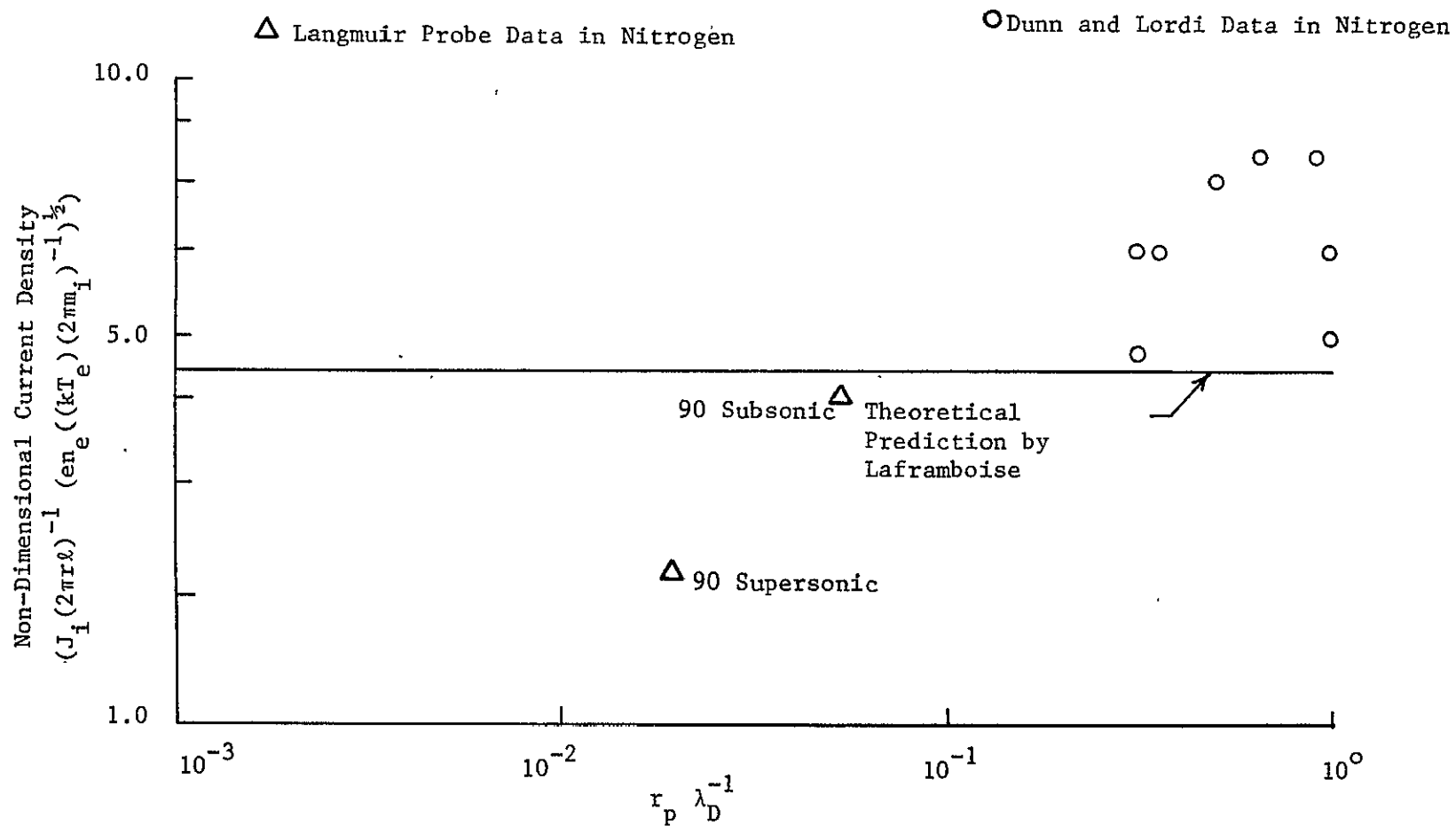
Figure 5.5   Comparison of Langmuir Probe Data with Theory for Collisionless Regime

5.4.4 Indicated Extent of Recombination of the Plasma in the Flow from Source to Test Station

Considering the loss of electrons and ions due to recombination, it can be formulated (51) that

$$\frac{dn_i}{dt} = \frac{dn_e}{dt} = - \alpha\, n_i n_e \qquad (5.4.11)$$

Since $n_i = n_e$ this can be integrated to give

$$\alpha = \frac{1}{t} \left[\frac{1}{n_e} - \frac{1}{n_{e0}} \right] \qquad (5.4.12)$$

On that basis, an experimental value of the recombination coefficient, (α) EXP, can be computed by estimating the electron density in the glow source, the electron density in the test jet, and the time for the particles to flow between the two. Table 12 presents the values of recombination coefficient determined using Eq. (5.4.12). The values of the recombination coefficient listed are orders of magnitude higher than recombination coefficients reported in classical studies (52–55) with short period quenching behavior ($\alpha = 1.8 \times 10^{-6}$ cm^3 sec^{-1} for N_2 at 9 Torr). One physical difference here is the much longer time involved in the flow from source to test station; also, there is considerable contact of plasma with the wall during the flow passage.

The magnitude of the recombination coefficients does seem to indicate that dissociative recombination (53) is the predominant loss process. It should be noted Kasner and Biondi (54) have measured recombination coefficients in nitrogen on the order of 10^{-6} cm^3 sec^{-1}.

Table 12:   Recombination Coefficients Indicated for the Flowing Plasma

ALT	α_{sub}	α_{sup}
km	cm^3/sec^{-1}	cm^3/sec^{-1}
90	4.3×10^{-6}	2.28×10^{-3}
80	9.2×10^{-5}	6.66×10^{-3}
70	1.1×10^{-4}	2.26×10^{-3}

They used microwave, mass spectrometric, and optical techniques to study the recombination rates in the afterglow of a microwave discharge. These researchers point out that such high values of α can only be attributed to the process of dissociative recombination between molecular ions and electrons in the weakly ionized plasma. In such a process a radiationless transition occurs in molecules; the molecules gain kinetic energy from their mutual repulsive forces making the neutralization process permanent (55). The time of the microwave discharge was only on the order of 10^{-3} sec. Recombination coefficients greater than 10^{-6} cm^3 sec^{-1} could be recorded for longer discharge times after excitation of the reactions between the species.

5.5 Evaluation of Plasma Properties from Blunt Electrostatic Probe Data and Comparison with Langmuir Probe Results

5.5.1 Introduction

The Langmuir double probe was used to obtain reference plasma properties in the scaled-D-region environment. These results establish reference conditions in the plasma at the modeled 70, 80 and 90 km regimes. Insertion of the blunt probe into the presumably known plasma environment will serve to indicate the validity of the blunt probe's operation and basic theory.

At present, blunt probe theories for the continuum regime have been developed by Lam (56), Touryan and Chung (57), Hoult (38), Sonin (19) and Lai (2). The theories formulated by Lam, and Touryan and Chung, however, generally are not valid in D-region probe flows because the assumption $\lambda_D r_p^{-1} << R_n^{-1/2}$ in their theory is not satisfied. Hoult's ion collection theory assumes that the charged particle density

in the plasma is low enough that the applied electric field of the probe

dominates the space charge electric field. The path of the attracted

particles in the theory is controlled by convection until very near

the probe surface where diffusion governs the dynamics of the particles.

Sonin's theory extended the theory developed by Hoult to include

supersonic moving probes. Sonin's ion collection theory is equivalent

to Hoult's theory in the D-region of the ionosphere because the strong

field condition, outlined in the theory, is satisfied throughout the

D-region (2). Sonin accounted for convection by assuming that at

large Reynolds numbers, R_n, the flow separates into two regions. In

the outer inviscid region, the particle concentrations remain constant,

while in the very near field of the probe a thin ($\delta << D_p$) boundary

layer exists. At the probe surface, the velocity and concentration of

the particles falls to zero. In Sonin's theory the electric field is

constant from the probe surface to the ambient plasma. It is therefore

observed that Hoult's theory assumes a very small perturbed region

(diffusion layer), while Sonin's theory does not include any perturbed

region outside the relatively thin boundary layer. In the absence of

any sheath region the electric field extends far from the probe

surface, but the collection of particles is dominated by convection

until near the probe surface. For a positive biased probe in a

continuum regime, however, the electron's high mobility and small mass

will result in an effective collecting surface at a large distance from

the probe surface; within this region the field induced velocities will

dominate and an analysis completely different from Hoult's and Sonin's

is necessary.

The theory outlined by Lai (2) is an analysis of electron

collection for blunt probes in the continuum regime of the D-region.

This theory was developed for subsonic probes and is based on a

dominant mobility concept. Starting at the probe surface, the probe's

field of influence is separated into the diffusion layer, mobility

layer and the convection and mobility region. When the electron drift

velocity (V_D) is found to dominate the imposed flow velocity (U) and

electron thermal velocity (V_T), the perturbed thickness (particle

collection layer) is determined by using an analysis for the static

probe. The static probe analysis is reasoned to be valid when $V_D \gg U$,

because the magnitude of the electron motion is the vector sum of U and

V_D. Therefore, although this probe theory was outlined for subsonic

probes, it can also be useful for supersonic flow configurations.

The blunt electrostatic probe electron collection theory (2) for

subsonic flowing plasma is based on a dominant mobility concept in

the continuum particle collection regime. The probe's field of

influence is separated into the diffusion layer, mobility layer, and

the convection and mobility region; these regions are shown in Figure

5.6 (2). For a positively biased probe, the electrons in the ambient

plasma (outer region) first encounter the influence of the probe at

the outer boundary of the convection and mobility region, γ_A. In the

present flow experiment, the electron drift velocity, V_D, dominates the

imposed flow velocity, U, and electron thermal velocity, V_T, so the

region, in theory, where convection would dominate is irrelevant. The

mobility layer, with outer boundary at γ_B, is the next inner layer and

is that region where the dynamics of the electrons are controlled by
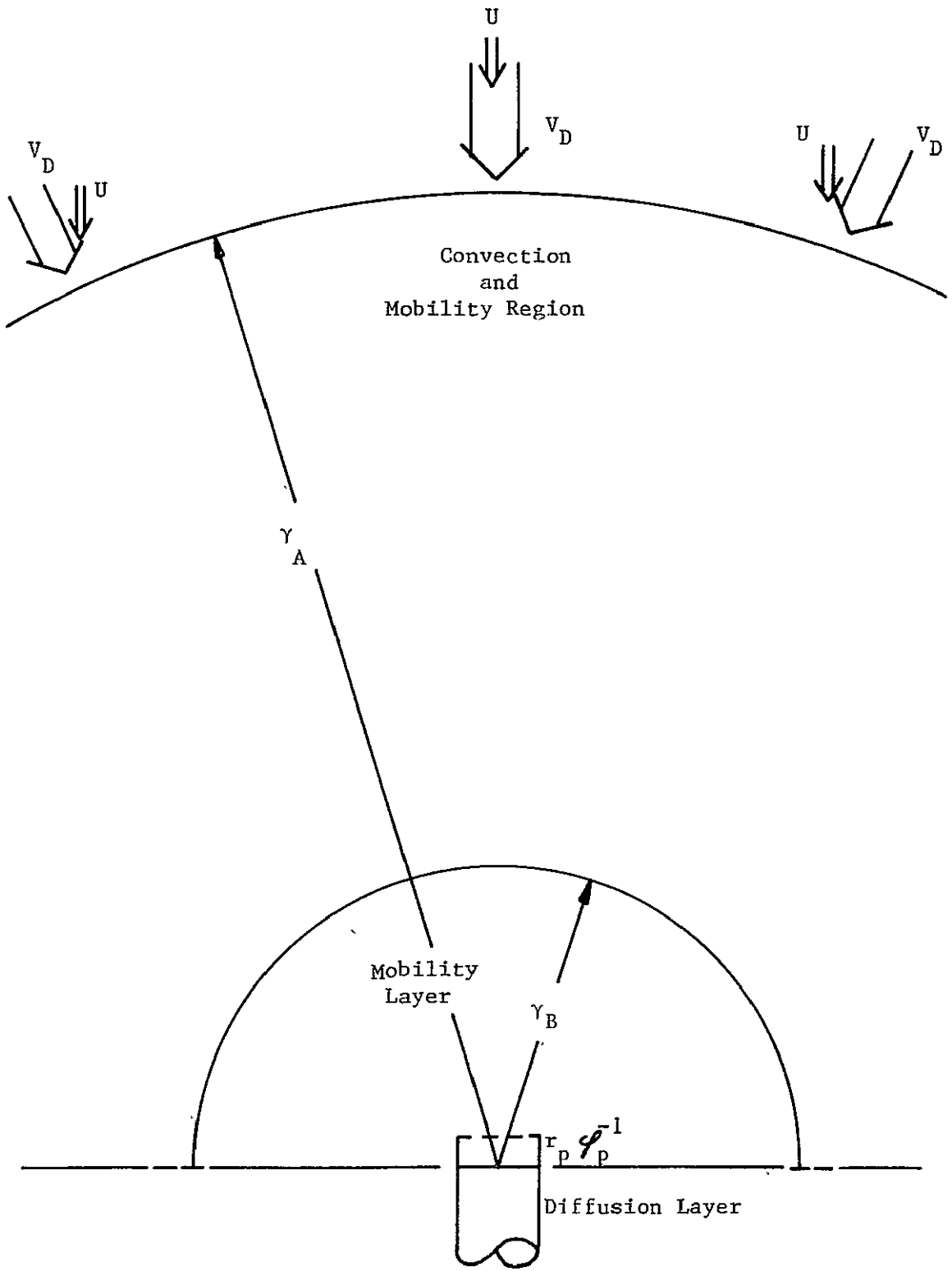
Figure 5.6 Blunt Electrostatic Probe Regions for Electron
Collection

the electric field of the probe. The electrons enter at γ_B with two velocity components, V_D and U, and the magnitude of V_D relation to U enables the mobility processes to dominate the motion and path of the electrons. The region closest to the probe surface is the diffusion layer, with outer boundary at $r_p \phi_p^{-1}$, where both electron diffusion and mobility are dominant processes. The diffusion layer is relatively thin compared to γ_B and allows a uniform and constant electric field to form. Within $r_p \phi_p^{-1}$, there is an exponential decay of electron concentration because of the proximity to the probe surface. However, there is also a simultaneous increase in density from the ambient plasma due to the mobility process. Thus, for a specific probe potential and operating pressure the combined effect of diffusion and mobility processes leaves the electron number density in the diffusion layer a constant.

Again, the primary interest here is to determine electron density from the electron collection regime of the blunt probe characteristic. The Debye length, λ_D, can be used only as an approximate indicator of the position of an effective collection surface for a probe of an effective collection surface for a probe in the test plasma, because the criterion for its validity, $\phi_p \ll 1$, is not satisfied. The theory presented by Lai (2) develops a different criterion for a scaling length indicative of the sphere of influence of the blunt probe; in that work, γ_0 was specified as a static plasma perturbed radius (boundary of a sheath region). For a moving probe, γ_B, was derived; generally, γ_0 and γ_B are comparable for low values of velocity. Further, the dominance of drift velocity, V_D, over flow velocity, U, enables γ_0, γ_B

to be used as the position of the surface where the particle flux to the probe is determined. The formulation of γ_0, γ_B by Lai, however, was developed for a particle collection radius much larger than the radius of the probe, $\gamma_0 \gg r_p$. If γ_0 is approximately the same order as the radius of the probe, $\gamma_0 \sim r_p$. an alteration of Lai's formulation of γ_0 for the continuum regimes is necessary.

The perturbed thickness for $\gamma_0 \sim r_p$ was formulated from the electric field distribution on the surface of a flat, circular, conducting collector disc modeling the probe. The collector disc is an equipotential surface where the charge distribution is symmetric about the axis and in the plane containing the disc. The electric field distribution for a circular disc where the probe radius is the same order as the radius of interest is (2)

$$\Phi = \frac{2V_d}{\pi} \left[\frac{r_p}{r^2 + r_p^2} \right] \qquad (5.5.1)$$

where r is the radial location of a surface of interest, V_d is the applied probe potential, and r_p is the radius of the probe electrode. Near the surface of the probe, $r \ll r_p$ and the electric field is

$$\Phi_p = \frac{2V_d}{\pi r_p} \qquad (5.5.2)$$

From conservation of flux between some collection surface A_0 at radius r_0, and the surface of particle collection on the probe, the electric field due to the probe is expressed by

$$\Phi_0 = \Phi_p \frac{A_{COL}}{A_0} \tag{5.5.3}$$

where A_0 is the area of the collection surface displaced from the probe, and $A_{COL} = \pi r_{COL}^2$ is the area of the collector disc (probe surface). Combining Eqs. (5.5.3, 5.5.2 and 5.5.1) the collection area at the boundary of the perturbed region is determined by

$$A_0 = A_{COL} \left[\frac{r_0^2 + r_p^2}{r_p^2} \right] \tag{5.5.4}$$

Dividing Eq. (5.5.3) by the static pressure, P, and substituting Eq. (5.5.4),

$$\frac{\Phi_0}{P} = \frac{\Phi}{P} \left[\frac{r_p^2}{r_0^2 + r_p^2} \right] \tag{5.5.5}$$

Following Lai (2), with $\Phi_o/P = 4 \times 10^{-2}$ volt cm^{-1} mm Hg at $r_0 \equiv \gamma_0$ for electron collection on nitrogen gas,

$$\gamma_0^2 = 25 \ r_p^2 \left(\frac{\Phi}{P} \right) - r_p^2, \ \text{(cgs)} \quad . \tag{5.5.6}$$

The data obtained by the blunt probe in the static and flow regimes were analyzed by first considering the relationship between the collected particle mean free path, λ_{s-n}, and the blunt probe size, r_p. The parameters that categorize collisions between charged and neutral particles enable the plasma−probe interaction states to be specified. Analyses appropriate for these states were then applied.

The approximate magnitude of the mean free paths between electron-neutral, λ_{e-n}, ion-neutral, λ_{i-n}, and neutral-neutral, λ_{n-n}, particles, . specified in section 5.4 and as listed in Table 2, were compared with the blunt probe size, r_p = 0.5 mm. With these approximate values, it was determined that for electron collection in the static and subsonic plasma regime, $\lambda_{e-n} > r_p$ (collisionless) at 90 km, and $\lambda_{e-n} > r_p$ (continuum) at 80 and 70 km. In the supersonic configuration $\lambda_{e-n} > r_p$ (collisionless) .at 90 and 80 km and $\lambda_{e-n} < r_p$ (continuum) at 70 km.

5.5.2 Static Source Plasma

In the static plasma configuration, current-voltage data was obtained with the blunt probe.positioned similar to the Langmuir probe. The blunt probe was found to conduct measurable current at locations, y = 1 cm to y = 4 cm from the center of the plasma source, within the glow discharge chamber.

Figure 5.7 represents typical current voltage characteristics for ion and electron collection by the blunt probe in the static continuum (70 km) plasma case. It should be noted that the extent of charge particle saturation decreases as the probe is moved further away from the plasma source, similar to behavior indicated by the Langmuir probe.

Figure 5.8 shows the electron collection, current-voltage characteristics for the pressure regimes studied in the static plasma configuration. The blunt probe indicates more pronounced saturation effects with increasing pressure; this trend is opposite to that observed with the Langmuir probe. This behavior could occur here because of the decreasing
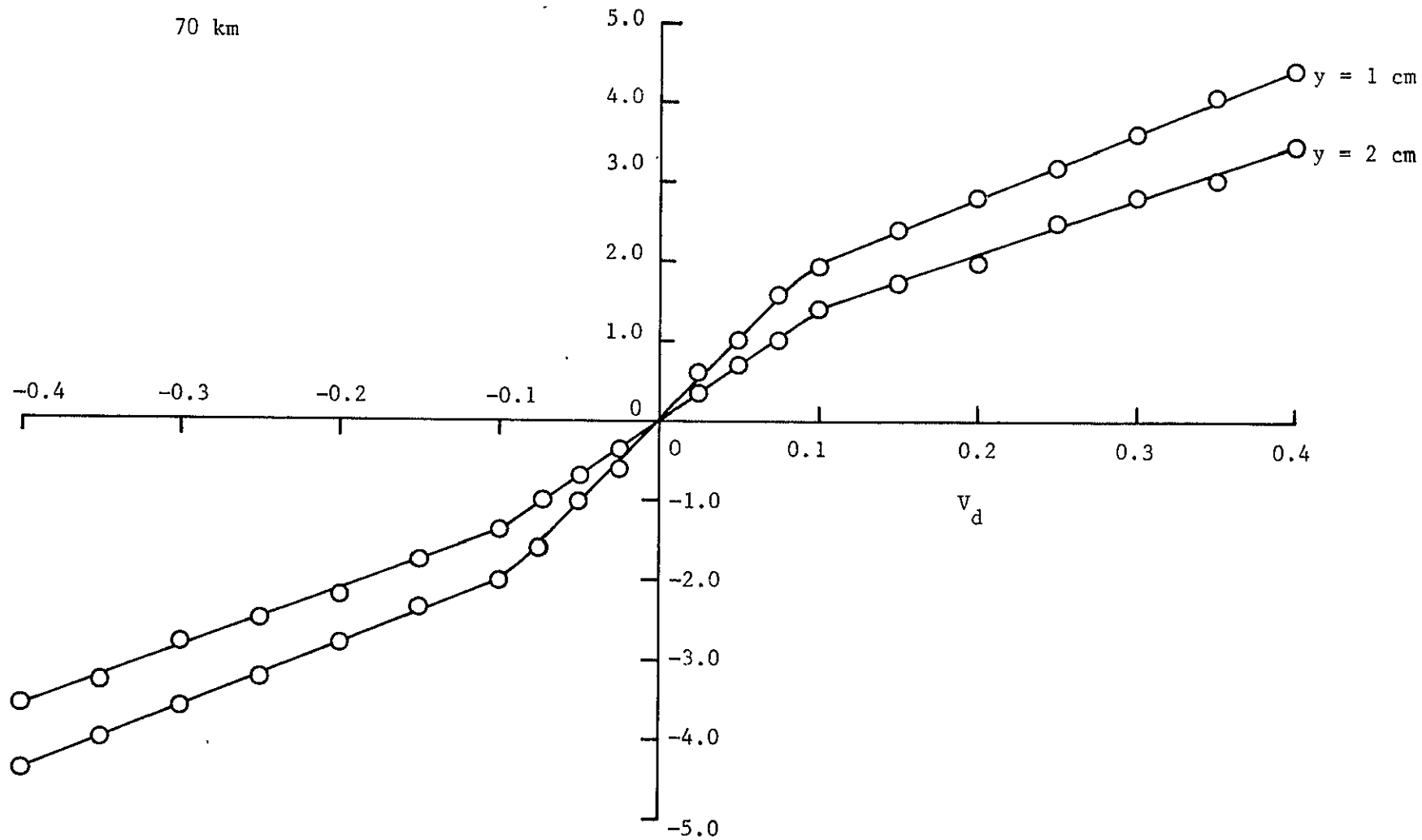
Figure 5.7 Current-Voltage Characteristics for Ion and Electron Collection in Static Plasma by the Scaled Blunt Probe at 70 km
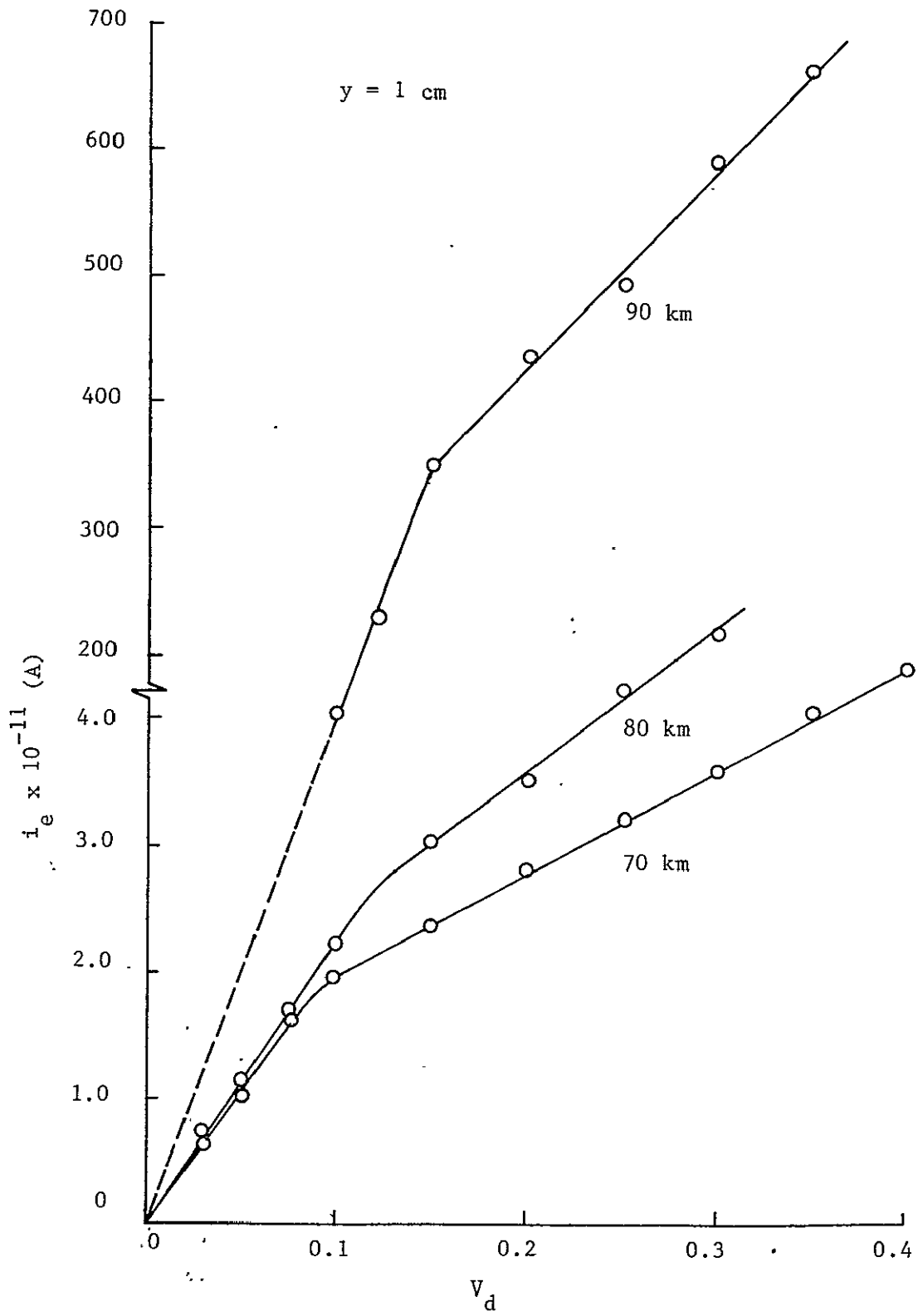
Figure 5.8   Blunt Probe Electron Current – Voltage
Characteristics for Static Plasma in the
70, 80 and 90 km Regimes

thickness of the perturbed region γ_0, which results from the increasing pressure. Also, an increased glow discharge potential was required to maintain the plasma at higher test pressure (500 V at the 90 km regime to 1500 V at the 70 km regime). It should be noted that the electron current conducted by the blunt probe in the 90 km regime was on the order of 10^{-9} A, the same order of magnitude as the current to the Langmuir probe in the 90 km regime. This indicates that γ_0 should also be the same order of magnitude as λ_D. In the 80 and 70 km regimes, electron current, i_e, was on the order of 10^{-11} A, a reduction by two orders of magnitude from the current conducted by the Langmuir probe at these conditions, thus indicating a smaller γ_0 for the blunt probe in the static continuum regime than λ_D.

The raw data obtained in the static plasma configuration with the blunt probe allows the plasma and sheath operational domains to be identified: $\gamma_0 > \lambda_{e-n} > r_p$ (γ_0 = 9.44 mm) or collisionless at 90 km; at 80 km (γ_0 = 4.18 mm), and 70 km (γ_0 = 1.51 mm), $\gamma_0 > r_p > \lambda_{e-n}$, or continuum.

In the continuum pressure regime (80 and 70 km) with static plasma, the values of n_e were determined by employing the probe analysis presented by Lai (2). The analysis is based on the formulation of the perturbed thickness, γ_0, appropriate when $\gamma_0 > r_p$, based on the above estimates. Lai's formulation (Eq. 4.3.12), n_e was determined from

$$n_e = 1.29 \times 10^{14} \, P \left(\frac{\Delta J_e}{\Delta V_p} \right) SAT \qquad (5.5.7)$$

In the collisionless, static plasma regime (90 km) the diffusion layer concept, as discussed by Lai (2) is not relevant because $r_p \mathcal{Y}_p <$ λ_{e-n}. The absence of collisions within the very near field of the blunt probe, therefore, requires the use of a theory, such as Child's-Langmuir (47), to evaluate data with a collisionless surface layer. A theory such as Laframboise (17) for the orbital-motion-limit in the collisionless regime does not apply for the blunt probes either, because particle orbits do not form due to the probe's geometry (33); for a constant operating pressure and discharge potential the effective collection area of the probe is a constant. The blunt probe data with $\gamma_0 > \lambda_{e-n} > r_p$ was therefore evaluated by the Child's-Langmuir relation (47), given by

$$n_{e0} = \left(\frac{\Delta j_e}{\Delta V_p} \right)_{SAT} \left(\frac{3}{2} \right) \left(\frac{m_e}{2e} \right)^{1/2} \left(\frac{kT_e}{e^2} \right) \left(V_p + \frac{kT_e}{e} \right)^{-1/2} \tag{5.5.8}$$

where n_{e0} is the electron number density in the undisturbed plasma, $(\Delta j_e / \Delta V_p)_{SAT}$ is the electron current slope after saturation, and γ_e is the electron current density. The Child's-Langmuir relation is valid for $V_p \, e \, (kT_e)^{-1} >> 1$ and $\lambda_{e-n} > r_p$. The electron number density was determined by the diagnostic form of Eq. (5.5.8) by

$$n_{e0} = 1.42 \times 10^{14} \left(\frac{\Delta J_e}{\Delta V_p} \right)_{SAT} \mathcal{Y}_p^{-1} \left[\frac{V_p \mathcal{Y}_p}{1 + \mathcal{Y}_p} \right]^{1/2} \tag{5.5.9}$$

where $\Delta J_e (\Delta V_p)^{-1} {}_{SAT}$ is the slope of the electron saturation region from the current-voltage characteristic and $\mathcal{Y}_p = eV_p (kT_e)^{-1}$ the

nondimensional plasma potential. The electron temperature was determined by Eq. (5.4.1) using the double Langmuir probe data. The values of n_{e0} and T_e for the static case are presented in Table 13.

5.5.3 Flowing Plasma at Test Station

The current voltage data in the flow configuration was obtained with the blunt probe at locations similar to those previously specified for the Langmuir probe. The probe was positioned at $y = 8.5$ cm from the center of the plasma source on the flow axis, at the exit plane of the nozzles.

For the subsonic flow configuration, Figure 5.9 shows the electron collection, current-voltage characteristics. As in the static plasma case, there is a continual increase in the degree of saturation with pressure. With flow, T_e reduces to 707°K at 90 km, 893°K at 80 km and 828°K at 70 km, which is an order of magnitude reduction below static plasma values. The values of T_e were determined from the Langmuir probe by Eq. (5.4.1). It was found that γ_0 is about the same magnitude as in the static plasma, which would be expected in a region where $V_D \gg U$. Also, at 90 km, γ_0 is about 3.85 mm, which is as large as the Langmuir probe particle collection dimension, λ_D; at 80 and 70 km, γ_0 is 1.41 mm and 0.40 mm, respectively, which is an order of magnitude smaller than γ_D. The values of γ_0 and γ_B, however, are two orders of magnitude smaller than the values Lai calculated due to the flow scaling by two orders of magnitude.

Table 13: Blunt Probe – Static Plasma Properties

ALT (km)	T_e ($^{\circ}$K)	n_e (cm^{-3})	λ_{e-n} (mm)	$\mathscr{S}_d$	γ_0 (mm)
90	1160	3.8×10^5	2.600	1.74	9.40
80	1857	1.47×10^4	0.442	0.66	4.18
70	830	2.8×10^4	0.130	1.40	1.51
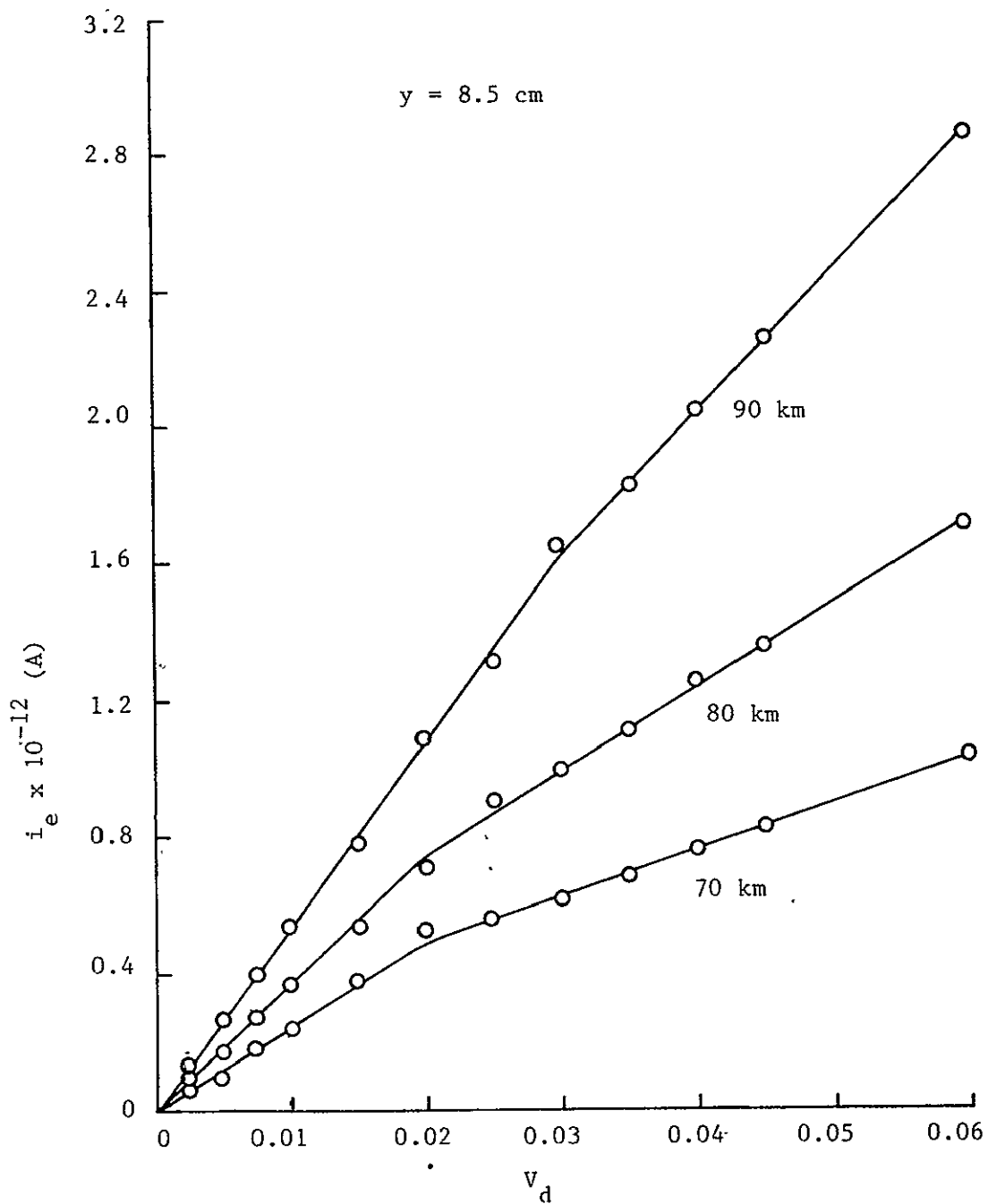
Figure 5.9   Blunt Probe Electron Current-Voltage Characteristics
for Subsonic Flow in the 70, 80 and 90 km Regimes

From the subsonic, blunt probe raw data, the operational regimes for the probe were determined. It was found that at the 90 km regime $\gamma_0 > \lambda_{e-n} > r_p$ (collisionless), at 80 km $\gamma_0 > r_p > \lambda_{e-n}$ (continuum), and at the 70 km regime $\gamma_0 > r_p > \lambda_{e-n}$ (continuum).

In the subsonic flow configuration at the 90 km test regime, the operational plasma and sheath domain $(\gamma_0 > \lambda_{e-n} > r_p)$, $\gamma_0 = 3.85$ mm, indicates the existance of a collisionless surface layer. The value of n_e was obtained by the Child's-Langmuir relation (47). Eq. (5.5.9) was used to obtain a value of n_e; a value $n_e = 8.99 \times 10^4$ cm^{-3} was obtained.

In the continuum regimes at 80 and 70 km the values of n_e were determined from Lai's (2) theory (Eq. 4.3.52). Lai's formulation of Eq. 4.3.52 was reformulated for the blunt probe in the 80 and 70 km test regimes. For the 80 km regime the value of n_e was determined by

$$n_e = 4.03 \times 10^{14} P_E \left[\frac{\Delta J_e}{\Delta V_p} \right]_{SAT} \tag{5.5.10}$$

where P_E is the static test pressure at the exit plane of the flow nozzle (y = 8.5 cm) and $(\Delta J_e / \Delta V_p)_{SAT}$ is the electron current slope after saturation. In the 70 km regime n_e was determined by

$$n_e = 3.05 \times 10^{14} P_E \left[\frac{\Delta J_e}{\Delta V_p} \right]_{SAT} \tag{5.5.11}$$

This data is presented in Table 15, at the end of this section. The values of n_e obtained by the blunt probe are relatively the same magnitude as the values obtained by the Langmuir probe.

In the supersonic flow configuration, a detached shock wave can be expected to form in front of the blunt probe. The values of Knudsen numbers ($K_n \equiv \lambda_{nn}/r_p$) in the supersonic flow in front of the blunt probe collection surface are: 19.38, 0.54 and 0.08 for 90, 80 and 70 km scaled conditions, respectively. The flow interaction can be concluded to be free molecular at 90 km, and slip flow at 80 and 70 km, scaled. As discussed in section 5.4.3, free stream plasma conditions will be calculated assuming that temperature and density jumps occur in standard fashion across a shock wave, before particles reach the collection surface. Calculations to account for compression and heating by the shock wave ($M_N = 2.0$) were necessary to obtain correct free stream properties.

Figure 5.10 shows the electron collection, current-voltage characteristics for the supersonic flow configuration. The saturation voltage continues to increase with pressure, while the magnitude of the conducted current continues to decrease below subsonic levels. T_e was determined from Eq. (5.4.1). The values of T_e are: $340^{\circ}K$ at 90 km, $269^{\circ}K$ at 80 km and $268^{\circ}K$ at 70 km.

It was found from the data that the magnitude of γ_0 is about twice that in the subsonic flow case but an order of magnitude smaller than λ_D for the Langmuir probe. As in the subsonic flow configuration, the reduction in magnitude of the conducted probe current appears related to the smaller sheath or field affected, mobility region. In the subsonic flow, γ_B was about twice the magnitude of γ_0, whereas in the supersonic flow configuration γ_B is 1.64 mm at 90 km, 0.62 mm at 80 km, and 0.27 mm at 70 km; these values are about one-third the size of γ_0. In the 70 km regime $r_p \mathcal{G}_d^{-1}$ is 0.12 mm, which is one-third that in the subsonic flow case.
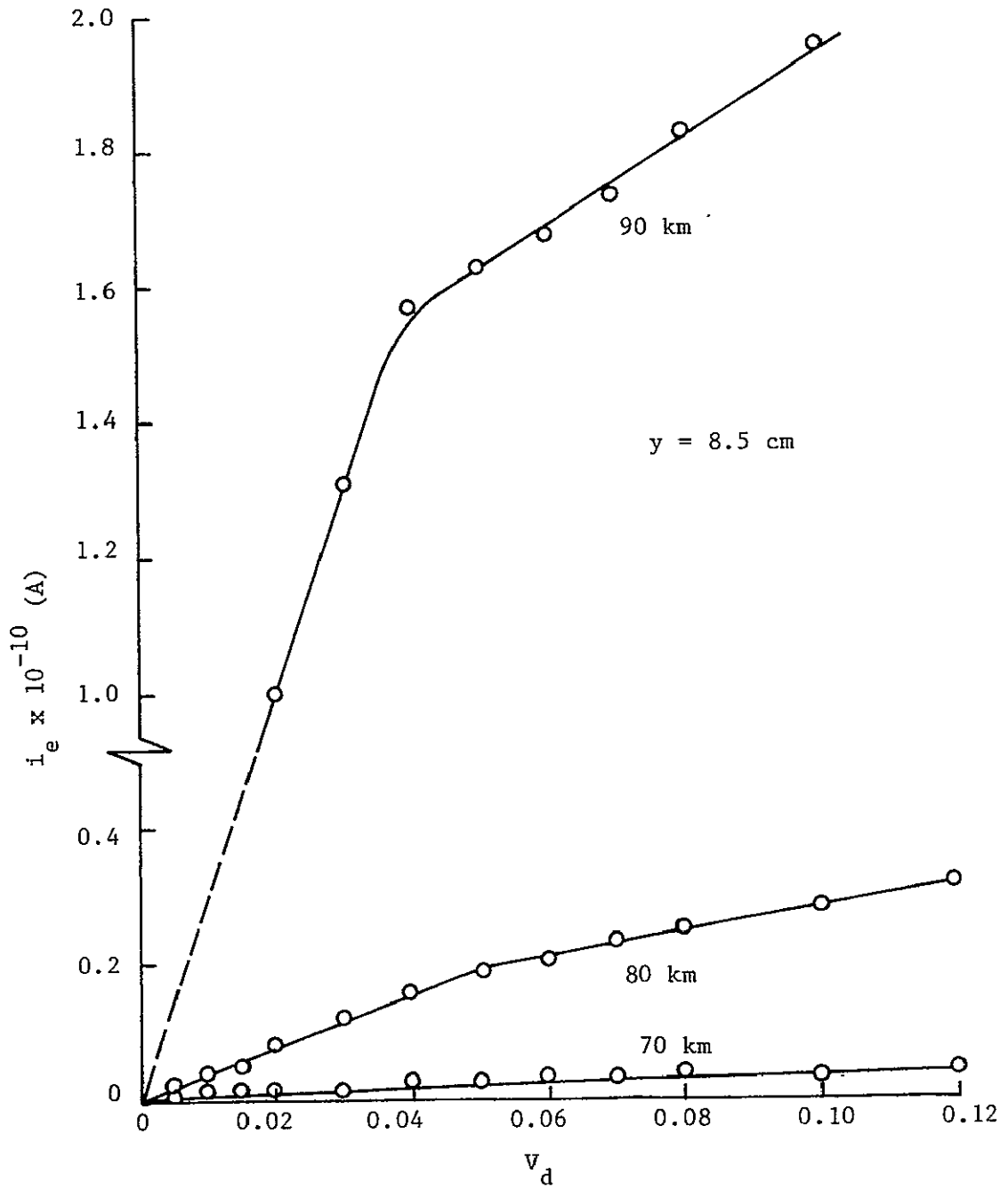
Figure 5.10   Blunt Probe Electron Current-Voltage Characteristics
for Supersonic Flow in the 70, 80 and 90 km Regimes

The operational domains for the blunt probe in the supersonic flow configuration were determined from the data, and provide for the specification of the collisionless or continuum probe theories. At the 90 km regime $\lambda_{e-n} \gg \gamma_0 > r_p$ (collisionless), at 80 km $\lambda_{e-n} > \gamma_0 > r_p$ (collisionless) and at the 70 km $\gamma_0 > r_p > \lambda_{e-n}$ (continuum). The operational domains for the flow and static configurations are summarized in Table 14.

The values of n_e in the collisionless test regimes at 90 and 80 km were determined from the Child's-Langmuir relation (47). Eq. (5.5.9) is the diagnostic form of the Child's Langmuir relation Eq. (5.5.8) used to evaluate the collisionless states. The values of n_e in the continuum regime (70 km) were determined from a reformulation of Lai's (2) theory Eq. (4.3.52) and is given by

$$n_e = 5.47 \times 10^{14} P_E \left[\frac{\Delta J_e}{\Delta V_p} \right]_{SAT} \qquad (5.5.12)$$

The values of n_e are presented in Table 15, at the end of this section.

Table 15 is a summary of the properties of plasma in the scaled flow facility obtained with the scaled blunt probe; it is useful for comparison with the properties obtained with the Langmuir probe.

5.6 Comparison of Electron Densities in the Scaled Laboratory Experiment as Indicated by Various Blunt Probe Theories

The values of the electron densities in the scaled plasma flow laboratory experiment were evaluated from double probe and blunt probe data using available theories. The blunt probe particle collection theories reported by Lai (2) and Mitchell (58), Hale and Hoult (4) have not

Table 14: Operational Regimes for the Scaled Blunt Probe

ALT	STATIC PLASMA			SUBSONIC FLOW			SUPERSONIC FLOW		
(km)	γ_0	λ_{e-n}	r_p	γ_0	λ_{e-n}	r_p	γ_0	λ_{e-n}	r_p
	(mm)	(mm)	(mm)	(mm)	(mm)	(mm)	(mm)	(mm)	(mm)
90	Collisionless			Collisionless			Collisionless		
	9.40 > 2.600 > 0.50			3.85 > 3.14 > 0.50			5.64 < 10.80 > 0.50		
80	Continuum			Continuum			Collisionless		
	4.18 > 0.442 < 0.50			1.41 > 0.31 < 0.50			2.91 > 2.11 > 0.50		
70	Continuum			Continuum			Continuum		
	1.51 > 0.139 < 0.50			0.40 > 0.17 < 0.50			1.5 > 0.54 ≈ 0.50		

Table 15:   Blunt Probe – Plasma Properties

STATIC PLASMA	T_e	n_e	λ_{e-n}	p	γ_O	γ_B	$r_p \wp_p^{-1}$
	$^\circ K$	(cm^{-3})	(mm)		(mm)	(mm)	(mm)
90 km	1160	3.8×10^5	2.600	1.74	9.40		
80 km	1857	1.46×10^4	0.442	1.66	4.18		0.30
70 km	830	2.80×10^4	0.139	1.40	1.51		0.36
SUBSONIC FLOW							
90 km	707	8.99×10^4	3.14	1.65	3.85	8.72	
80 km	893	7.66×10^3	0.31	1.40	1.41	3.14	0.36
70 km	828	1.62×10^3	0.17	1,43	0.40	1.43	0.35
SUPERSONIC FLOW							
90 km	664	5.18×10^3	10.80	3.10	5.64	1.64	
80 km	476	9.6×10^2	2.11	3.30	2.95	0.62	
70 km	284	1.34×10^3	0.54	3.18	1.57	0.27	0.12

as yet, been tested or substantiated by controlled laboratory experiments. Electrostatic probe response using a double Langmuir probe and a scaled blunt probe in static and flowing plasmas was studied and allows for an experimental comparison of the indications of number density from the various probe theories formulated for D-region probe flows.

Lai's theory (2) was developed for continuum electron collection by static and subsonic moving probes and presents an analysis of the several perturbed regimes adjacent to the probe's surface. The Mitchell (58), Hale and Hoult (4) theory has primarily been used to describe ion particle collection but was also used to indicate electron densities with rocket-borne probe data. Mitchell calculated the particle concentration in the D-region from the data obtained by Hale's rocket-borne blunt probes. The electron densities, n_e, in the present experiment without negative ions, are determined by

$$n_e = \frac{\sigma_-}{e\mu_e} \tag{5.6.1}$$

where μ_e is the electron mobility and σ_- is the electron conductivity.

In the collisionless regimes the response from the Langmuir double probe was evaluated from the theory developed by Laframboise (17). In the collisionless regime, the response from the blunt probe was evaluated by a new application of the Child-Langmuir theory (47).

In the transition regimes electron densities were evaluated from the particle collection theory formulated by Kirchhoff et al., (22).

Figure 5.11 presents a comparison of electron densities evaluated with various particle collection theories in the subsonic flow configuration; Figure 5.12 presents densities determined in the supersonic flow
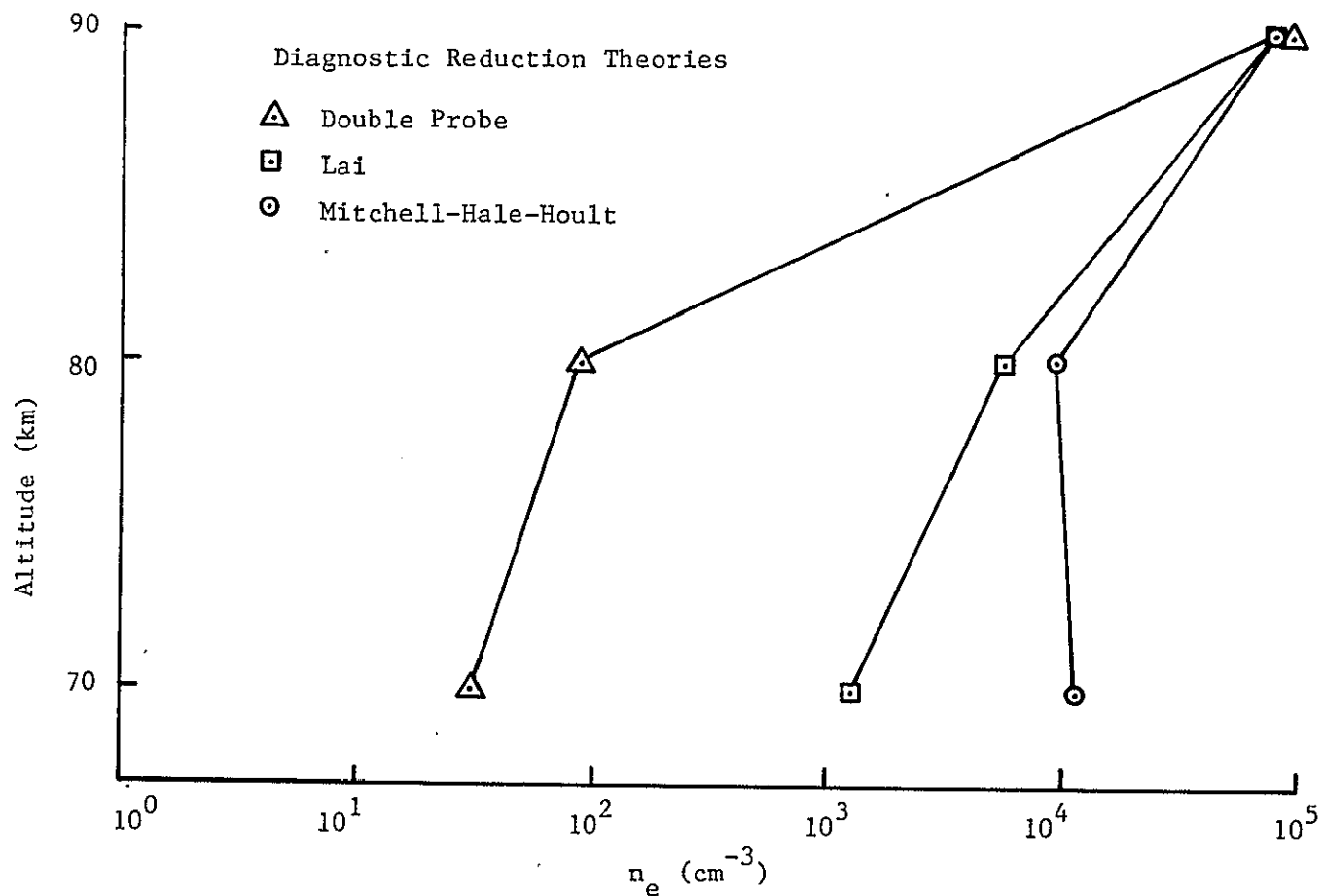
Figure 5.11   Comparison of Electron Densities Indicated by Different Diagnostic
Reduction Theories in Subsonic Flow
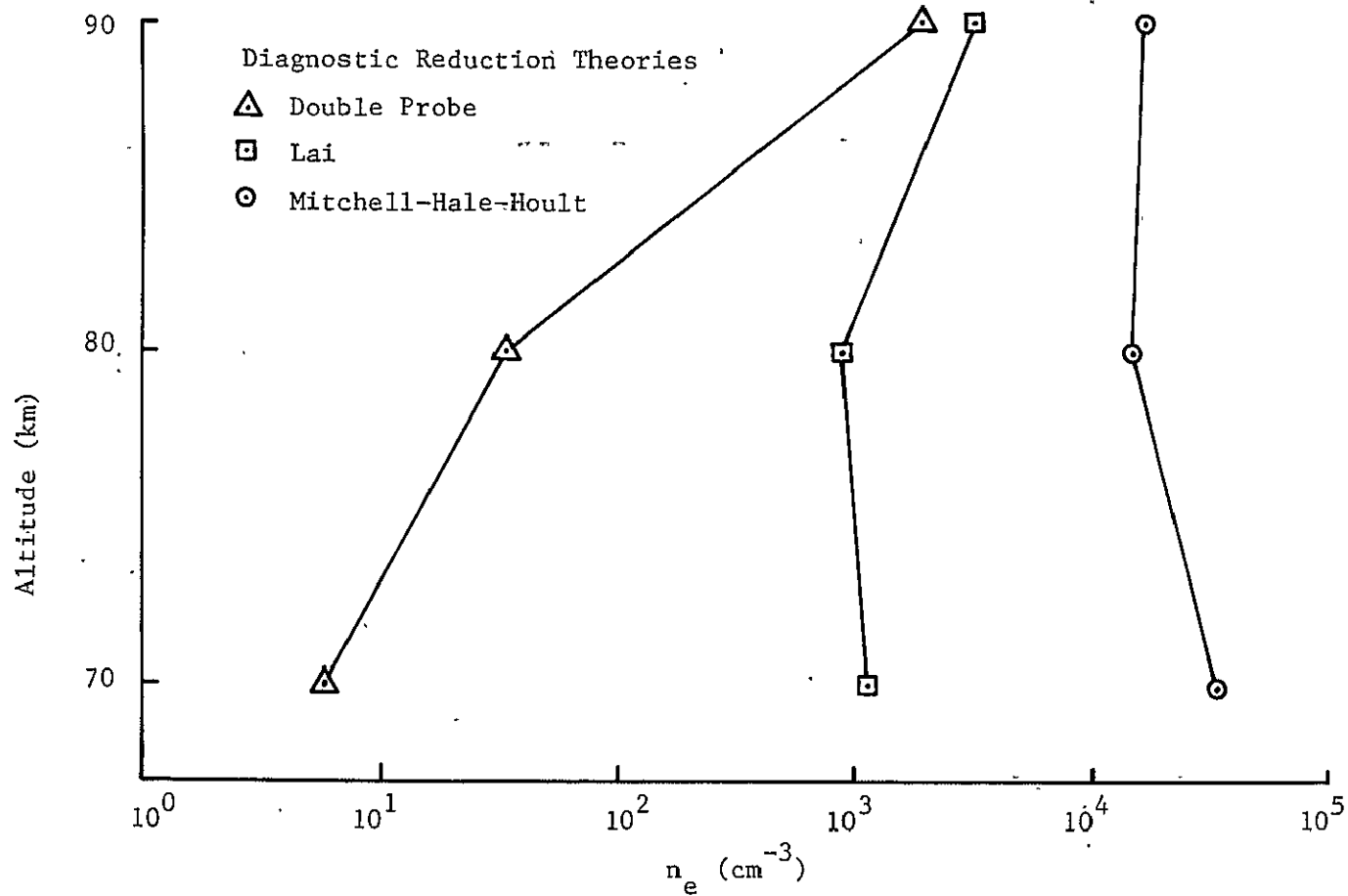
Figure 5.12   Comparison of Electron Densities Indicated by Different
Diagnostic Reduction Theories in Supersonic Flow

configuration. Generally, there are relatively small differences in indicated values of n_e in the 90 km collisionless regime. The procedure used to determine particle concentrations from Laframboise's theory (17) for the double Langmuir probe, utilizes the electron-retarding region of the probe's current-voltage characteristic. In this region the electrons are absorbed by the probe while the ions are repelled. In the Child-Langmuir theory (47) for the blunt probe, however, the values of n_e are determined from the slope of potentials above the saturation of the probe characteristic. In such a model the dynamics of the electrons are determined within the sheath. The electron. current is collected by the continual collisionless flux of particles through a constant area sheath at a boundary which increases in thickness with increasing probe potential.

There are dissimilar indications of n_e in the continuum regimes. Under continuum test conditions with a blunt probe, there is a relatively constant sheath thickness for a specific operating pressure. As the applied blunt probe potential, V_d, is increased the collection surface area generally remains constant. For the cylindrical double probe, however, the sheath collection surface area continually increases proportional to $V_d^{1/2}$ (33).

The values of n_e indicated for the supersonic flow configuration are generally smaller in magnitude than concentrations obtained in the subsonic flow configuration. Some differences may be due to the shock wave which is presumed to form in front of both geometries of probes. Shock compression would not only increase the density in the flow, but also would increase the recombination rate between positive ions and

electrons. While temperature jumps across shocks would appear, there would only be recovery of lower initial temperatures due to expansion. Any correction to the data to account for changes in density due to the shock wave, cannot recover the loss of electrons from recombination. Also, the position of a shock forward of the probe surface could be outside any detached effective collecting surface, as shown in Figure 5.4, and cause extraneous effects in the particle collection process.

The electron density reduction method used by Mitchell (58), Hale and Hoult (4), predicts densities that are generally one order of magnitude higher than predicted by Lai (2) and one to three orders of magnitude higher than predicted by the double probe diagnostic. These results are not unexpected, because the theory developed by Mitchell (58), Hale and Hoult (4) correctly models ion collection which takes place close to the probe surface. This theory does not account for the relatively thick "sheath" or perturbed region, which forms when electrons are collected by a positive biased probe. Therefore, only an analysis which includes the structure of a region with enhanced electron activity sheath and accounts for the particle dynamics within this perturbed region, can be expected to be valid for electron collection. Lai's theory (2) appears to give better agreement with double probe indications of electron density. However, it will be noted that some double probe indications of electron density are anomalously low, 10^1-10^2 cm^{-3}, and their validity is questionable.

The differences in the electron densities indicated by the various probes and theories must be considered relative to some significant factors. First, the theories to reduce double probe data never precisely

matched the experimental conditions. The data shows that there were few distinct, definable regimes of operation that are either collisionless, transitional, or continuum. The general inability to apply a theory which precisely fits the experiment, resulted in approximate analyses being applied in the reduction procedures. Further, Laframboise (59) has recently pointed out that the standard double probe method for determining the value of the electron temperature, T_e, will result in an overestimation as the Debye length increases under continuum or transitional plasma regimes. Laframboise discusses an improved theory for determining the correct values of T_e; such a theory should be explored further. At the present time, the implications of Laframboise's new theory have not, as yet, been fully explored. However, the indicated values of T_e that have been presented could be higher than more correct values; such a situation would also imply higher densities for the double probe.

Another influence on the differences in the evaluated magnitudes of the electron densities relates to the detailed construction of the blunt probe. The blunt probe's design did not precisely fit the requirement of $r_p \gg r_{COL}$, because of the large gap between the guard ring and collection surface. If, however, $r_p = r_{COL}$ then the values of n_e would be four times smaller using Lai's theory (2) with the present experiments.

In brief summary, it will be reemphasized that for the first time, a series of controlled laboratory tests with ionospheric plasma was conducted to examine electron collection by blunt probes. Several

theories that had not been tested or verified under controlled conditions were used to reduce electron density estimates from the data. The results presented here show that, generally, the theoretical studies of particle collection by electrostatic probes should be continued and improved before the present experimental results can be satisfactorily resolved.

———

CHAPTER VI

CONCLUSION

6.1 Summary

Rocket-borne blunt probe flows have been simulated in a weakly
ionized plasma. A steady state plasma flow system adequately simulated
the electron temperatures and number densities indicative of the
D-region of the ionosphere. The equivalence of the flow parameters
(M_n, R_n and K_n) in the actual and simulated regimes were achieved by
scaling the neutral gas density and probe diameter over two orders of
magnitude. The glow discharge source plasma produced satisfactory ̇
electron temperatures and densities. The control of these properties
was achieved by varying the electrode configurations in the discharge
chamber and by allowing relaxation of the cross flow from the discharge
chamber through a baffle system. Subsonic and supersonic flows were
produced to model the flight configurations of actual rocket-borne
probes through the ionosphere.

The electron collection theory outlined by Lai was specifically
considered. It was concluded that this theory, which was formulated
for subsonic and static blunt probes, appears to be valid for super-
sonic probes when the electron drift velocity dominates the imposed
flow velocity.

The laboratory data obtained from the scaled blunt probe were ·
reduced and compared with the Langmuir double probe predictions of n_e
in the subsonic and supersonic flow configuration. They were found to
be in mixed agreement. The electron densities indicated by Lai's
theory were then compared with those indicated by the ion

collection theory of Mitchell, Hale, Hoult. It was found that these reduction procedures resulted in electron densities that were one order of magnitude or more higher than the densities evaluated by Lai's electron collection theory. These results were not unexpected because of the basic formulation of the ion theories, which do not account for the relatively thick sheath formation when electrons are collected.

The recent development of a new theoretical formulation for deriving the electron temperature in large Debye length, continuum-transitional, plasmas is noted. While this work must be further explored, values of T_e would be overestimated if this theory is shown to be substantiated.

The work presented here is the first controlled laboratory test for electron collection from ionospheric plasma. Further work is required, for precise corroboration of electron collection theories by electrostatic blunt probes.

6.2 Improvement of Plasma Discharge System for D-Region Probe Flow Modeling

As an improved plasma discharge flow modeling system, the employment of a cold-cathode discharge system along with the multiphase baffle and flow nozzle arrangement would provide a means for obtaining low electron temperatures ($T_e \sim 10^2$ °K) and number densities ($n_e \sim 10^3$ cm^{-3}) at the test section in the experimental facility. A cold-cathode discharge system is produced by using brush cathodes as the electrode configuration (26). Brush cathodes produce a stable plasma discharge in the abnormal glow region of the glow discharge (26). The negative glow typically produced in laboratory plasmas by the usual glow discharge electrode configuration, is generally too small to be of significance for

diagnostic probing. However, if brush cathodes are employed the resulting negative flow typically extends one or two orders of magnitude further longitudinally than the normal cathode glow. Within the negative glow region of the discharge there are no striations or instabilities, which are usually associated with a glow discharge plasmas. The negative glow plasma is a reliable means for attaining desired, reproducible values of electron temperatures and number densities.

Specifically, the employment of brush electrodes in a discharge tube where its length to diameter ratio is about sic, is proposed. Two brush cathodes located opposite to each other and one brush anode positioned off-set from the center of the discharge tube between each cathode is suggested. This arrangement would provide a uniform electron gas in the energy range of 1 to 10 KV (26), and enable the gas cross flow in the discharge chamber to remain long enough to reach equilibrium with the entire volume of plasma before entering the baffle system. The relatively long distance between the cathodes and anode would require the operating discharge current to be maintained at about 150 mA. This current is necessary to provide sufficient kinetic energy to the ions for continued and sufficient ion bombardment at the cathodes, such that electrons could attain energetic trajectories for a uniform and concentrated discharge beam.

Persson (26) has used brush electrodes in a similar arrangement. Helium was used as the test gas, and single collisionless Langmuir probes were employed for diagnostic probing. The negative glow discharge beam is a field-free plasma and was observed by Persson to fill the

entire discharge. tube. Electron temperatures of order 10^2 $^{\circ}$K were obtained in this experimental arrangement. It was found that the high energy of the electrons in the discharge beam prohibit the beam from interacting with the different plasma wave mechanisms. Energy only associated with electrons released in ionization and recombination processes is transmitted to the plasma, thus enabling low electron temperatures. Electron densities of order 10^{12} cm^{-3} were obtained and are characteristic of negative glows produced in helium. The use of multiphase baffles, however, in the proposed experimental arrangement with air as the test gas, would reduce the densities sufficiently such that characteristic D-region electron number densities would be achieved.

REFERENCES

1. Nicolet, M. and A. C. Aikin, The formation of the D-region of the ionosphere, Journal of Geophysical Research, 65, 1469, 1960.

2. Lai, T., Electron collection theory for a D-region subsonic blunt electrostatic probe, Ionosphere Research Laboratory , The Pennsylvania State University, Scientific Report No. 424, 1974.

3. York, T. M., Laboratory simulation of lower ionosphere probe flows, Ionosphere Research Laboratory, The Pennsylvania State University, Internal Report, 1973.

4. Hale, L. C. and D. P. Hoult, A subsonic D-region probe theory and instrumentation, Ionosphere Research Laboratory, The Pennsylvania State University, Scientific Report No. 247, 1965.

5. Whipple, E. C., An imposed technique for obtaining atmospheric ion mobility distribution, Journal of Geophysical Research, 65, 3679, 1960.

6. Bordeau, R. E., E. C. Whipple and J. F. J. Clark, Analytic and experimental electrical conductivity between the stratosphere and the ionosphere, Journal of Geophysical Research, 64, 1369, 1959.

7. Chung, P. M., L. Talbot and K. J. Touryan, Electric probes in stationary and flowing plasmas, Part I and II, AIAA Journal, 12, 133, 1974.

8. Hale, L. C., Positive-ions in the mesosphere, Proceedings of the COSPAR Symposium on Methods of Measurements and Results of Lower Ionosphere Structure, Konstanze, 1973.

9. Burkhard, W. J., D-region blunt probe data analysis using hybrid computer techniques, Ionosphere Research Laboratory, The Pennsylvania State University, Scientific Report No. 415, 1973.

10. French, J. B., Langmuir probes in a flowing low density plasma, UTIAS Report No. 79, 1961.

11. Dunn, M. G. and J. A. Lordi, Thin-wire Langmuir probe measurements in the transition and free molecular flow regimes, AIAA Journal, 8, 1077, 1970.

12. Sonin, A. A., The behavior of free molecular cylindrical Langmuir probes in supersonic flows and their application to the study of the blunt body stagnation layer, UTIAS Report No. 109, 1965.

13. Sonin, A. A., Free-molecule Langmuir probe and its use in flow-field studies, AIAA Journal, 4, 1588, 1966.

14. Smetana, F. O. and Iachetta, F. A., Experiments on the current collected by a cylindrical Langmuir probe in a rarefied plasma streaming with high velocity, Rarefied Gas Dynamics, Edited by Trilling-Wachman, Academic Press, New York, 2, 65, 1963.

15. Segall, S. B. and D. W. Koopman, Application of cylindrical Langmuir probes to streaming plasma diagnostics, Physics of Fluids, 16, 1149, 1973.

16. Heatley, A. H., Collector theory for ions with Maxwellian and drift velocities, Physical Review, 52, 235, 1973.

17. Laframboise, J. G., Theory of spherical and cylindrical Langmuir probes in a collisionless Maxwellian plasma at rest, UTIAS Report No. 100, 1966.

18. Jakubowski, A. K., Effect of angle of incidence on the response of cylindrical electrostatic probes at supersonic speeds, AIAA Journal, 10, 988, 1972.

19. Sonin, A. A., Theory of ion collection by a supersonic atmospheric sounding rocket, Journal of Geophysical Research, 72, 4547, 1967.

20. Llewellyn-Jones, F., The Glow Discharge, John Wiley and Sons, Inc., New York, 1966.

21. Enkenhus, K. R., Pressure probes at very low density, UTIA Report No. 43, 1957.

22. Kirchhoff, R. H., E. W. Peterson and L. Talbot, An experimental study of the cylindrical Langmuir probe response in the transition regime, AIAA Journal, 9, 1686, 1971.

23. Hale, L. C., Parameters of the low ionosphere at night deduced from parachute borne blunt probe measurements, Space Research XII, Edited by R. L. Smith-Rose, North Holland Publishing Company, Amsterdam, 1967.

24. Cobine, J. D., Gaseous Conductors, Dover Publications, Inc., New York, 1958.

25. Johnson, E. O. and L. Malter, A floating double probe method for measurements in gas discharges, Physical Review, 80, 1950.

26. Persson, K. B., Brush cathodes - a well behaved plasma, Journal of Applied Physics, 36, 3086, 1965.

27. Bunting, W. D. and W. J. Keikkila, Transient ion sheath effects on probe admittance, Journal of Applied Physics, 42, 1136, 1970.

28. Katzer, M. M. and J. P. Finnegan, An analytical and developmental analysis of a resistance heated thruster, Undergraduate Thesis, Department of Aerospace Engineering, The Pennsylvania State University, University Park, Pennsylvania, 1969.

29. RCA Receiving Tube Manual, Technical Series RC-20, RCA, Harrison, New Jersey, 1960.

30. McDaniel, E. W., Collision Phenomena in Ionized Gases, John Wiley and Sons, Inc., New York, 1964.

31. Rogers, K. W., J. B. Wainwright and K. J. Touryan, Impace and static pressure measurements in high speed flows with transitional Knudsen numbers, Rarefied Gas Dynamics, Edited by H. J. deLeeuw, Academic Press, New York, 2, 1966.

32. Schaaf, S. A. and P. L. Chambre, Flow of Rarefied Gases, Princeton University Press, Princeton, New Jersey, 1961.

33. Chen, F. F., in Plasma Diagnostic Techniques, Edited by Huddlestone-Leonard, Academic Press, New York, 1965.

34. Wehner, G. and G. Medicus, Reliability of probe measurements in hot cathode gas diodes, Journal of Applied Physics, 23, 1035, 1952.

35. Liepman, H. W. and A. Roshko, Elements of Gasdynamics, John Wiley and Sons, Inc., New York, 1957.

36. Abramovich, G. N., The Theory of Turbulent Jets, M.I.T. Press, Cambridge, Massachusetts, 1963.

37. Ashkenas, H. and F. S. Sherman, The structure and utilization of supersonic free jets in low density wind tunnels, Rarefied Gas Dynamics, Edited by H. J. deLeeuw, Academic Press, New York, 2, 1966.

38. Hoult, D. P., D-region probe theory, Journal of Geophysical Research, 70, 3183, 1965.

39. Petersen, E. W. and L. Talbot, Collisionless electrostatic single-probe and double-probe measurements, AIAA Journal, 8, 2215, 1970.

40. Chou, Y. S., L. Talbot and D. R. Willis, Kinetic theory for a spherical electrostatic probe in stationary weakly ionized plasma, Physics of Fluids, 9, 2150, 1966.

41. Talbot, L. and Y. S. Chou, Langmuir probe response in the transitional regime, Rarefied Gas Dynamics, Edited by Trilling-Wachman, Academic Press, New York, 2, 1969.

42. Kaegi, E. M. and R. Chin, Stagnation region shock layer ionization measurements in hypersonic air flows, AIAA Paper No. 66, 1966.

43. Thornton, J. A., Comparison of theory and experiment for ion collection by spherical and cylindrical probes in a collisional plasma, AIAA Journal, 9, 342, 1971.

44. Kiel, R. E., Continuum electrostatic probe theory for large sheaths on spheres and cylinders, Journal of Applied Physics, 40, 3668, 1969.

45. Chung, P. M. and V. D. Blankenship, Theory of electrostatic double probe comprised of two parallel plates, AIAA Journal, 4, 442, 1966.

46. Chung, P. M., Diagnostic equations of electrostatic double probes for continuum plasmas, Journal of Spacecraft and Rockets, 4, 1105, 1967.

47. Sutton, G. W. and A. Sherman, Engineering Magnetohydrodynamics, McGraw-Hill, New York, 1965.

48. Graf, K. A., The determination of spatially non-uniform electron density distribution, UTIAS Report No. 108, 1965.

49. McKenna, K. F., Hypersonic low density shock layer structure on flat faced cylinders, M.S. Thesis, Department of Aerospace Engineering, The Pennsylvania State University, University Park, Pennsylvania, 1970.

50. Hester, S. D. and A. A. Sonin, Ion temperature sensitive end effects in cylindrical Langmuir probe response at ionosphere satellite conditions, Physics of Fluids, 13, 1265, 1970.

51. Nasser, E., Fundamentals of Gaseous Ionization and Plasma Electronics, John Wiley and Sons, Inc., New York, 1971.

52. Weston, G. F., Cold Cathode Glow Discharge Tubes, ILIFFE Books Ltd., London, 1968.

53. Bates, D. R., Dissociative recombination, Physical Review, 78, 492, 1950.

54. Kasner, W. H. and M. A. Biondi, Electron-ion recombination in nitrogen, Physical Review, 137, A317, 1965.

55. McDaniel, E. W., Collision Phenomena in Ionized Gases, John Wiley and Sons, Inc., New York, 1964.

56. Lam, S. H., A general theory for the flow of weakly ionized gases, AIAA Journal, 2, 256, 1964.

57. Touryan, K. J. and P. M. Chung, Flush-mounted electrostatic probe in the presence of negative ions, AIAA Journal, 9, 365, 1971.

58. Mitchell, J. D., An experimental investigation of mesospheric ionization, Ionosphere Research Laboratory, The Pennsylvania State University, Scientific Report No. 416, 1973.

59. Laframboise, J. G. and J. Chang,Probe theory for arbitrary shape in a large Debye length, stationary plasma, Physics of Fluids, 19, 25, 1977.

Kaplan, Lee Bernard, Laboratory Simulation of Rocket-Borne D-Region Blunt Probe
    Flows, The Ionosphere Research Laboratory, Electrical Engineering East,
    University Park, Pennsylvania, 16802, 1977

PSU-IRL-SCI-456

Classification Numbers

1 5   Ionosphere
1.5 1   D-Region

The flow of weakly ionized plasmas that is similar to the flow that occurs over rocket-borne blunt probes as they pass through the lower ionosphere has been simulated in a scaled laboratory environment, and electron collection D-region blunt probe theories have been evaluated.

A scaled steady state plasma flow simulated the electron temperatures ($T_e \sim 10^2$ °K) and number densities ($n_e \sim 10^2$ cm^{-3}) characteristic of the lower ionosphere (D-region). A glow discharge was used to produce the source plasma; source electron temperatures and densities were controlled by varying the electrode configuration. The test section conditions were also controlled by relaxation of the plasma from the cross flow in the discharge chamber and through a baffle system Subsonic ($M_n = 0.3$) and supersonic ($M_n = 2.0$) flows were produced Equivalence of the flow parameters ($M_n \sim 0.3$, $R_n \sim 10^2$, and $K_n \sim 10^{-2}$) was reproduced by appropriately scaling both the neutral gas density and probe diameter to two orders of magnitude.

The state of the plasma in the glow source and test section jet was indicated from a Langmuir (collisionless) double probe response. A scaled version of a rocket-borne blunt probe was also evaluated in this controlled flow experiment The various blunt probe theories for particle collection were analyzed, and electron densities evaluated from double Langmuir and scaled blunt probe data using these theories were compared with mixed results The theory by Mitchell, Hale, Hoult is felt to correctly describe the processes in the relatively thin perturbed layer adjacent to the probe surface that is dominant in ion collection. However, for electron collection, the theory proposed by Lai appears to more correctly describe the particle motion and processes occurring in the several perturbed layers adjacent to the blunt probe surface, and indicated number densities show better agreement with those indicated by the double probe

Kaplan, Lee Bernard, Laboratory Simulation of Rocket-Borne D-Region Blunt Probe Flows, The Ionosphere Research Laboratory, Electrical Engineering East, University Park, Pennsylvania, 16802, 1977.

PSU-IRL-SCI-456

Classification Numbers

1.5 Ionosphere
1.5.1 D-Region

The flow of weakly ionized plasmas that is similar to the flow that occurs over rocket-borne blunt probes as they pass through the lower ionosphere has been simulated in a scaled laboratory environment, and electron collection D-region blunt probe theories have been evaluated.

A scaled steady state plasma flow simulated the electron temperatures ($T_e \sim 10^2$ °K) and number densities ($n_e \sim 10^2$ cm^{-3}) characteristic of the lower ionosphere (D-region). A glow discharge was used to produce the source plasma, source electron temperatures and densities were controlled by varying the electrode configuration. The test section conditions were also controlled by relaxation of the plasma from the cross flow in the discharge chamber and through a baffle system. Subsonic ($M_n = 0.3$) and supersonic ($M_n = 2.0$) flows were produced. Equivalence of the flow parameters ($M_n \sim 0.3$, $R_n \sim 10^2$, and $K_n \sim 10^{-2}$) was reproduced by appropriately scaling both the neutral gas density and probe diameter to two orders of magnitude.

The state of the plasma in the glow source and test section jet was indicated from a Langmuir (collisionless) double probe response. A scaled version of a rocket-borne blunt probe was also evaluated in this controlled flow experiment. The various blunt probe theories for particle collection were analyzed, and electron densities evaluated from double Langmuir and scaled blunt probe data using these theories were compared with mixed results. The theory by Mitchell, Hale, Hoult is felt to correctly describe the processes in the relatively thin perturbed layer adjacent to the probe surface that is dominant in ion collection. However, for electron collection, the theory proposed by Lai appears to more correctly describe the particle motion and processes occurring in the several perturbed layers adjacent to the blunt probe surface, and indicated number densities show better agreement with those indicated by the double probe